AD-A122 359 METALLIC HALIDE OPTICAL GLASSES: SYNTHESIS AND CHARACTERIZATION OF IR TRA..(U) CATHOLIC UNIV OF AMERICA WASHINGTON DC C T MOYNIHAN ET AL. OCT 82 1/3

UNCLASSIFIED RADC-TR-82-264 F19628-81-K-0010 F/G 11/2 NL

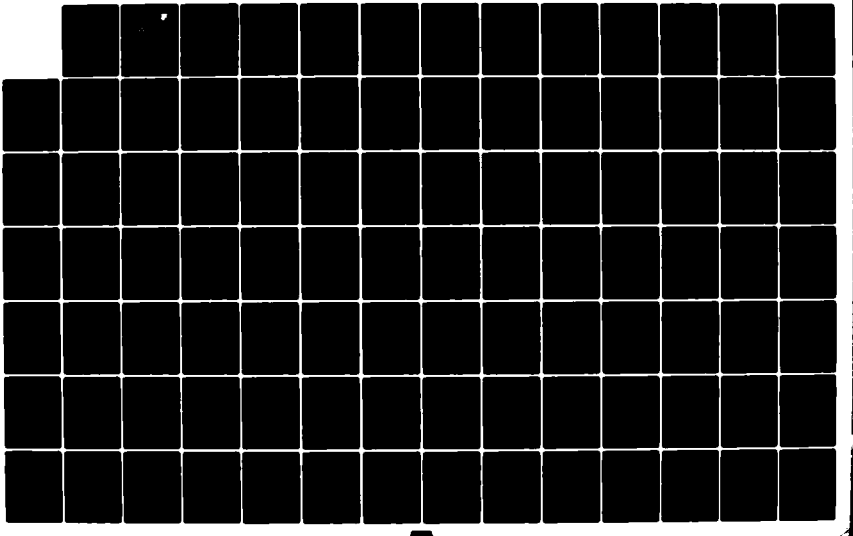

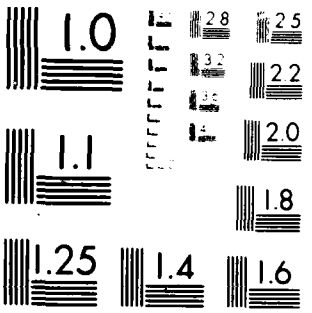

(15)

RADC-TR-82-264
Final Technical Report
October 1982

METALLIC HALIDE OPTICAL GLASSES: SYNTHESIS AND CHARACTERIZATION OF IR TRANSMITTING FLUORIDE GLASSES

The Catholic University of America

C. T. Moynihan
K. -H. Chung
D. L. Gavin
A. J. Bruce
E. O. Gbogi
M. Boulos

APPROVED FOR PUBLIC RELEASE; DISTRIBUTION UNLIMITED

ROME AIR DEVELOPMENT CENTER
Air Force Systems Command
Griffiss Air Force Base, NY 13441

This report has been reviewed by the RADC Public Affairs Office (PA) and is releasable to the National Technical Information Service (NTIS). At NTIS it will be releasable to the general public, including foreign nations.

RADC-TR-82-264 has been reviewed and is approved for publication.

APPROVED: 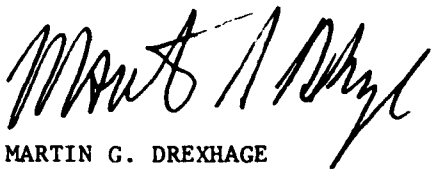

MARTIN G. DREXHAGE
Project Engineer

APPROVED: 

HAROLD ROTH, Director
Solid State Sciences Division

FOR THE COMMANDER: 

JOHN P. HUSS
Acting Chief, Plans Office

If your address has changed or if you wish to be removed from the RADC mailing list, or if the addressee is no longer employed by your organization, please notify RADC (ESM) Hanscom AFB MA 01731. This will assist us in maintaining a current mailing list.

Do not return copies of this report unless contractual obligations or notices on a specific document requires that it be returned.

UNCLASSIFIED

SECURITY CLASSIFICATION OF THIS PAGE (When Data Entered)

REPORT DOCUMENTATION PAGE

READ INSTRUCTIONS BEFORE COMPLETING FORM

1 REPORT NUMBER: RADC-TR-82-264	2 GOVT ACCESSION NO.: AD-A122 357
	3 RECIPIENT'S CATALOG NUMBER:
4 TITLE (and Subtitle): METALLIC HALIDE OPTICAL GLASSES: SYNTHESIS AND CHARACTERIZATION OF IR TRANSMITTING FLUORIDE GLASSES	5 TYPE OF REPORT & PERIOD COVERED: Final Technical Report 23 Jan 81 - 30 Sep 82
	6 PERFORMING ORG REPORT NUMBER: N/A
7 AUTHOR(s): C. T. Moynihan, A. J. Bruce, K. -H. Chung, E. O. Ebogi, D. L. Gavin, M. Boulos	8 CONTRACT OR GRANT NUMBER(s): F19628-81-K-0010
9 PERFORMING ORGANIZATION NAME AND ADDRESS: The Catholic University of America, Washington DC 20064	10 PROGRAM ELEMENT, PROJECT, TASK AREA & WORK UNIT NUMBERS: 62702F, 46001744
11 CONTROLLING OFFICE NAME AND ADDRESS: Rome Air Development Center (ESM), Hanscom AFB MA 01731	12 REPORT DATE: October 1982
	13 NUMBER OF PAGES: 208
14 MONITORING AGENCY NAME & ADDRESS (if different from Controlling Office): Same	15 SECURITY CLASS. (of this report): UNCLASSIFIED
	15a DECLASSIFICATION/DOWNGRADING SCHEDULE: N/A

16 DISTRIBUTION STATEMENT (of this Report)

Approved for public release; distribution unlimited.

17 DISTRIBUTION STATEMENT (of the abstract entered in Block 20, if different from Report)

Same

18 SUPPLEMENTARY NOTES

RADC Project Engineer: Dr. Martin G. Drexhage (ESM)

19 KEY WORDS (Continue on reverse side if necessary and identify by block number)

Fluoride Glass
Infrared Transmission
Glass Transition Temperature
Crystallization
Heat Capacity
Multiphonon Absorption
Reactive Atmosphere Melting

20 ABSTRACT (Continue on reverse side if necessary and identify by block number)

Heavy metal fluoride glasses, e.g., those based on ZrF_4, HfF_4 and BaF_2/ThF_4, were prepared by fusion of the fluorides at 800-1000°C. These glasses exhibit considerable promise as high transparency materials from the UV to the IR.

At the moment there are several problems with these glasses which are addressed in this report. One major problem is that the materials are not

DD FORM 1 JAN 73 1473 EDITION OF 1 NOV 65 IS OBSOLETE

UNCLASSIFIED

SECURITY CLASSIFICATION OF THIS PAGE (When Data Entered)

extremely good glass formers and tend to crystallize on cooling. In addition, absorptions due to -OH and metal oxyfluoride impurities are likely to be the substantial sources of extrinsic loss in the mid-IR.

Improvements in the glass forming abilities of the fluorozirconate and fluorohafnate glasses (as reflected by an increase in the difference between the glass transition and crystallization temperatures) could be achieved by adding CsF, PbF_2 or AlF_3 as additional components. The BaF_2/ThF_4 glasses could be improved by adding NaF, LiF or AlF_3 or by the substitution of LuF_3 for YbF_3.

On a per gram-atom basis the glass heat capacities $\bar{C}p$ at ambient temperature were all close to 5.2 cal/g-at.K and near the glass transition approached the Dulong-Petit limit of 3R. The values of $\Delta\bar{C}p$ at the glass transition were large compared to those for oxide glasses.

The IR spectra of the fluoride glasses showed peaks at 2.9 m and either 7 μm or 9 μm due respectively to -OH and metal oxyfluoride impurities. For glasses melted under reactive atmospheres and peaks at 2.9 m were found to be due almost entirely to surface -OH. It was generally found that melting in a closed reactor with CCl_4 atmosphere was best for removing -OH. A CCl_4 atmosphere was also found best for removing oxide impurities. Removal of -OH and oxide absorption by reactive atmosphere processing was generally easier and more complete for the BaF_2/ThF_4 glasses than for the ZrF_4 - or HfF_4 -based glasses.

For the fluorizirconate and fluorohafnate glasses the main contributors to multiphonon absorption on the IR edge at 7 μm were found to be ZrF_4 and HfF_4 respectively. Components such as BaF_2 , LaF_3 , ThF_4 and NaF had little effect on the IR edge absorption. The BaF_2 /ThF_4 glasses had IR edges at longer wavelenghts (9 μm) than glasses based on ZrF_4 or HfF_4 , due to the absence of these latter components. Addition of AlF_3 shifted the IR edge to shorter wavelengths for all the glasses.

TABLE OF CONTENTS

LIST OF APPENDICES

LIST OF FIGURES

LIST OF TABLES

CHAPTER I

INTRODUCTION

There are several potential uses for infrared optical glasses transparent in the frequency region beyond the IR edge of fused silica, say in the 2 to 10 μm wavelength range. BeF_2 and multicomponent systems based on BeF_2 (fluoroberyllates) show good glass formation capability. BeF_2-based glasses have the lowest refractive indices and the lowest optical dispersions of any inorganic glasses. However, there is only a small shift of the IR edge to longer wavelengths with respect to that of fused silica, and so there is little to be gained in terms of IR transparency with these glasses. Moreover, there are disadvantages associated with the high toxicity of Be (which complicates the processing of the glass) and the hygroscopicity of many of the compositions. Chalcogenide glasses possess a wide range of infrared transparency - to 12 μm and beyond with certain compositions - but again there are drawbacks, namely, toxicity, relatively poor mechanical characteristics, lack of transparency in the visible, and difficulties with the elimination of hydrogen impurities.

Recently synthesized heavy metal fluoride glasses, particularly those based on ZrF_4 and HfF_4, exhibit considerable promise as ultrahigh transparency materials for the mid-IR (2-5 μm). This makes them attractive for use as optical waveguides or laser windows and raises the prospect of achieving very long (>100 km), repeaterless fiber links for transoceanic or transcontinental communications. Fluorozirconate and

fluorohafnate glasses contain a large percentage (50 - 60 mol%) of ZrF_4 or HfH_4 as the primary constituent, along with lesser amounts of alkaline earth, rare earth or actinide fluorides as secondary components. Very recently, heavy metal fluoride compositions with even better IR transparency and reasonable glassforming ability which contain no ZrF_4 or HfF_4 have also been developed. At the moment, however, there are some substantial problems with heavy metal fluoride glasses. An absorption band at 2.9 μm due to hydroxyl (-OH) impurities is likely to be a substantial source of extrinsic loss in the mid-IR. In addition, oxide ion and the oxygen in bulk -OH will be bonded to the cations in the glass, and these metal oxyfluoride species can contribute to excess absorption on the IR absorption edge at about 7 μm. These glasses also have relatively close glass transition and crystallization temperatures, which indicates a tendency toward devitrification (crystallization) during slow cooling from the melt.

The goal of this study was to develop ways of synthesizing fluoride glasses which (a) eliminate undesirable IR absorption due to oxide and -OH and (b) minimize the tendency toward devitrification. These two aims are possibly not mutually exclusive. There is some evidence that oxide impurities which are poorly soluble in the melt or which result from attack of atmospheric water on the glass during forming and casting tend to form nucleation sites for crystal growth. From this work a greater understanding of the intrinsic (i.e., impurity free) IR edge absorption characteristics of these glasses should be obtained. This will in turn allow a determination of the true potential of these

glasses as ultrahigh transparency mid-IR optical materials.

Results reported here summarize much of the effort of an ongoing research program in these glasses which commenced at Catholic University of America in the fall of 1979 and moved to Rensselaer Polytechnic Institute in the fall of 1981. Some of the work was carried out in collaboration with colleagues at Rome Air Development Center (RADC), Hanscom Air Force Base, Massachusetts. In particular, some glass samples were prepared by M. G. Drexhage and O.H. El-Bayoumi at RADC.

CHAPTER II

PREVIOUS WORK ON HEAVY METAL FLUORIDE GLASSES

II. 1. Glass Forming Compositions

In contrast to oxides, glass formation in oxygen-free fluorides was until recently limited to materials based on BeF_2 or AlF_3 [1,2]. BeF_2 is the only fluoride which easily forms a glass by itself on cooling from the molten state [3]. The AlF_3 systems require other components for glass formation and must be rapidly quenched [2,4].

Glass formation in heavy metal fluoride systems was first reported by Poulain et al. for systems in which ZrF_4 was the main component [5]. The first glass of this type was obtained accidentally by Michel Poulain at the University of Rennes, France, on March 15, 1974 [6] while attempting to prepare a $2ZrF_4$-BaF_2-NaF-NdF_3 crystal with a large cation in the center of the hole in a $SmZrF_7$ structure. The preparation was carried out in a sealed Ni tube. Small pieces (3-4 mm) of glass, which Michel Poulain [6] initially thought might be single crystals, were obtained. However, x-ray diffraction showed an amorphous structure with only a few sharp peaks due to NdF_3 crystals in glass. A composition melted without NdF_3 did not show these peaks and gave a good glass. Poulain then explored the ternary NaF-BaF_2-ZrF_4 system for glass formation. Development of other glass-forming compositions followed.

These glasses, termed "fluorozirconate", contain large amounts (>50 mol %) of ZrF_4 [7] along with lesser amounts of alkaline earth, rare earth or actinide fluorides. Analogous fluorohafnate glasses can

be prepared by replacing ZrF_4 with HfF_4 [8]. In fluorozirconate type glasses (ternary systems including ZrF_4 or HfF_4), ZrF_4 (or HfF_4) has been called the glass-former, BaF_2, due to the size of Ba^{2+}, has been called a primary network modifier, and one or more other fluorides have been called secondary modifiers [7]. These last may include fluorides of the inner transition metals (e.g., ThF_4 or NdF_3), group III fluorides (e.g., LaF_3 or GaF_3), and alkalis fluorides (e.g. KF or CsF). The above terminology, which is derived from that for network oxide glasses such as silicates or borates, is not necessarily appropriate for these materials, since they are highly ionic and may have structures not at all analogous to the network oxide materials.

Fluorozirconate glasses tend to crystallize easily, and the regions of glass formation in the different systems are usually quite small, although it is usually possible to enlarge the glass formation region by adding further components to the melt. The limits of the vitreous areas for several ZrF_4-based ternary systems reported in the literature [7,9,10] are shown in Fig. 1. Tables III-IV show some representative ZrF_4 (or HfF_4) containing glass compositions which have been synthesized. Some glass - forming binary compositions do exist, but these require rapid quenching and are hence more difficult to prepare than the ternary compositions [11-13].

Glass formation has also been reported in a variety of heavy metal fluoride systems which do not contain ZrF_4 or HfF_4 [14-18]. Many of these compositions, however, require rapid quenching (e.g., pressing a melt between metal plates), to yield even thin ($\sim$1.0 mm) plates of glass.

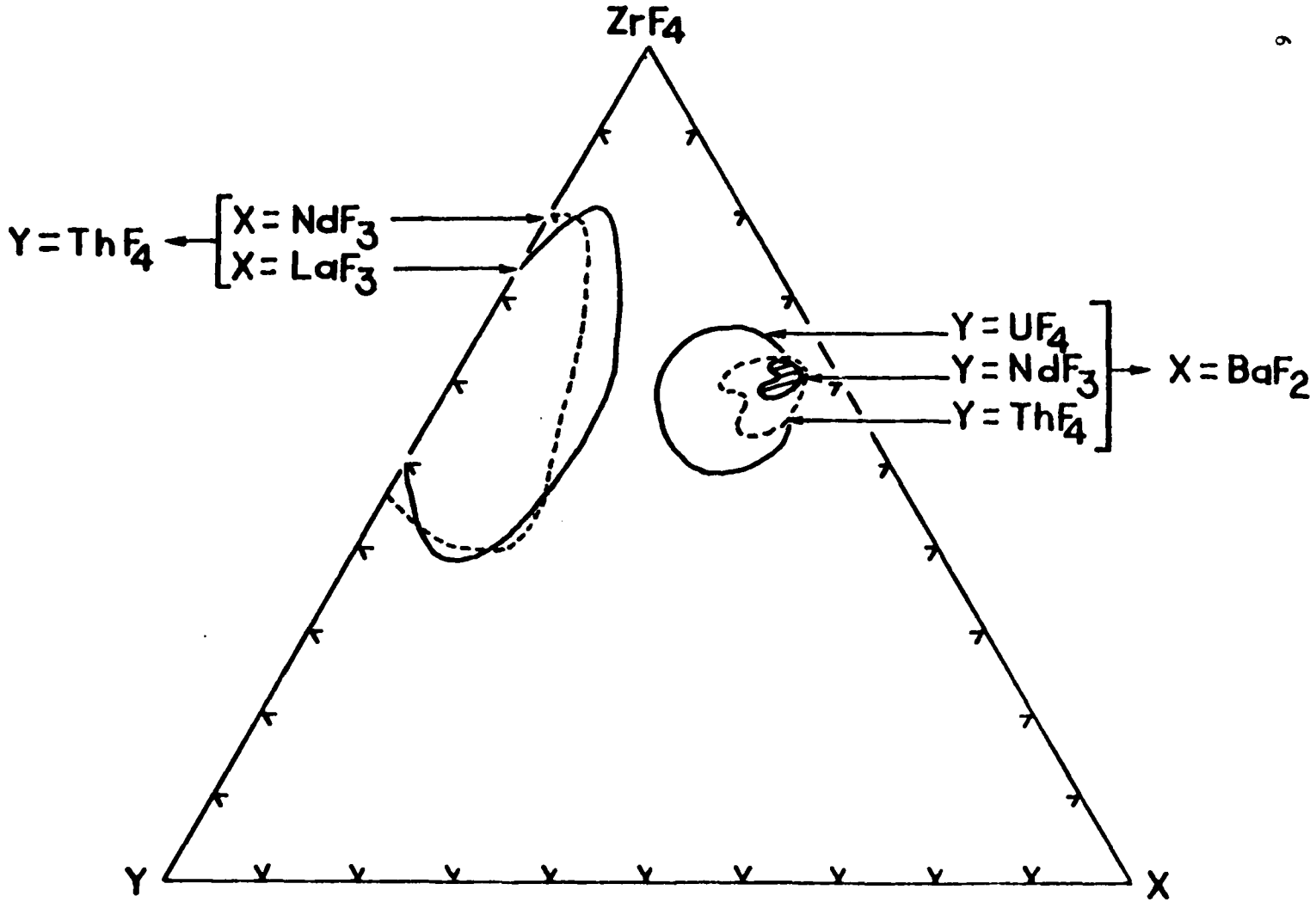

FIG. 1

However, some compositions containing BaF_2 and ThF_4 in conjunction with ZnF_2, YF_3, YbF_3, LuF_3 or AlF_3 [17,18] yield glasses whose quality and size are comparable to that of the ZrF_4- and HfF_4-based glasses. Some of these non-fluorozirconate multicomponent glass compositions are listed in Tables V and VI.

In summary, four main types of heavy metal fluoride glasses have been prepared to date: (1) Fluorozirconate or fluorohafnate glasses;

ZrF_4 or HfF_4 (50-60 mol%) - BaF_2 (~30 mol%) - other fluorides (e.g., LaF_3, NdF_3, ThF_4, UF_4)

(2) Thorium fluoride-based glasses:

$ThF_4 - BaF_2 - MF_2$ (M = Mn, Zn)

$ThF_4 - BaF_2 - LnF_3$ (Ln = Tm, Yb, Y, Lu)

(3) Rare earth fluoride-based glasses:

$LnF_3 - ZnF_2 - BaF_2$ (Ln = Any Rare Earth)

$LnF_3 - MnF_2 - BaF_2$ (Ln = Dy, Ho, Er, Tm, Yb, Y, Lu)

(4) Transition metal fluoride glasses:

$PbF_2 - XF_2 - YF_3$ (X = Mn, Zn, Fe, Co, Ni, Cu, Y = V, Cr, Ga)

As noted above, additional fluoride components can be incorporated in small to moderate amounts in these glasses.

II. 2. Criteria for Glass Formation

There are several explanations for glass formation in oxide systems which would be applied to heavy metal fluoride glasses. These are based on network structure (Zachariasen), packing (Poulain), bond strength (Sun), and nucleation and crystal growth kinetics.

II. 2.1 Network Formation à la Zachariasen

The classical silicate, germanate and phosphate glasses have been extensively studied and their network structure based on tetrahedral units (e.g., SiO_4) has been clearly established. The basic structural units of $ZnCl_2$, BeF_2 and GeS_2 glasses are also tetrahedral. In pure B_2O_3 the basic network structural units are triangular BO_3 groups; however, in alkali borates both triangular BO_3 and tetrahedral BO_4 structural units exist.

In crystalline ZrF_4 each Zr atom is located at the center of square archimedian antiprism, thus being surrounded by 8 F atoms. Each F atoms is coordinated by 2 Zr atoms. The antiprisms are joined together by sharing all eight corners, thus forming a three-dimensional array. The eight-fold coordination of the Zr^{4+} ion is justified in part by the large anion/cation radius ratio in ZrF_4 (0.57 for Zr/F vs. 0.22 for Be/F). According to Zachariasen's criteria [19] for glass formation, the coordination number of (oxygen or fluoride ions) about the central cation must be small (4 or less) for a compound to be favored as a glass-former. While this rule is apparently applicable for fluoroberyllates, it is no longer valid for the fluorozirconates if the short-range order of ZrF_4 is assumed to be similar in the crystalline and vitreous states. Given the

large ionic radius ratio, the basic molecular structure unit should be at least an octahedron [7]. Thus, fluorozirconate glasses represent an entirely new class of materials, which accounts for a general lack of understanding of their structure. Crystals having general formulas $MZrF_6$ and $LnZrF_7$ (where M is a divalent metal and Ln is a rare earth) have the Zr atoms in octahedral coordination with fluorine. Seven and eight coordinated Zr atoms also occur in crystalline fluorozirconates and may be present in non-stoichiometric compounds such as $(M, Zr)F_{3+x}$ [20].

Poulain et al. [21] suggested that the Zr and Th atoms in the ZrF_4-BaF_2-ThF_4 glass system also form a common network of polyhedra with coordination numbers varying from 6 to 8, joined together by sharing corners (ThF_4 is isomorphic with ZrF_4). The network is broken down by the modifying Ba^{2+} ions.

A structural model of ZrF_4-ThF_4-LnF_3 glasses (where Ln = La,Nd) was proposed by Matecki et al. [11] based upon physical property behavior. The authors considered ThF_4 and LnF_3 to act as network stabilizers (similar to the role of intermediates in oxide glasses). This hypothesis was supported by the increase in Tg, liquidus temperature and chemical durability and the decrease in the thermal expansion coefficient of these glasses when compared with BaF_2-containing systems. The stabilizing role played by LnF_3 and ThF_4 was explained by the significant size of the Ln^{3+} and Th^{4+} ions which may be surrounded by 9, 10 or 11 F^- ions, thus lowering the coordination number of the Zr atoms and thereby reducing the number of F-F pairs in close proximity.

Almeida and Mackenzie [22] have proposed structures for binary

ZrF_4-BaF_2 glasses based upon IR and Raman spectra. The authors proposed three different model glasses: metazirconate, dizirconate and trizirconate. They suggested that barium dizirconate metal glass $2ZrF_4 \cdot BaF_2$ contains infinite chains of ZrF_6 octahedra sharing two corners each, plus a smaller amount of octahedral rings, mostly 8- and 9- membered. These chains and rings are cross-linked by Ba-F ionic bonds. The proposed barium metazirconate model glass $ZrF_4 \cdot BaF_2$ contains 7-coordinated Zr atoms, either in the form of $Zr_2F_{12}^{4-}$ dimeric anions (as in crystalline α-$BaZrF_6$) or else in a chain structure similar to the dizirconate, but made up of pentagonal bipyramids. The proposed barium trizirconate model glass $3ZrF_4 \cdot BaF_2$ has a more two-dimensional structure when compared with the dizirconate model glass such that, for example, double and triple chains of octahedra are now likely to occur and may even form sheetlike units with extensive bridging. A certain amount of five-coordinated fluorozirconate units are also likely to occur, as well as some isolated ZrF_6^{2-} octahedra ions.

II. 2.2. Poulain's Model

Poulain [23] has proposed structural and energetic conditions for glass formation in ionic systems and for ZrF_4-based glasses in particular. His proposals are based on the concept of order/disorder in non-stoichiometric compounds, and he addresses the problem of glass formation in terms of the stabilization factors for the non-periodic packing of the anions and cations in the fluoride glasses. Such non-periodic packing can occur for the anions in the fluoride rich phases $(Ln,Zr)F_{3+x}$ and for

the network cations due to the presence of larger Ba^{2+} ions in the ZrF_4-BaF_2-LnF_3 glasses. The mobilities of highly charged cations in ionic glasses will be low, and the formation of non-periodic structures will permit the cations to be inserted into the anionic network in several different ways.

The cations exhibiting a high field strength F (= Z/r, where Z and r are ionic charge and radius respectively) appear as potential glass formers, since they induce a strong ionic interaction and large anion/cation ratio, which increases the number of potentially available sites. Table I shows the calculated field strengths for various cations commonly incorporated into halide glasses. Poulain has suggested the criterion, $10 > {}^{F}c/F_A > 2.5$, for glass formation in ionic systems, where F_c and F_A are cationic and anionic field strength respectively.

II. 2.3 Sun's Bond Strength Model

Sun's bond strength approach [24], for interpreting the glass-forming, intermediate and modifying character of oxide glass constituents, has been applied to fluoride glasses by Baldwin and Mackenzie [25]. According to this theory, the single bond strength of a fluoride MFn is defined as the dissociation energy per mole of the cation (E_d) divided by its coordination number. E_d is given by:

$$E_d = \Delta H_f^o (MFn,c) - \Delta H_f^o (M,g) - n\Delta H_f^o (F,g) \qquad (II.1)$$

where ΔH_f^o is the enthalphy of formation and "c" and "g" refer to

Table I. Glass Forming Ability Of Various Cations With Respect To Anionic And Cationic Field Strength (Ref. 23).

Cation	Anion	F_A*	F_C*	F_C/F_A	Glass progenitor
Al^{3+}	F	0.78	5.6	7.2	Yes
Be^{2+}	F	0.78	7.4	9.5	Yes
Zr^{4+}	F	0.78	5	6.4	Yes
Hf^{4+}	F	0.78	5.2	6.7	Yes
Ga^{3+}	F	0.78	4.8	6.1	Yes
Fe^{3+}	F	0.78	4.7	6.0	Yes
Cr^{3+}	F	0.78	4.9	6.3	Yes
Th^{4+}	F	0.78	3.8	4.9	Yes
Y^{3+}	F	0.78	3.1	4.0	Yes
Zn^{2+}	F	0.78	2.8	3.6	Yes
Si^{4+}	F	0.78	15.4	19.7	No
Mo^{6+}	F	0.78	14.6	18.7	No
Ca^{2+}	F	0.78	1.78	2.3	No
Na^{+}	F	0.78	0.85	1.1	No
Zn^{2+}	Cl	0.55	3.33	6.0	Yes
Bi^{3+}	Cl	0.55	2.91	5.3	Yes

crystalline and gaseous states respectively. The assumption of this approach is that the more strongly bonded constituent cations in a glass melt are less likely to have their bonds ruptured and thus will be less likely to undergo reordering, which is a prerequisite for crystallization. Hence glass formation will be favored. Sun [24] defined three classes of cationic species, namely strongly bonded glass-formers which form the glassy network, less strongly bonded intermediates, and weakly bonded modifiers. Intermediates are not able to form glasses by themselves, but are able to be incorporated into a continuous glass network. Modifiers, on the other hand, break up or depolymerize the glass-forming network. Calculated values of the single bond strength for individual fluorides are shown in Table II.

II. 2.4. Kinetic Models

The basic idea behind the kinetic model is that liquids form glasses because they failed to crystallize on cooling. This means that the structural rearrangements necessary for crystal nucleation and/or growth are too slow to occur to an appreciable extent on the time scale dictated by the cooling rate. The ease of such structural rearrangements will be inversely proportional to the viscosity of the liquid. At sufficiently low temperature, near and below the glass transition region, the viscosity becomes sufficiently high that crystallization can not occur on perceptible time scales. The problem of glass formation is thus a question of whether the viscosity is sufficiently high to forestall crystallization while the melt is being cooled to the high viscosity

Table II. Relationship Of Glass Formation To Dissociation Energy For Fluorides (From Ref. 25).

M in MF_n	Valence	Dissociation energy per MF_n (kcal/mol)	Coordination number	Single bond strength (kcal/mol)
Glass formers				
Ti	4	585	6	98
Sc	3	539	6	90
Be	2	537	4	89
Hf	4	688	8	86
Zr	4	681	8	85
Al	3	496	6	83
Intermediates				
Cr	3	431	6	72
Y	3	570	8	71
B	3	275	4	69
Fe	3	408	6	68
Nd	3	537	8	67
Pb	4	350	6	58
Sb	3	340	6	57
Mg	2	339	6	57
Modifiers				
Si	4	319	6	53
Co	2	304	6	51
Ga	3	403	8	50
Ni	2	297	6	50
Mn	2	296	6	49
Ca	2	371	8	46
Sr	2	369	8	46
Ba	2	368	8	46
Zn	2	253	6	42
Cu	2	250	6	42
Bi	3	324	8	41
Cr	2	320	8	40
Li	1	203	6	34
Pb	2	245	8	31
Na	1	182	6	30
K	1	176	6	29
Cd	2	233	8	29
Ag	1	167	6	28
Cs	1	166	6	28
Tl	1	141	6	24
Hg	2	178	8	22

region. Therefore the best glass-forming systems (i.e., those that will form glasses under the slowest cooling rates) will be those that have high viscosities at their liquidus temperatures and whose viscosities increase rapidly at temperatures below the liquidus temperature. Heavy metal fluoride melts have low viscosities in their liquidus range [26,27] and are therefore inherently poor glass-formers. This is why it is necessary to use relatively rapid quenching rates in order to produce glasses from these melts.

In general the best glass-forming melts appear to be those with low liquidus temperatures, i.e., those with compositions in the eutectic regions of the phase diagrams for the components of each system. This is because the lower the liquidus temperature, the higher the viscosity of the melt at the liquidus and the shorter the temperature interval between the liquidus region and the high viscosity region near the glass transition. Heavy metal fluoride glasses appear to conform to this general pattern, since the low liquidus temperature regions calculated for ZrF_4-BaF_2-LaF_3 and ZrF_4-BaF_2-NaF systems by Kaufman et al. [28] are in excellent agreement with the glass-forming compositions reported in these systems by Poulain and his coworkers [9, 29].

II. 3. Glass Preparation

BeF_2, like SiO_2, easily forms a glass on cooling from the molten state [3,30]. Molten BeF_2 is highly viscous at the liquidus temperature (cf. II. 4.3 of this Thesis). The addition of modifying fluorides to BeF_2 substantially decreases the viscosity, crystallization is favored,

and glasses can no longer form when the amounts of modifying fluorides become large.

Heavy metal fluoride melts, like BeF_2, react with atmospheric water and with many crucible materials. Two approaches have been taken to the problem of melting and forming heavy metal fluoride glasses. The first involves direct fusion of the anhydrous fluorides in dry inert atmosphere at $700 \sim 1000^{\circ}C$ [7,21]. Suitable crucible materials include vitreous carbon, platinum, gold and nickel. To obtain high quality glass by this method it is of the utmost importance to avoid oxide and OH^- contamination of the raw materials during mixing and melting. These impurities lead to undesirable mid-IR absorptions and can enhance devitrification [10]. For fluoride melts, OH^- contamination readily occurs through hydrolysis [31]:

$$F^-(\ell) + H_2O(g) \rightleftarrows OH^-(\ell) + HF(g) \qquad \text{(II.2)}$$

where "ℓ" (for "liquid") refers to the melt. To eliminate the oxide and OH^- contamination Robinson et al. [32] have suggested melting such glasses under a CCl_4 atmosphere. Carbon tetrachloride reacts with water and oxide species in the melt:

$$CCl_4(g) + 2OH^-(\ell) \rightleftarrows CO_2(g) + 2HCl(g) + 2Cl^-(\ell) \qquad \text{(II.3)}$$

$$CCl_4(g) + 2H_2O(\ell) \rightleftarrows CO_2(g) + 4HCl(g) \qquad \text{(II.4)}$$

Moreover, CCl_4 pyrolytically cracks at temperatures above 400°C to give nascent chlorine, which compensates any fluoride deficiency in the melt [32]. To achieve the purity required in fiber optic and other applications, direct fusion of fluorides in a reactive atmosphere may be the best approach [10], as it introduces no intermediate steps into the glass preparation process. Moreover, technology for production of crystalline fluorides with exceptional purity is well developed as a result of research into high power laser window materials [33].

A second method of preparation [7,8,21] may preferentially be used when all or some of the starting materials are in the form of oxides. Since pure fluorides can present problems in handling due to their hygroscopic nature, oxides have generally been used as raw materials for preparing fluorozirconate glasses. These oxides are converted to fluorides through heating in the presence of ammonium bifluoride ($NH_4F \cdot HF$). The fluorination reaction may occur in two steps [7], namely formation of an ammonium fluorometallic complex (e.g., $(NH_4)_3ZrF_7$) at 150 ∿ 300°C, followed by decomposition to the metallic fluoride (e.g., ZrF_4) upon heating to about 400°C:

$$2ZrO_2(s) + 7NH_4F \cdot HF(s) \rightleftharpoons 2(NH_4)_3ZrF_7(s) + NH_3(g) + 4H_2O(g) \quad \text{(II.5)}$$

$$(NH_4)_3ZrF_7(s) \rightleftharpoons ZrF_4(s) + 3NH_4F(g) \quad \text{(II.6)}$$

Excess ammonium bifluoride is generally required to drive these reactions

to completion.

The melts are cast into glass pieces by pouring them into a mold either at room temperature or preheated mold to about 300°C. In cases where the melt devitrifies during this casting procedure, an attempt can be made to form very thin glass sheets by rapid quenching; a small amount of melt is poured onto a brass plate and a second plate quickly placed on top. Melting temperatures of non-fluorozirconate glasses (e.g., BaF_2-ZnF_2-YbF_3-ThF_4) are higher than for the fluorozirconate glasses. Rapid quenching is sometimes required to prevent devitrification, although reasonably thick samples of some multi-component glasses have been made.

II. 4. Properties

II. 4.1. Glass Transition and Crystallization Temperatures

Fig. 2 shows a typical DSC trace during heating of a HfF_4-based glass at 10K/min. Values for glass transition temperature Tg are generally taken as the extrapolated onset of the heat capacity change, as shown in Fig. 2. The glass transition temperature, Tg, marks the temperature region in which the glass begins to exhibit liquid-like properties and corresponds to a shear viscosity of 10^{12}-10^{13} poise (10^{11}-10^{12} Pa·S) [34]. The crystallization temperature is the temperature of onset of the crystallization exotherm during heating. The crystallization temperature presumably marks the temperature at which the viscosity of the melt becomes low enough that the crystal growth can proceed at a substantial rate. There are two operationally significant definitions of the crystallization temperature which have been employed in the past: the extrapolated onset of the crystallization peak (Tx in Fig. 2) and

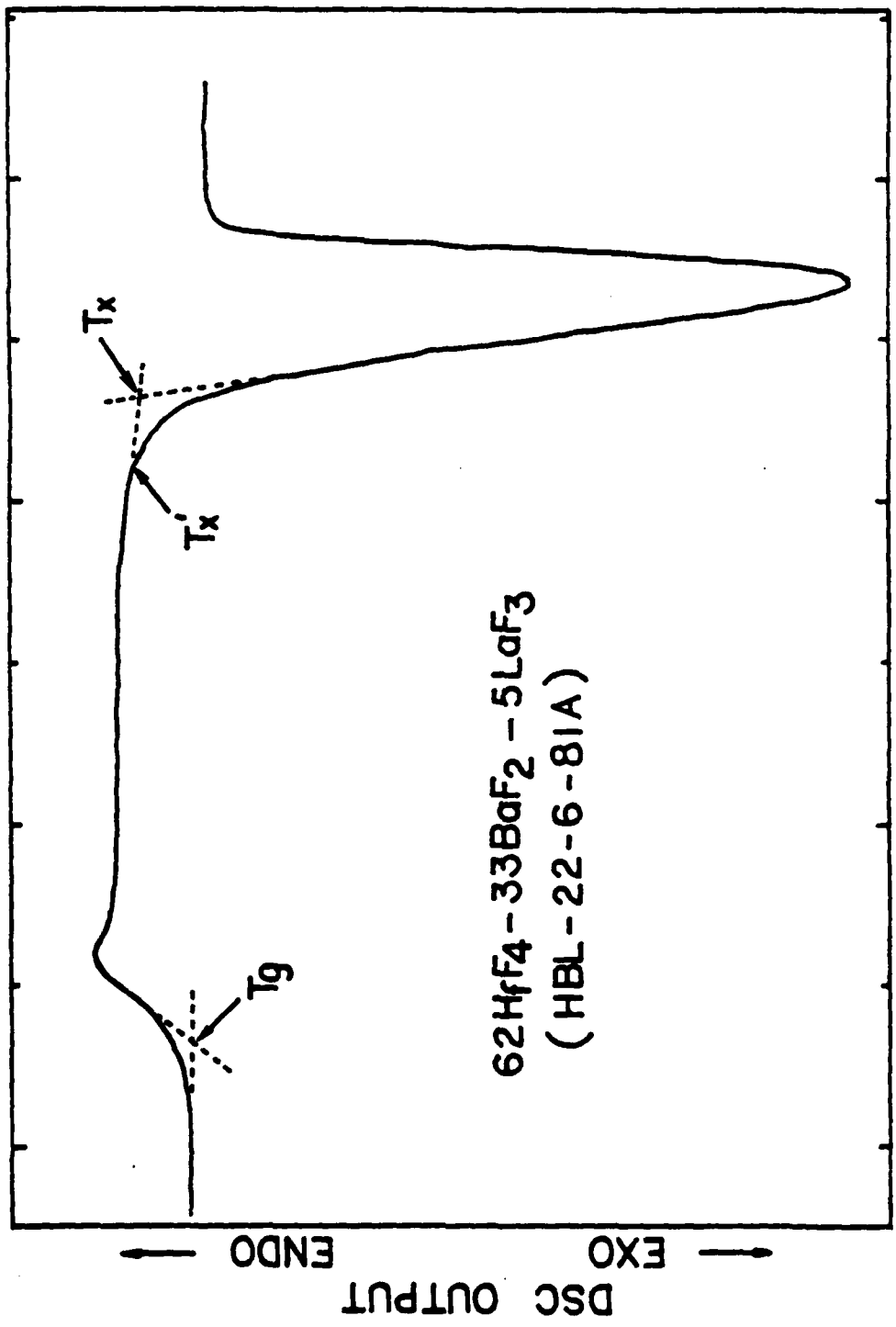
DSC OUTPUT
ENDO
EXO
300
340
380
420
T [°C]
62HfF4 - 33BaF2 - 5LaF3
(HBL - 22 - 6 - 81A)
Tg
Tx'
Tx

FIG. 2

the temperature at which the onset of crystallization is most perceptible on the DSC trace (Tx' in Fig. 2). Crystallization kinetics are complicated for multicomponent systems and depend on the viscosity, the presence of heterogeneous nuclei, and the thermodynamics of formation of the crystalline phase [1].

The glass transition temperatures of relatively stable multicomponent fluoroberyllate glasses are typically in the range of 160 to 280°C [30]. Values of Tg and Tx for a number of heavy metal fluoride glasses reported previously are shown in Tables III-VI. The compositions are given in mole percent metal fluoride. For ZrF_4-/HfF_4-based glasses the glass transition temperature is generally in the range 280-320°C, while the crystallization temperature is in the range 380-430°C. The Tg and Tx values of HfF_4-based glasses are a little higher than those of the corresponding ZrF_4-based glasses. Addition of an alkali fluoride decreases both Tg and Tx, while compositions without modifying compounds (e.g., BaF_2) show higher Tg and Tx values. Some non-fluorozirconate (BaF_2/ThF_4-based) multicomponent glasses have higher Tg's and Tx's than fluorozirconate glasses.

The heating rates used in studies by different groups are often not the same (usually between 2 and 50°C min^{-1}). Since both Tg and Tx depend on the heating rate used, comparison between the results of different authors is difficult. The relative proximity of the glass transition and crystallization temperatures (~80°C) in these glasses manifests the tendency for devitrification during slow cooling from the melt.

Table III (a). Compositions and Properties of Some ZrF_4-Based Glasses.

Compositions in mol%.

ZrF_4	BaF_2	ThF_4	NaF	AlF_3	GdF_3	NdF_3	SrF_2	CaF_2	Tg (°C)	Tx (°C)	d (g/cm^3)	n_D	ref.
67							33		290	340	-	--	12
63	33				4				310	390	-	1.529	37-39
60	35							5	320	-	4.5	1.51	29
60	34					6			320	380	4.56	1.5257	7,11,29
60	33	7							295	390	4.80	1.53	10,11, 31,32
60	32			4				4	297	366	4.45	1.516	36
60	28			4		8			306	366	4.51	1.519	36
52	24		20	4					247	325	4.28	1.494	36
50	25		25						240	300	4.5	1.50	7,29,35
50	20		25			5			-	-	4.5	1.56	5
50	20	7.5	22.5						270	320	4.52	1.504	7,29, 35,40

Table III (b). Compositions and Properties of Some ZrF_4-Based Glasses.

Compositions in mol%.													
ZrF_4	BaF_2	LaF_3	ThF_4	AlF_3	NdF_3	YF_3	EuF_3	$BaCl_2$	Tg (°C)	Tx (°C)	d (g/cm^3)	n_D	ref.
64	36								300	352	4.662	1.522	12,37
61.5	29.4		7				2.6		312	397	—	1.531	45
60.5	33.8	5.7							294	380	4.79	1.523	9,26
60	26		10	4					311	407	4.73	1.522	36
60	25	7	8						320	—	—	—	40
60		7	33						440	—	—	—	35,40
60		10	30						450	540	—	—	11
60		33			7				—	—	5.25	1.5473	11
57	36	3		4					310	390	4.61	1.524	41-43
55	20							25	246	271	4.405	—	12
54	35			4		7			313	380	4.52	1.510	36,44

Table IV. Compositions and Properties of Some ZrF_4-and/or HfF_4-Based Glasses.

Compositions in mol %.

ZrF_4	HfF_4	BaF_2	LaF_3	ThF_4	AlF_3	CsF	LiF	PbF_2	Tg (°C)	Tx (°C)	d (g/cm^3)	n_D	ref.
66.6		21.9	6.1		1.9		3.5		228	—	4.35	1.509	9,26
58		25	7				10		273	—	4.49	1.521	9
29	29	33		9					321	411	5.49	—	8,10
	70	25.7	4.3						312	395	5.78	1.514	10,26
	62	23	5			10			306	391	—	—	10
	62	15	5					18	292	362	—	—	10
	62	15	5		2	6		10	309	427	6.08	1.523	10,26,42
	60	33		7					320	430	6.2	—	8,10,31
	58	33	9						332	415	5.56	—	10,26
	57.5	25.3		8.75				8.44	331	—	6.3	1.524	46
	57	36	3		4				312	400	5.88	1.504	26,41,42

Table V. Compositions and Properties of Some Nonfluorozirconate (BaF_2/ThF_4-Based) Glasses.

Compositions in mol %.

BaF_2	ThF_4	ZnF_2	YbF_3	YF_3	LuF_3	AlF_3	CaF_2	MnF_2	Tg (°C)	Tx (°C)	d (g/cm^3)	n_D	ref.
20	40		40						436	482	6.75	—	14,17
20	20		30			30			462	591	5.74	1.486	48
20	26.7	26.7	26.7						350	423	6.41	—	17
22				16		40	22		430	535	4.0	1.44	47
20	20			30		30			450	541	4.98	1.488	48
20	22.4			28.8		28.8			446	554	5.10	1.489	18,26,41
10	55			35					423	467	6.08	—	17
20	20				30	30			469	598	5.77	1.485	48
20					30			50	316	339	5.55	—	49
20	20	40				20			347	460	5.29	1.496	50
10	50							40	326	395	5.75	—	15,49

Table VI. Compositions and Properties of Some Nonfluorozirconate (PbF_2-Containing) Glasses.

Compositions in mol%.

PbF_2	AlF_3	GaF_3	CaF_2	MF	CrF_3	MnF_2	FeF_3	CuF_2	Tg (°C)	Tx (°C)	d (g/cm^3)	n_D	ref.
50	50								255	278	—	—	4,37,51
50		50							285	329	—	—	52
50					25	25			261	310	5.9	1.663	52
50						25	25		238	283	—	—	52
33							33	33	239	293	5.65	1.593	52
25				30(K)			45		265	312	—	—	53
25				30(Na)	45				330	382	—	—	53
25		45		30(Li)					225	283	—	—	53
		45	25	30(Na)					312	373	—	—	53
		40	43					17	344	400	—	—	52

II. 4.2 Density

The density of BeF_2 glass is 1.98 g/cm^3 [30] and increases with addition of alkali or alkaline earth fluoride modifiers. Since the heavy metal fluoride glasses prepared so far contain cations of large mass numbers, their density is quite high (of the order of 2-3 times that of BeF_2 glass). Generally the densities of ZrF_4-based glasses are 4.5-5.0 g/cm^3 while those of HfF_4-based glasses are 5.5-6.0 g/cm^3. The densities for a number of typical compositions are shown in Tables III-VI.

II. 4.3 Viscosity

Molten BeF_2 is highly viscous with a viscosity of about 10^6 P near its liquidus temperature (550°C). The addition of modifying fluorides substantially decreases the viscosity [30].

Data from the work of Drexhage et al. [26, 42] indicates that viscosity values obtained with a rotational viscometer for a ZrF_4-BaF_2-LaF_3-AlF_3(ZBLA) glass are ~0.4 P at 670°C and ~4 P at 490°C. HfF_4-BaF_2-LaF_3-AlF_3 glass has a higher viscosity than the corresponding ZrF_4-based glass below the liquidus temperature. Also it was shown that viscosity decreases steeply above Tg in the viscosity-temperature profile.

Hu and Mackenzie [27] reported that the viscosity (at 540°C) and activation energy for $60ZrF_4$-$30BaF_2$-$10LaF_3$ glass are 3 P, and 25 kcal/mol respectively.

II. 4.4 Chemical Stability

Vitreous BeF_2 rapidly reacts with atmospheric water resulting clouding of the surface on exposure to air [3,30]. Beryllium fluoride is soluble in aqueous solutions especially at low pH, but appears to be insoluble in organic liquids such as benzene or toluene [30]. Additions of network intermediate fluorides such as AlF_3 or MgF_2 greatly enhance the chemical durability [2].

Only limited studies of chemical durabilities have been performed for heavy metal fluoride glasses. The ZrF_4-based glasses such as ZrF_4-BaF_2-ThF_4 and ZrF_4-BaF_2-NaF have been found to be stable with respect to fluorinating agents such as F_2, HF, ClF_3 and UF_6 [7,21]. The reason is that all the cations present in the glass are already in their highest possible oxidation state and can not be further oxidized by fluorine [7, 21]. ZrF_4-BaF_2-ThF_4 glasses are slightly attacked on the surface after several hours in water at 20°C or after exposure to 100% relative humidity [5,21,31]. However, they are stable in air at 350°C. HfF_4-BaF_2-ThF_4 glasses also appear to be slowly attacked by water [31]. The rate of dissolution of $57ZrF_4$-$34BaF_2$-$9ThF_4$ glass in boiling water has been determined as 4.7×10^{-5} g $cm^{-2}m^{-1}$ [30]. ThF_4-AlF_3-LnF_3-BaF_2 glasses (where Ln = rare earths or yttrium) have been found to show no change in weight or signs of attack even after several hours exposure to gaseous F_2 or to boiling aqueous HF [48]. These glasses are fairly resistant to attack by water. However, it is found that this resistance is lowered by the addition of NaF to the batch [48].

II. 4.5 Radiation Hardness

In comparison with silicate glasses fluorohafnate and fluorozirconate glasses seem to be much less sensitive to γ-irradiation. It has been reported that there is no incremental optical transmission loss in the 2.5-4 μm region for a fluorozirconate glass irradiated with 45 Mrad of γ-rays [54], and tests at RADC have indicated no observable changes of 2-6 μm transmission within experimental error in several fluoride glasses irradiated to 10^6 rads with a ^{60}Co source [13]. These tests were carried out on bulk specimens a few mm thick, so that small radiation induced optical losses which would cause marked attenuation in optical fibers have not been assessed. Nonetheless these glasses show particular promise in applications involving harsh nuclear environments or low bit rate military communication systems.

II. 4.6 Thermal Properties

The thermal expansion coefficient α of vitreous BeF_2 has been found to be 68 x 10^{-7} $^oC^{-1}$ and most fluoroberyllates have thermal expansion coefficients ranging from 100 to 250 x 10^{-7} $^oC^{-1}$ [30]. Thermal expansion coefficients for fluorozirconate, fluorohafnate [26,31,32,37,38, 41,42] and non-fluorozirconate (e.g., BaF_2-ZnF_2-YF_3-ThF_4 or PbF_2-AlF_3) glasses [4,18,26,47,50] have been reported in the range 150 x 10^{-7} - 200 x 10^{-7} $^oC^{-1}$. Hence the α values for heavy metal fluoride glasses are high compared to those for typical silicate glasses (e.g., soda-lime silicate, α = 92 x 10^{-7} $^oC^{-1}$).

The heat of crystallization of a ThF_4-YF_3-AlF_3-BaF_2 [18] glass

has been found to be 70-80 J/g while for PbF_2 containing glasses [4,52,53] values are in the range 20-70 J/g. Only two heat capacity values of heavy metal fluoride glasses have been reported, for $60ZrF_4$-$33BaF_2$-$7ThF_4$ (C_p = 0.51 $J\,g^{-1}\,{}^oC^{-1}$ at 45°C) [31,32] and for $60HfF_4$-$33BaF_2$-$7ThF_4$ (C_p = 0.43 $J\,g^{-1}\,{}^oC^{-1}$ at 45°C) [32]. A Debye temperature θ_D of 300K has been reported for $58ZrF_4$-$34BaF_2$-$8ThF_4$ [55] glass and was calculated from observed ultrasonic velocities using:

$$\theta_D = \frac{h}{k}\left(\frac{3N}{4\pi}\right)^{1/3} Cm \qquad (II.7)$$

where Cm is the mean sound velocity, N is the number of atoms per unit volume, and h and k are the Planck and Boltzmann constants respectively.

So far no thermal conductivities have been reported for heavy metal fluoride glasses.

II. 4.7 Electrical Properties

Vitreous BeF_2 is a good insulator whose electrical conduction mechanism appears to derive from fluoride ion transport; the conductivity is very sensitive to hydroxyl impurities [56,57]. The activation energy for conduction of water-free BeF_2 is 36.7 $kcal\cdot mol^{-1}$, as compared to 25 $kcal\cdot mol^{-1}$ for hydroxyl containing BeF_2 [56,57]. Simple binary alkali fluoroberyllate glasses exhibit unusual conduction behavior; small additions of alkali modifiers to BeF_2 decrease the electrical conductivity by several orders of magnitude, and this compositional behavior is reversed with further alkali fluoride additives [60]. This conductivity

anomaly has been explained as a consequence of two competing fluoride transport mechanisms. At low alkali concentrations, the conductivity is controlled by fluoride ions in anti-Frenkel defect sites, whereas at high alkali-concentrations non-bridging fluoride ions are the primary current carrying species.

Leroy and Ravaine [61] have reported that ZrF_4-based glasses are fluoride ion conductors. These glasses exhibited ionic conductivities which obey an Arrhenius law ($\sigma = \sigma_o \exp(-E/kT)$) in the temperature range 100 ~ 250°C, where σ is the electrical conductivity, σ_o a pre-exponential constant, and E the activation energy for conduction [35,61,62]. For the fluorozirconate glasses, conductivities are $\sim 10^{-5} - 10^{-6}\ \Omega^{-1}cm^{-1}$ and activation energies are ~16-20 kcal mol^{-1} at 200-250°C [12,40,61,62]. The substitution of Ba by Na in the ZrF_4-BaF_2-ThF_4 system decreases the conductivity [35,62], however contradictory trends in the associated activation energy have been found [35,62].

II. 4.3 Mechanical Properties

Vickers hardness and Young's modulus of BeF_2 glass are 200 kg/mm^2 and 5.92×10^4 MPa, as compared to 540-580 kg/mm^2 and 6.9×10^4 MPa for soda-lime glass [3,63]. The mechanical properties of some selected heavy metal fluoride glasses along with some comparison glasses are given in Table VII. From Table VII it appears that the mechanical properties of heavy metal fluoride glasses are comparable to those of chalcogenide glasses (i.e., smaller hardness and elastic moduli) and inferior to those of silicates. However, it is important to note that the compositions

Table VII. Mechanical Properties of Some Heavy Metal Fluoride, Silicate and Chalcogenide Glasses.

	Hardness, kg/mm^2	Elastic Modulus, MPa x 10^4	Bulk Modulus, MPa x 10^4	Shear Modulus, MPa x 10^4	Poisson's ratio	Fracture Strength MPa	Stress Corrosion Susceptibility	Ref.
$60ZrF_4$-$33BaF_2$-$7ThF_4$	250					62		31
$58ZrF_4$-$34BaF_2$-$8ThF_4$		5.97	4.5		0.279			55
$60HfF_4$-$33BaF_2$-$7ThF_4$						62		31
$57ZrF_4$-$36BaF_2$-$3LaF_3$-$4AlF_3$	228±3	5.5±0.1	4.8±0.1	2.1±0.1	0.3	11±4	12±5	43
$57HfF_4$-$36BaF_2$-$3LaF_3$-$4AlF_3$	233+7	5.6±0.1	4.8±0.1	2.1±0.1	0.3	-	11±4	43
$57.5HfF_4$-$8.75ThF_4$-$25.3BaF_2$-$8.44PbF_2$	267							46
$22BaF_2$-$22LaF_3$-$16YF_3$-$40AlF_3$	360							47
soda-lime	540-580	6.9						63
chalcogenide	100-200					20		64

have not been optimized for mechanical properties, and projections for improvement are good [43].

II. 4.9 Optical Properties

II. 4.9.1 Optical Attenuation

The attenuation of an optical beam as it passes through a material is described by Beer's Law:

$$I = I_o e^{-\alpha x} \tag{II.8}$$

where I_o and I are the intensities of the beam before and after passing a distance x through the material, and α is the attenuation coefficient. α has units of distance^{-1} (usually cm^{-1}). Often in fiber-optic studies the attenuation coefficient is expressed in dB/km:

$$\alpha(\text{dB/km}) = (10/x) \log_{10} (I_o/I) \tag{II.9}$$

where x is the distance in km transversed by the light beam. The conversion factor between the two units for α is:

$$\alpha(\text{dB/km}) = 4.3 \times 10^5 \, \alpha(\text{cm}^{-1}) \tag{II.10}$$

The optical transmission loss for a glass arises from two independent processes: scattering and absorption. Thus

$$\alpha_T = \alpha_S + \alpha_A \tag{II.11}$$

where α_T, α_s and α_A are the total, scattering and absorptive attenuation coefficients respectively. The contributions to intrinsic losses in an insulator are illustrated schematically in Fig. 3. The minimum intrinsic optical loss occurs at the intersection of the intrinsic (mainly Rayleigh for glass) scattering curve on the high frequency side and the multiphenon edge on the low frequency side. In most IR transparent crystals the attenuation at this point is extremely small ($\sim 10^{-8}$ cm^{-1} ($\sim 10^{-3}$ dB/km)). By contrast the losses in fused silica are 4.65×10^{-7} cm^{-1} (0.2 dB/km) at the minimum ($\sim$1.6 μm) in the curve [65]. For fluorozirconate glasses several studies have indicated that the intrinsic attenuation minimum will occur in the vicinity of 3-4 μm [10,39,46,66]. Absorption coefficients at the DF laser wavelength (3.8 μm) have been reported: $\alpha = 2 \times 10^{-3}$ cm^{-1} (8.6×10^{2} dB/km) for ZrF_4-BaF_2-ThF_4 [31], 8.7×10^{-3} cm^{-1} (3.74×10^{3} dB/km) for ZrF_4-BaF_2-LaF_3-AlF_3 and 3.97×10^{-3} cm^{-1} (1.71×10^{3} dB/km) for HfF_4-BaF_2-LaF_3-AlF_3 [64]. These values are 5 orders of magnitude greater than the theoretical minimum losses (2.33×10^{-8} cm^{-1} (10^{-2} dB/km) at 4.4 μm) [46] and indicate sizeable extrinsic contributions to the observed losses. Recently Mitachi et al. [67] reported that they formed a step index profile fiber optic waveguide from glass compositions in the BaF_2-GdF_3-ZrF_4-AlF_3 system. A minimum loss of 8.6×10^{-5} cm^{-1} (37 dB/km) at 2.6 μm was measured for this fiber.

II. 4.9.1.1 Scattering Losses

The light scattering processes may be divided into Mie, Brillouin and Rayleigh scattering. Mie scattering is caused by inhomogeneities

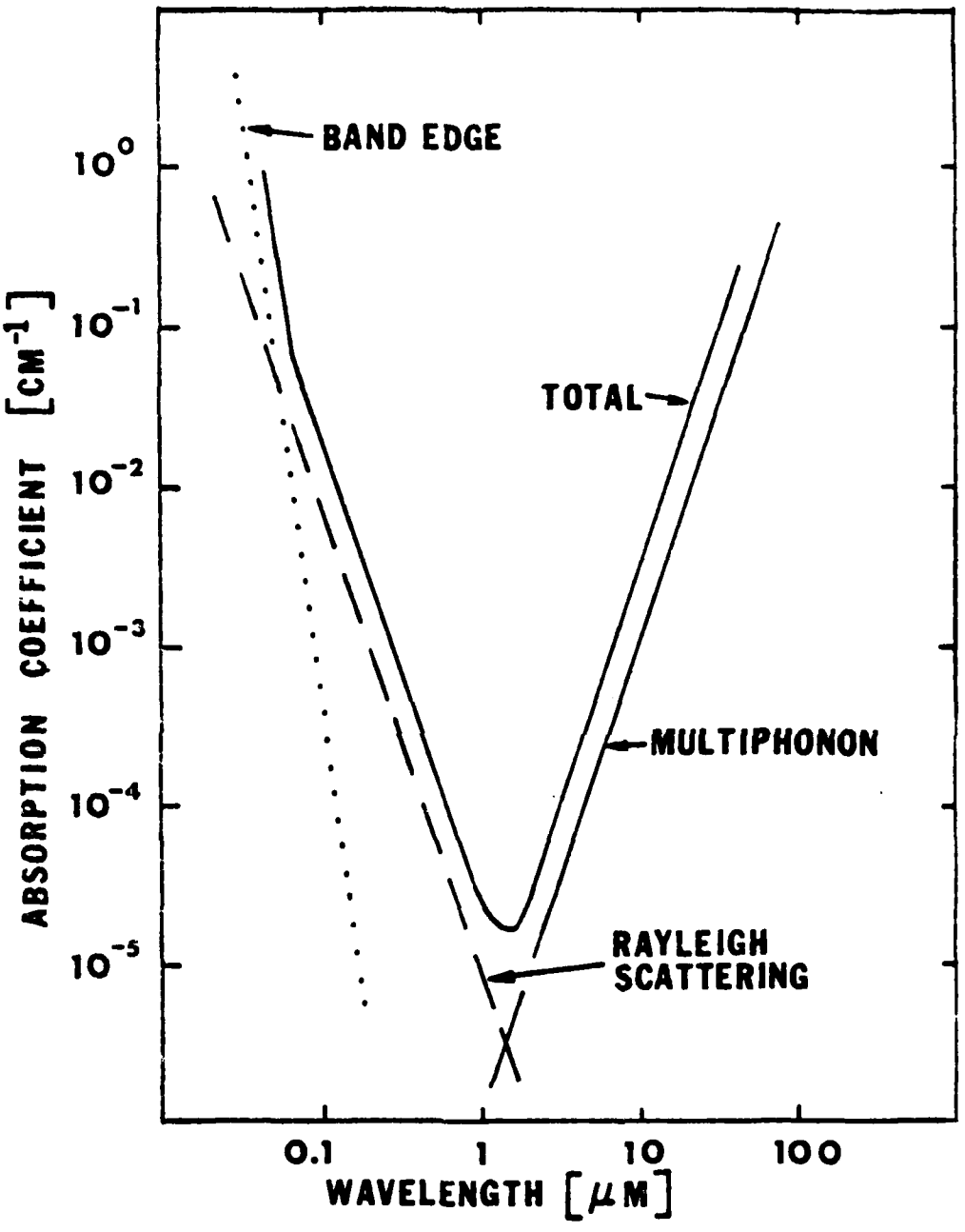
BAND EDGE
TOTAL
MULTIPHONON
RAYLEIGH
SCATTERING
ABSORPTION COEFFICIENT [CM⁻¹]
10⁰
10⁻¹
10⁻²
10⁻³
10⁻⁴
10⁻⁵
0.1
1
10
100
WAVELENGTH [μM]

FIG. 3

comparable in size to the wavelength of the light used. This undesirable feature can be eliminated with care in glass preparation and melting.

Brillouin scattering is due to scattering of light from thermally excited sound waves. The Brillouin attenuation coefficient (α_B) is given by [68]

$$\alpha_B = (8\pi^3/3)(n^8P^2/\lambda^4)\ k\ Tg\ \beta_T \qquad \text{(II.12)}$$

where λ is the wavelength, n is the refractive index, P is the photoelastic (Pockel) coefficient, k is the Boltzmann constant, Tg is the glass transition temperature and β_T is the isothermal compressibility. An approximation to the n^8P^2 factor in Eq. (II.12) can be made from the electronic oscillator strengths [69,70]:

$$n^8P^2 \sim D^2Za^2/E_o^4 \qquad \text{(II.13)}$$

where E_o is the average energy gap of the glass, Za is the formal chemical valence of the anion and D is a dimensionless structural factor. Eq. (II.13) reveals that fluorides (Za = 1) provide an intrinsic factor-of-4 improvement over oxides (Za = 2). In addition, the lower Tg's of fluoride glasses compared to oxides should also work to reduce the Brillouin scattering.

Rayleigh scattering, which generally dominates the scattering in glasses, is caused by small periodic changes in refractive index which may result from compositional and density fluctuations. The total

scattering attenuation coefficient (α_s) is given by:

$$\alpha_s = \alpha_B (1 + R_{LP}) \qquad \text{(II.14)}$$

where R_{LP} (the Landau-Placzek ratio) is defined as the ratio of the Rayleigh scattering intensity to the total Brillouin scattering intensity. For ideal crystals, $R_{LP} = 0$, while R_{LP} is 0.2 [71] for good quality SiO_2 single crystals and 21-28 for SiO_2 glass.

The attenuation coefficient due to scattering encountered in optical grade oxide glasses is of the order of 10^{-4} cm^{-1} (10 dB/km) or less [72]. Definitive values of the scattering losses in fluoride glasses are not yet available, except for a recent report of total integrated scatter (as the fraction of incident light scattered) of ZrF_4-BaF_2-LaF_3-AlF_3 (ZBLA) and HfF_4-BaF_2-LaF_3-AlF_3 (HBLA) glasses at 3.39 μm (Table VIII) [64]. Even if the absolute scattering cross section is larger for heavy metal fluoride glasses than for silicates, the actual value of the scattering loss in their contemplated operating frequency range may be lower. This is because the scattering losses exhibit a λ^{-4} dependence, and the IR absorption edges of the heavy metal fluoride glasses occur at longer wavelengths than for oxide glasses. The intersection of the multiphonon and scattering curves will therefore occur at longer wavelengths and the corresponding minimum absorption coefficients will hopefully be reduced (cf. Fig. 3). The lower values of Za, Tg and Eo [69] for fluorides compared to silicates also tend to make α_B smaller than for oxides.

Table VIII. 3.39 μm Scattering of Fluorozirconates.

Data from Ref. 64.

		BEST	AVERAGE
ZBLA	THIN	3×10^{-4}	1.1×10^{-3}
	THICK	3.2×10^{-3}	6.2×10^{-3}
HBLA	# 107	8×10^{-4}	2.1×10^{-3}
	# 153	1.2×10^{-2}	2.1×10^{-2}

Comparison Values MgF_2 $\sim 10^{-2}$, spinel plates $\sim 10^{-3}$
Spinel domes $\sim 10^{-2}$, sapphire $\sim 10^{-4}$

II. 4.9.1.2. Absorption Losses

Absorption losses in glasses can either be intrinsic (due to the bulk glass components) or extrinsic (due to impurities and defects). Intrinsic absorption occurs in the ultraviolet region due to the electronic excitation of atoms of the bulk glass and in the infrared region due to the resonant vibrations of the atoms or ions. Fig. 4 shows the spectra from UV to IR of typical heavy metal fluoride glasses along with that for silica glass. The shift of the IR edges to longer wavelengths is the primary reason for interest in heavy metal fluoride glasses.

II. 4.9.1.2.1 UV Losses and Electronic Absorption

The UV cut-off of BeF_2 is below 0.15 μm [30]. Fluorozirconate and fluorohafnate glasses possess UV edges in the vicinity of 0.25 μm (5 eV) [72]; 0.21 μm for ZrF_4-BaF_2-LaF_3 and 0.24 μm for HfF_4-BaF_2-LaF_3 [10,74]. This red shift in the UV edge is expected when a lighter element is replaced by a heavier element in the same group [8,46]. Aluminum containing glasses (ZrF_4-BaF_2-LaF_3-AlF_3 or HfF_4-BaF_2-LaF_3-AlF_3) have their UV edges at longer wavelengths (0.29 μm) [73]. Glasses containing YbF_3 (e.g., BaF_2-ZnF_2-YbF_3-ThF_4) possess a sharp electronic absorption band at ∿0.9 μm [75]. Replacing the YbF_3 with YF_3 or LuF_3 removes this band. Substantial structure is displayed in all the UV edges of fluorozirconate and fluorohafnate glasses, and the UV edge characteristics are extremely sensitive to the presence of small amounts of impurities [73]. Some glasses prepared in CCl_4 atmospheres are yellow in color, and their UV edges are found to be shifted to considerably

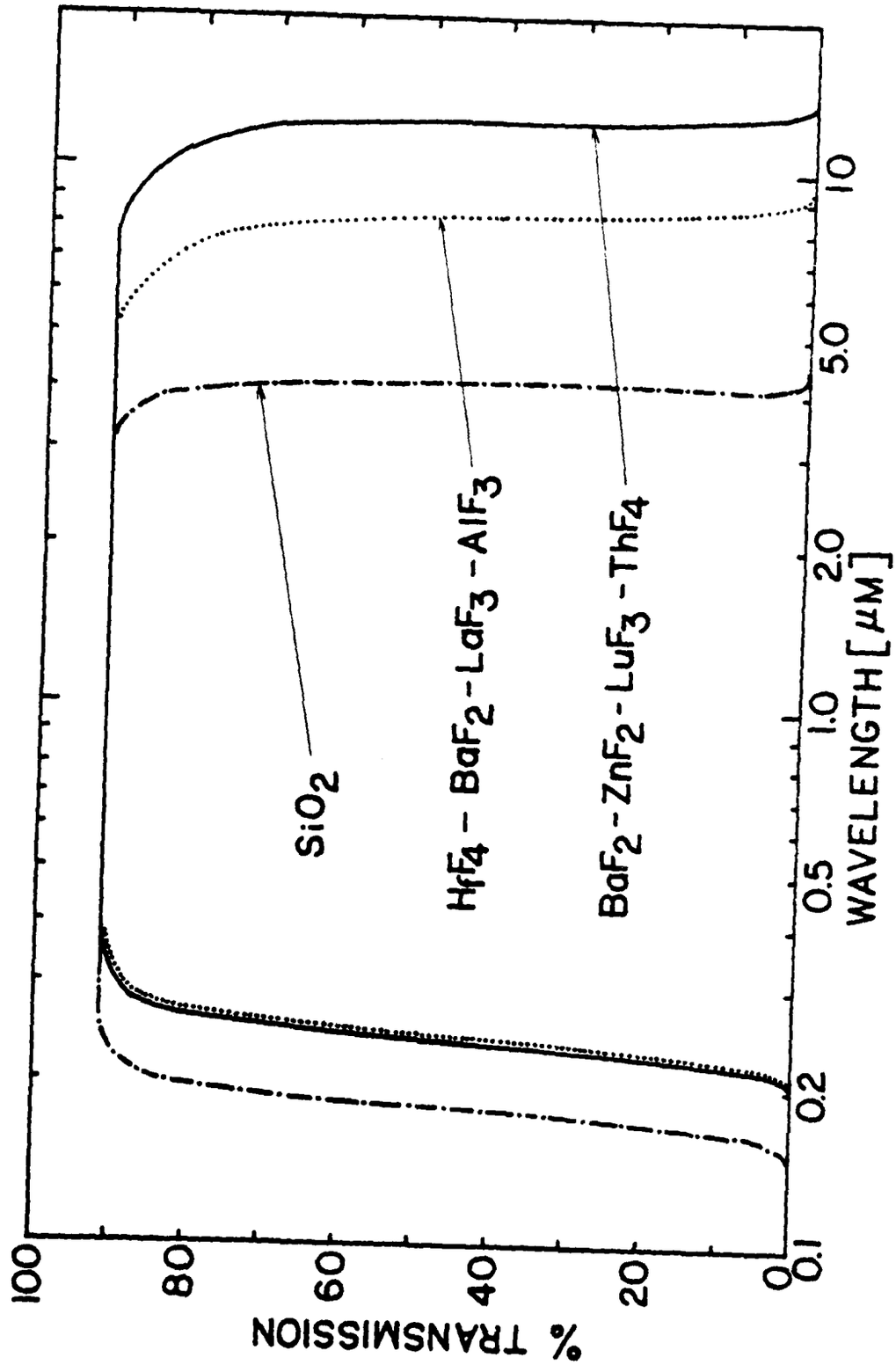
% TRANSMISSION
100
80
60
40
20
0
0.1
0.2
0.5
1.0
2.0
5.0
10
WAVELENGTH [μM]
SiO2
HfF4 - BaF2 - LaF3 - AlF3
BaF2 - ZnF2 - LuF3 - ThF4

FIG. 4

longer wavelengths when prepared in Pt crucibles as opposed to vitreous carbon crucibles [73]. A broad feature has been observed in the spectra of glasses prepared under reactive atmosphere (CCl_4, Cl_2) near 0.36 μm (3.5 eV) which indicates the presence of Cl_2 in glasses. Use of Pt crucibles leads to greater Cl_2 contamination than does vitreous carbon crucibles. Bands at 0.45 μm and 0.27 μm in the spectra of glasses in the binary ZrF_4-BaF_2 system have been assigned to Pt and Fe contamination respectively [12].

II. 4.9.1.2.2. Intrinsic IR Losses

II. 4.9.1.2.2.A. Fundamental Region

The infrared spectrum of vitreous BeF_2 shows a very strong absorption band at 770 cm^{-1} due to the fundamental Be-F stretching mode and three weak bands at 248, 420 and 910 cm^{-1} [30]. The fundamental IR spectra of fluorozirconate and fluorohafnate glasses are composed of two well separated relatively broad peaks centered near 250 cm^{-1} (150 - 300 cm^{-1}) and 525 cm^{-1} (400 - 600 cm^{-1}), the high frequency peak being considerably more intense [76,77]. The 525 cm^{-1} peak is attributed to Zr-F (or Hf-F) stretching vibrations and the 250 cm^{-1} peak may originate from Ba-F stretching vibrations and/or Zr-F (or Hf-F) bending modes [76-78]. In ternary ZrF_4- and HfF_4-based glasses the third component (usually LaF_3 or ThF_4) has a negligible effect on the IR spectrum. The maximum reflectivity (~45%) [41] and corresponding absorption oscillator strength is lower in fluorohafnate than in fluorozirconate [76,77]. In the spectrum of ZrF_4-BaF_2-$BaCl_2$ glasses a peak at 460 - 480 cm^{-1} [12],

which is related to the presence of chlorine in the glass, occurs in addition to the 525 cm^{-1} peak. For BaF_2-ZnF_2-YF_3/YbF_3-ThF_4 glasses peaks are observed at 400 cm^{-1} and 250 cm^{-1} for the YF_3 containing glass, and 435 cm^{-1} and 250 cm^{-1} for the YbF_3 containing glass. On the addition of AlF_3 to the system a peak appears at $\sim$625 cm^{-1} and the IR edge is shifted to a higher frequency [41].

The Raman spectrum of vitreous BeF_2 shows a strong polarized peak at 280 cm^{-1} and three medium band at 380, 750 and 810 cm^{-1} [30]. Fluorozirconate and fluorohafnate glasses have a dominant Raman peak in their polarized VV spectra in the vicinity of 580 cm^{-1} with a corresponding deep minimum in the depolarization spectrum [12,76,78,79]. This peak is attributed to the symmetric stretching vibrations associated with ZrF_x^{4-x} and HfF_x^{4-x} (where $5 \leq x \leq 8$) [78,79]. The HfF_4- and ZrF_4-based glasses show this peak at the same frequency (580 cm^{-1}), possibly due to the Hf-F bond having a higher force constant than the Zr-F bond [79], offsetting the mass difference. A broad depolarized feature in the viscinity of $\sim$250 cm^{-1} is displayed [76,78] in ZrF_4- and HfF_4-based glasses, suggesting that the principal low frequency Raman peak also stems from vibrations (possibly of the bending type) associated with Zr-F or Hf-F complexes [78]. In ternary fluorozirconate and fluorohafnate glasses the spectra are relatively unaffected by changing the third component (LaF_3 or ThF_4) [79].

II. 4.9.1.2.2.B. Multiphonon Region

The IR edge in a transmission spectrum is due to multiphonon processes. In solids, multiphonon absorption takes place when a high

energy photon couples weakly with a transverse optical (TO) mode of the material; this TO mode then decays into two or more lower energy phonons of frequencies corresponding to fundamental vibrational modes. The net effect is that the material appears to show absorption due to overtones or harmonics of the fundamental vibration frequencies. The frequency region corresponding to roughly twice the frequency of the strong high frequency fundamental band is called the two-phonon region, three times the fundamental frequency the three-phonon region, etc.

The intrinsic absorption coefficient (α_A) in the IR multiphonon absorption region depends on frequency (ω) and temperature (T). The multiphonon absorption coefficient on the IR edge has an approximate exponential dependence on frequency [80]:

$$\alpha_A(\omega) = A \exp(-B\omega) \qquad \text{(II.15)}$$

where A and B are constants. In most cases, ionic materials display relatively little structure in their multiphonon spectra, and virtually none at all at room temperature and above. The IR edges of heavy metal fluoride glasses tend to be rather featureless, suggesting that the glasses are fairly ionic [77]. This behavior contrasts with that for semiconductors, where marked structure often persists into the three-phonon regimes, even above room temperature [81]. These differences in spectral characteristics are attributed to the larger anharmonicity and substantially broader vibrational density of states of ionic materials compared to semiconductors [81].

The temperature dependence of the absorption coefficient in the multiphonon region is given by [82,83]:

$$\alpha_A(T) = \alpha_o \, [N(\omega_o) + 1]^{\omega/\omega_o} \, [N(\omega) + 1]^{-1} \qquad (II.16)$$

where $N(\omega)$ is the Bose-Einstein (thermal occupancy) function, $N(\omega) = [\exp(\omega/kT) - 1]^{-1}$, $\omega_o = \omega_o(T)$ is a typical optical phonon frequency and α_o is the absorption at absolute zero. Combining equations (II.15) and (II.16):

$$\alpha(\omega,T) = \alpha_o \, [N(\omega_o) + 1]^{\omega/\omega_o} \, [N(\omega) + 1]^{-1} \exp(-B\omega) \qquad (II.17)$$

Bendow et al. [84] have shown that the equation corresponds reasonably well with experimental multiphonon data for $58ZrF_4$-$33BaF_2$-$9ThF_4$ glass. The best fit parameters for data taken over the temperature range 100 to 550°C and the frequency region 1200 to 1700cm^{-1} were:

$$\alpha_o = 2.97 \times 10^5 cm^{-1}, \quad B = 8.8 \times 10^{-3} cm, \quad \omega_o = 500 cm^{-1}$$

For samples a few mm thick the infrared cut-off due to multiphonon processes for vitreous BeF_2 is in the 4-5 μm region [30]. The IR absorption edge of fluorozirconate and fluorohafnate is at ∿7 μm (the fluorohafnate edge being at a wavelength 0.025 - 0.033 μm higher than that for the corresponding fluorozirconate) [8]. For BaF_2-ZnF_2-YF_3/YbF_3-ThF_4 glasses the edge is at ∿9 μm [14,16]. On the addition of

AlF_3 to the system the IR edge is shifted to a lower wavelength [41].

II. 4.9.1.2.3. Extrinsic IR Losses

At shorter IR wavelengths (2 μm to 10 μm) the residual absorption of all insulating materials is limited by extrinsic processes either due to bulk or surface absorption. The principal source of the residual bulk absorption in the IR-transmitting materials is believed to be largely associated with substitutional molecular inpurities, although other sources such as macroscopic inclusions have been considered. The major impurities affecting the optical transparency of heavy metal fluoride glasses are transition metal ions (and/or rare-earth ions), hydroxyl groups (-OH) and oxide species. The hydroxyl absorption band at 2.9 μm is likely to be a substantial source of extrinsic loss in the mid-IR region. In addition, oxide ions and the oxygen in bulk -OH will be bonded to the cations in the glass, and these metal oxyfluoride species can contribute to excess absorption on the IR absorption edge at ~7 μm, as will be discussed in detail in the later sections of this thesis.

II. 4.9.2 Refractive Index and Material Dispersion

Vitreous BeF_2 has very low refractive index (n_D = 1.2747) and high Abbe number (ν = 106.8) [85]. The Abbe number is defined by

$$\nu = (n_D - 1)/(n_F - n_c) \qquad \text{(II.18)}$$

where n_D is the refractive index at the wavelength of the sodium doublet (582.29 nm) and n_F and n_c the indices at the wavelengths of two lines of

the hydrogen spectrum (486.13 nm and 656.27 nm respectively). The Abbe number is related to the dispersion of the refractive index in the visible; the higher the Abbe number, the smaller the dependence of the index on wavelength. Addition of modifying fluorides to BeF_2 increases n_D and decreases ν. For ZrF_4-based glasses n_D is typically 1.50-1.54 (Table III-VI), while ν is usually in the range 70-80 [7,9,11,26,42,86]. The refractive index usually increases when a less polarizable element is replaced by a more polarizable one, for example, Pb compounds are often added to increase the refractive indices of glasses. For atoms or ions of similar valence electron configuration, increased atomic mass generally is accompanied by increased polarizability. However for the heavy metal fluoride glasses substitution of heavier HfF_4 for lighter ZrF_4 leads to a glass of lower refractive index. This may be due to a difference in the atomic packing of the ZrF_4- and HfF_4-based glasses. The variation of refractive indices in the IR regime for a $62ZrF_4$-$33BaF_2$-$5LaF_3$ glass (ZBL) and $62HfF_4$-$33BaF_2$-$5LaF_3$ glass (HBL) with wavelength is compared with that of fused silica in Fig. 5 [87].

The material dispersion, M is defined by

$$M = -(\lambda/c)(d^2n/d\lambda^2) \qquad \text{(II.19)}$$

where c is velocity of light in vacuum and $d^2n/d\lambda^2$ is the second derivative of the refractive index n with respect to wavelength λ. The quantity $d^2n/d\lambda^2$ is directly related to the bandwidth of an optical fiber; the maximum bandwidth occurs at a wavelength λ_o where $d^2n/d\lambda^2$ is zero.

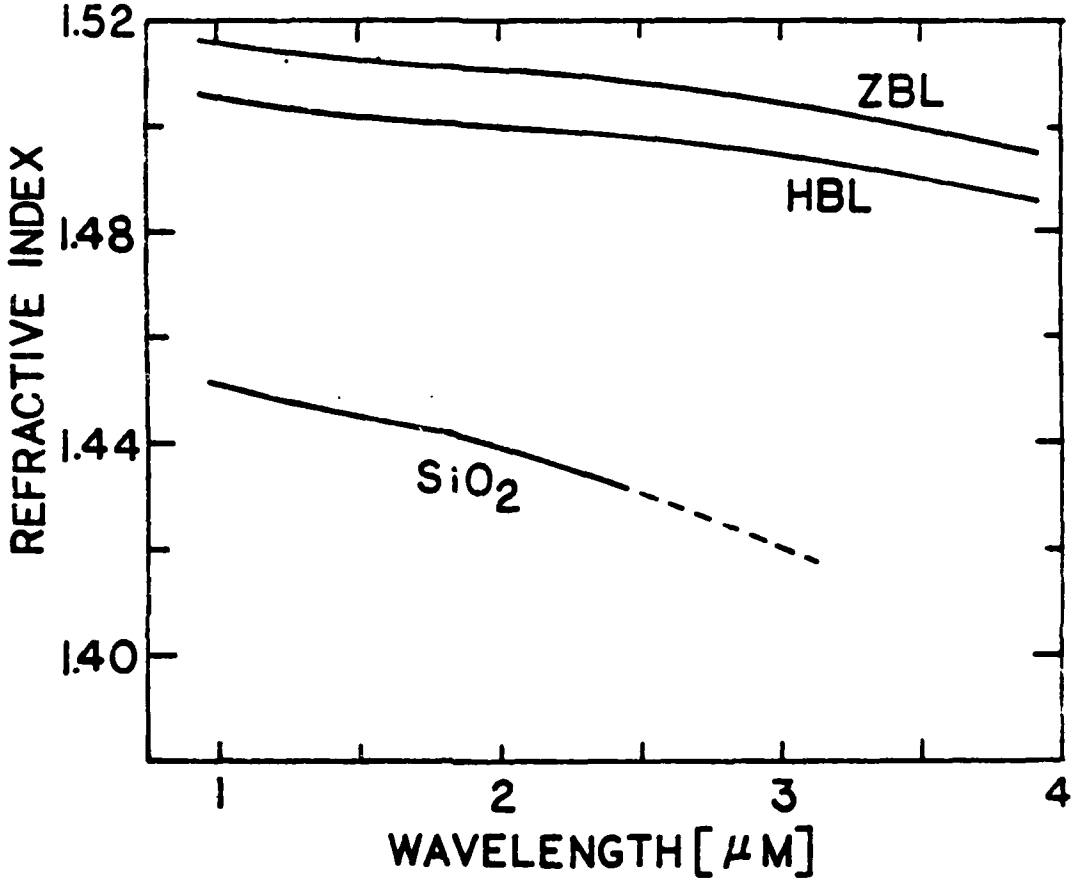
1.52
1.48
1.44
1.40
REFRACTIVE INDEX
ZBL
HBL
SiO2
1
2
3
4
WAVELENGTH [μM]

FIG. 5

Ideally, λ_o falls within the ultralow loss regime of the material between the electronic and infrared edges. Bendow et a. [87] and Jeunhomme et al. [88] have found that $d^2n/d\lambda^2$ is nearly the same for fluorozirconate and fluorohafnate glasses, λ_o being at ~1.7 μm. This is in good agreement with the theoretically predicted value [89]. Thus the material dispersion zero wavelength is not in the ultra low loss region (3-4 μm) predicted for these glasses. In contrast to fused silica, however, the dispersion curve (Fig. 6) for the fluoride glasses is considerably flatter and the dispersion smaller as one moves away from λ_o to longer wavelengths [87,88]. Thus for the heavy metal fluoride glasses the material dispersion at 3 μm (1.3 μm away from λ_o) is the same as that for fused silica at 1.7 μm (only 0.4 μm away from λ_o) [87]. Calculations show that even at 3 μm it should be possible to attain bandwidths in excess of $GH_z \cdot km$ in fibers made from these materials [87].

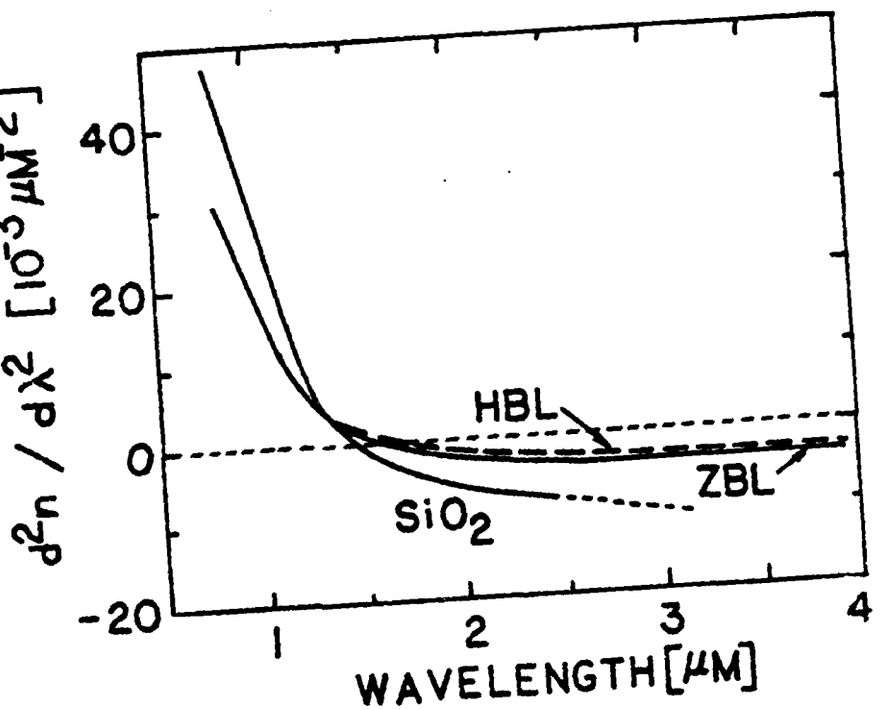
$d^2n / d\lambda^2$ [$10^{-3}\mu M^{-2}$]
40
20
0
-20
1
2
3
4
WAVELENGTH [μM]
HBL
ZBL
SiO_2

FIG. 6

CHAPTER III

EXPERIMENTAL PROCEDURE

III.1 Materials

The chemicals used in the glass synthesis are listed in Table IX. The glasses were melted in crucibles of platinum (100 mL and 25 mL) or vitreous carbon (2 in D x 2 in H; Fluorocarbon, Anaheim, CA). The tongs used to handle the crucibles were platinum tipped to prevent contamination of the melt with transition metals.

The glass compositions are designated by using acronyms formed from the first letters of the chemical symbols of the cations of the components or the full chemical symbols in cases where the same first letters appear for different components (Table X). Individual glass samples are identified by the day-month-year when they were melted, e.g., ZBL-21-7-81 identifies a ZrF_4-BaF_2-LaF_3 glass melted on 21 July 81. The three general types of glasses studied here were ZBL and HBL, ZBLA and HBLA and BZnYbT.

III.2. Synthesis Procedures

Two general types of reactor were used for the melting. In the first type (the "open" reactor) a controlled atmosphere was flowed over the batch during melting, but the reactor was not tightly closed against the ambient atmosphere. The second type (the "closed" reactor) was tightly closed to prevent exposure of the melt to the ambient atmosphere.

Table IX. Chemicals Used in Heavy Metal Fluoride Glass Syntheses

Chemical	Purity	Source
Al	99.9% metal powder	Alfa Products
AlF_3	99.5%	Cerac, Inc.
BaF_2	99%	Alfa Products
BaF_2	99.9%	Cerac. Inc.
CsF	99.9%	Alfa Products; Cerac. Inc.
Gd_2O_3	99.9%	Alfa Products
HfF_4	99.9%	Cerac. Inc.
HfO_2	97%	Teledyne Wah Chang Albany
HfO_2	99.999%	Apache Chemicals, Inc.
LaF_3	99.9%	Cerac. Inc.
La_2O_3	99.999%	Aldrich Chemical Co.
$NH_4F \cdot HF$	97+%	Alfa Products
$NH_4F \cdot HF$	99.9%	Cerac. Inc.
PbF_2	98%	Alfa Products
PbF_2	99.9%	Cerac. Inc.
KF	99.9+% (Fisher Certified)	Fisher Scientific Co.
ThF_4	99.9%	Alfa Products; Cerac. Inc.
YF_3	99.9%	Cerac. Inc.
YbF_3	99.9%	Cerac. Inc.
ZnF_2	99.5%	Cerac. Inc.
ZrF_4	99.5%	Cerac. Inc.
ZrO_2	99+%	Alfa Products
Ar gas	99.997%, H_2O(3ppm), O_2(5ppm)	Union Carbide Co.
CCl_4	ACS grade	Fisher Scientific Co.
Cl_2 gas	3½% Cl_2 in N_2	Matheson
N_2 gas	99.997%, H_2O(3ppm), O_2(5ppm)	Matheson; Union Carbide

Table X. Acronyms Used For Glass Designation

abbreviation	component	abbreviation	component
A	AlF_3	N	NaF
B	BaF_2	Nd	NdF_3
Bi	BiF_3	P	PbF_2
C	CsF	R	RbF
G	GdF_3	T	ThF_4
H	HfF_4	U	UF_4
K	KF	Y	YF_3
L	LaF_3	Yb	YbF_3
Li	LiF	Z	ZrF_4
Lu	LuF_3	Zn	ZnF_2

III. 2.1 Melting in the Open Reactor

During earlier parts of this study (up until 14 October 1980) glass was melted in the open reactor. A diagram of this is shown in Fig. 7. The reactor was placed in the fume hood because of corrosive vapors evolved during melting. The furnace in which both fluorination and melting were carried out was a Hoskins FD-104 crucible furnace (5 inD x 5 inH heating chamber) controlled with an Omega Model 52 temperature controller. The chromel-alumel thermocouple (T.C.) connected to the controller entered through the bottom of the furnace. The furnace temperature was determined with a chromel-alumel thermocouple which entered through the top whose output was monitored in the early part of the study by a Keithly Model 177 difital multimeter and later by an Omega Model 199 Type K digital thermometer. The top of the furnace was closed with a cover of Transite or Marinite; the cover contained two or three small holes, which were used for insertion of the thermocouple and as an escape hole for water vapor and NH_4F and ZrF_4 particles evolved during glass synthesis. The glasses were melted mostly in a 100 mL platinum crucible which was loosely covered with Pt foil to minimize the evaporation of fluorides during melting. The gas stream ($\sim$2.0 ℓ/min) was introduced through a Vycor glass tube which entered through the bottom of the furnace and was connected through a flowmeter to the regulator of the cylinder with 3/8 in OD Tygon tubing.

The open reactor was preferred when all or some of the starting materials were in the form of oxides. The glass batch (typically 20 g of metal oxides and fluorides) was weighed into a plastic jar and

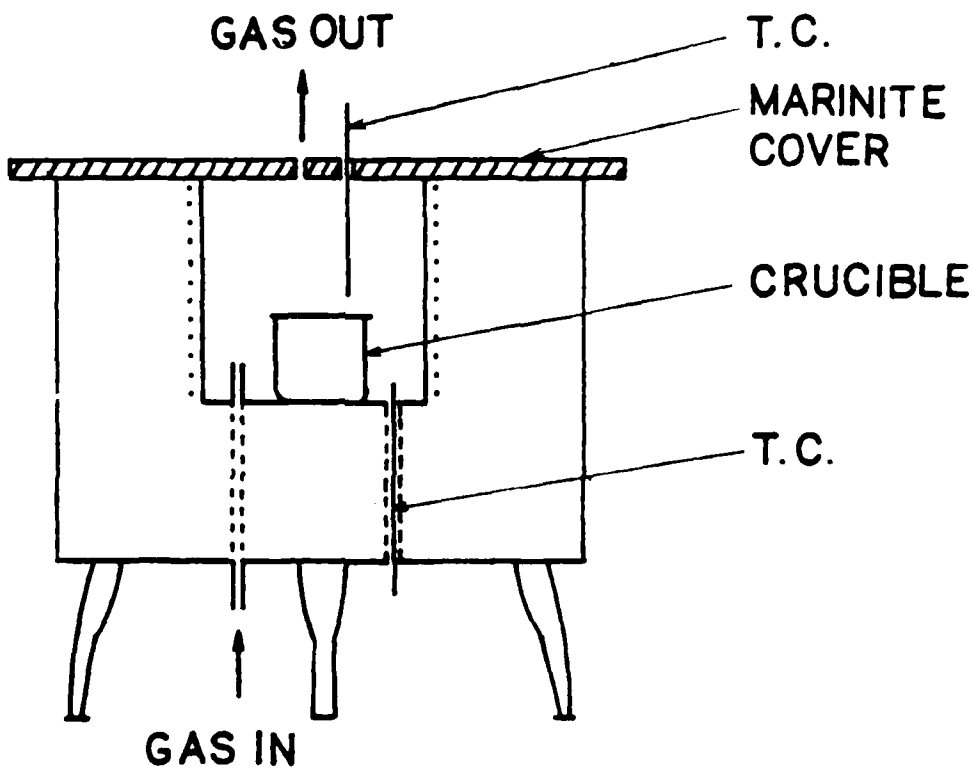

FIG. 7

thoroughly mixed with a large excess of $NH_4F \cdot HF$ (~30 g). To avoid the presence of unfluorinated phases or inclusions which might lead to devitrification during casting, it was beneficial to add 4 to 6 times the stoichiometric amount of $NH_4F \cdot HF$ to the glass batch. The crucible and lid were dried at 200°C for 30 min before melting. Melting was carried out under dry, inert (N_2) atmosphere introduced into the furnace interior. The batch was placed in the furnace for 1 hr at about 320°C to allow fluorination to occur. The crucible was then removed from the furnace, and the hot crystalline mixture was broken up with a ceramic rod in the crucible and then mixed with an additional 10-20 g $NH_4F \cdot HF$. The crucible was covered and reintroduced into the furnace at 320°C and held for 10 min to ensure complete fluorination. The furnace temperature was then raised at the rate of ~15°C min^{-1} to the melting temperature (~750°C for ZBL & HBL, ~850°C for ZBLA & HBLA, ~950°C for BZnYbT) and held there until heavy evolution of NH_4F fumes had abated (~20 min). The melt was then kept at this temperature for an additional 10 min. At this point the fluoride mixture should be completely molten. However, sometimes the Pt crucible had a white deposit on the cooler parts of the inner walls, probably due to volatilized ZrF_4. In order to avoid contaminating the melt with these solid particles during casting, the melt was sometimes poured into a clean 25 mL Pt crucible, an additional (~10 g) $NH_4F \cdot HF$ added to the surface, and the loosely covered crucible replaced in the furnace at the melting temperature. It was again heated until heavy evolution of fumes had stopped and, after an additional 10 min,

was removed briefly from the furnace for inspection. The melt at this point was usually clear. If it had a gravish color (probably due to the presence of lower valent metallic cations), it was reheated at the melting temperature for an additional 5-10 min. This generally caused the melt to become clear, presumably by oxidation of the lower valent species, since oxygen had been admitted to the furnace atmosphere in removing the melt for inspection.

To improve the quality of the glass high purity metal fluorides were used as the starting materials in later experiments (from 21 January 1981). In these later experiments a modified version of the open reactor sketched in Fig. 8 and with a provision for reactive atmosphere melting was used. The large Al_2O_3 crucible in the furnace was used as a furnace liner to prevent corrosion of the walls of the furnace by the vapors evolved while melting. The furnace cover contained two or three small holes, which were used to insertion of the gas inlet, the thermocouple and to allow $NH_4F \cdot HF$ decomposition products to escape. The gas stream (0.1 - 0.2 ℓ/min) was introduced through an Al_2O_3 tube (1/4" OD) which entered through the top of the furnace. The gas flow line shown on the right hand side of Fig. 9 was constructed of Teflon tubing (1/4 in OD; Cole-Palmer, Chicago IL) and Teflon fittings (Chemplast, Wayne, NJ). The cross purging line between N_2 cylinder and Cl_2 cylinder was used to purge Cl_2 from the Cl_2 regulator at the end of an experiment to prevent corrosion of the regulator. CCl_4 vapor for reactive atmosphere processing was generated by either (1) bubbling nitrogen through a gas washing bottle with a fritted disc (Fisher) filled with liquid CCl_4 or (2) by passing

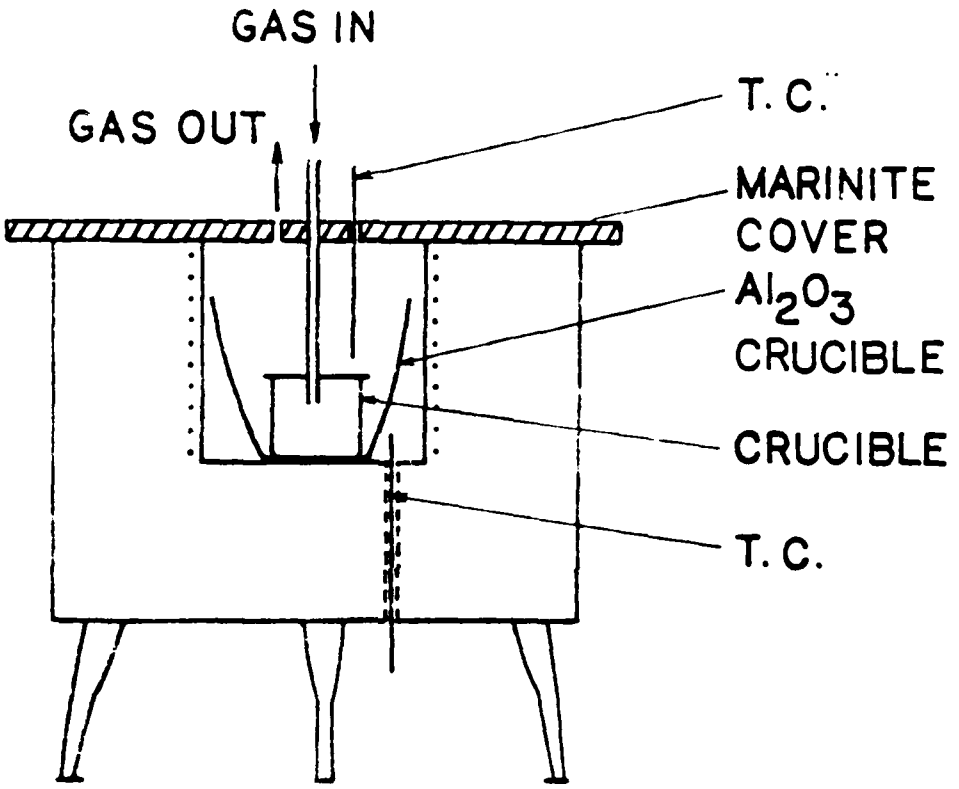

FIG. 8

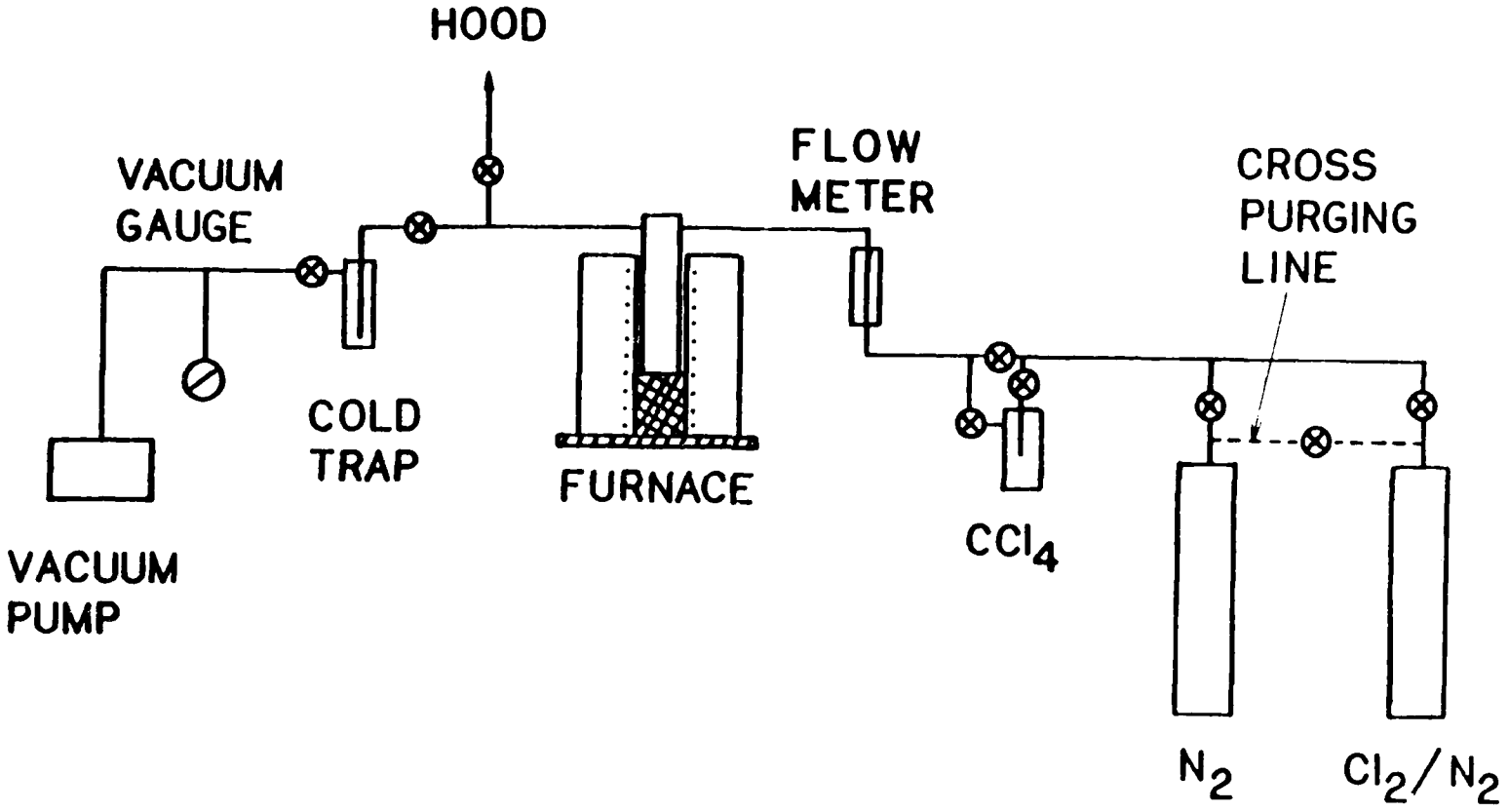
HOOD
VACUUM GAUGE
FLOW METER
CROSS PURGING LINE
COLD TRAP
FURNACE
VACUUM PUMP
CCl_4
N_2
Cl_2/N_2

FIG. 9

nitrogen over the surface of liquid CCl_4. Glasses were melted in both vitreous carbon and Pt crucibles with a Pt foil lid. The lid contained a 3/8 in diameter hole at the center for insertion of the gas inlet tube and to allow $NH_4F \cdot HF$ decomposition products to escape. The Pt crucibles were preferred, because the vitreous carbon crucibles were gradually eroded at elevated temperatures by $NH_4F \cdot HF$ decomposition products and also because they were easier to handle.

Some of the fluoride starting materials (e.g., ZrF_4) are hygroscopic and probably contain small amounts of water. Two methods were tried to remove this, along with small amounts of oxide present in the starting materials or formed by reaction with the water: (1) drying at 300°C for 30 min while flowing a dry inert gas over the batch, (2) adding ammonium bifluoride to the batch (~1 g/4 g of batch) and subsequently heating for 30 min at 400°C while again flowing a dry inert gas. The temperature was then raised in two ways, either in one step or in several steps. In the one step method the temperature was gradually raised at the rate of ~15°C min^{-1} to the melting temperature (~750°C for ZBL and HBL, ~850°C for ZBLA and HBLA, ~950°C for BZnYbT). In the multi-step method the temperature was increased every 0.5 hr to 500°C, 600°C, 700°C, etc., up to the melting temperature. The flow of reactive gas (CCl_4 in N_2, 3 1/2% Cl_2 in N_2) was started at 500°C when the glass was prepared under the reactive atmosphere. The melt was held at the melting temperature for 10-20 min. The multi-step method was preferred, since it tended to produce a clear melt, but larger amounts of material sublimed from the batch due to the longer melting time.

III. 2.2 Melting in the Closed Reactor

During the later parts of the study (since 18 May 1981) the glasses were melted either in the modified open reactor (Fig. 8) or in the closed reactor, sketched in Fig. 10. The closed reactor was made from 2 1/2 in ID quartz tubing and capped with a ball-and-socket joint (CFQ 102/75; U.S. Quartz, Fairfield, NJ). This joint was grooved to accept a heat resistant rubber O-ring seal (3.5 in diameter) and was held together during use by means of a spring-loaded steel clamp. The reactor vessel was mounted vertically with the bottom inserted 8 inches into an Astro Model A 142 tubular furnace. Temperature was controlled with the Omega Model 52 temperature controller, and the furnace temperature in the region of the crucible was measured using a chromel-alumel thermocouple inserted between the outside of the quartz tube and the inner wall of the furnace. Thermocouple output was monitored by an Omega Model 199 Type K digital thermometer. The gas flowline in and out of the closed reactor is shown in Fig. 9. A Welch Model 1400 Duo-Seal Vacuum Pump could be used to evacuate the reactor; the vacuum was monitored with a vacuum gauge (Comptech Model 201 Thermocouple Gauge Control).

Glasses were melted mostly in a vitreous carbon crucibles which were loosely covered with vitreous carbon disc to minimize the evaporation of fluorides during melting. When the starting materials were in the form of fluorides the closed reactor was preferred, since the melt needs to be prevented from reaction with any ambient moisture or O_2. Before melting the starting materials (fluorides) were either (1) dried or (2) prefluorinated. Drying was effected in the closed reactor either

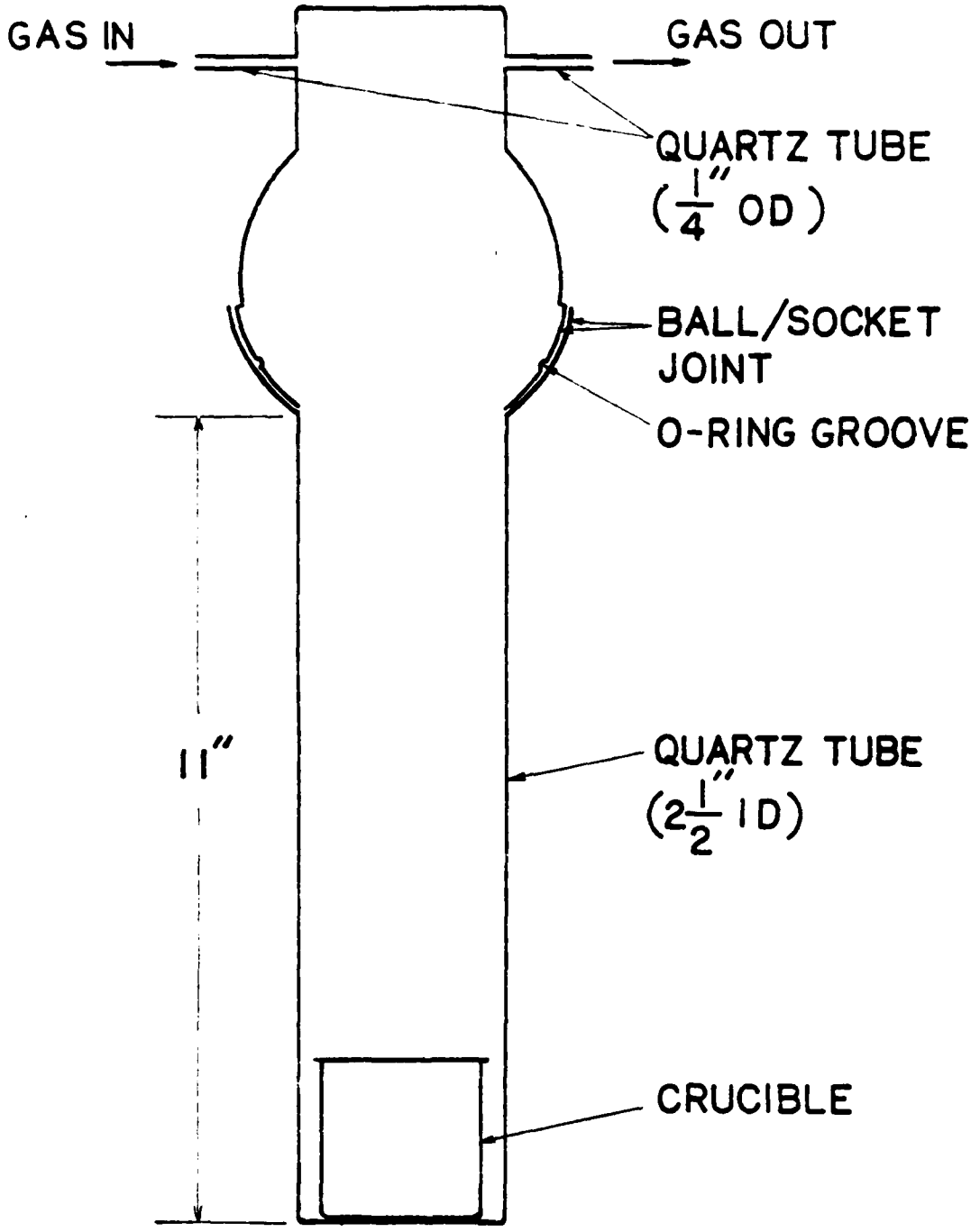
GAS IN
GAS OUT
QUARTZ TUBE
(1/4" OD)
BALL/SOCKET
JOINT
O-RING GROOVE
11"
QUARTZ TUBE
(2 1/2" ID)
CRUCIBLE

FIG. 10

by evacuating with vacuum pump at a low temperature (100-150°C) or by flowing a dry inert gas through the reactor at higher temperature (~300°C). Drying by evacuation at high temperature (~300°C) led to decomposition of the materials, and a relatively large amount of highly acidic water was condensed into the cold trap. Prefluorination was achieved by adding ammonium bifluoride to the batch (~1 g/4 g of batch) and heating the mixture in a crucible in the open reactor (Fig. 8) from 300°C to 500°C, raising the temperature in the multi-step mode under an atmosphere of inert gas. When the mixture ceased to fume at 500°C, the crucible was transferred to the closed reactor for melting. The modes of temperature increase and gas flow are indentical to those outlined in the previous section (III. 2.1). In the melting procedure, crucibles containing the glass substrate materials were placed at the bottom of the reactor vessel, and the ball-and-socket joint was sealed. The atmosphere in the vessel was controlled by flowing gas through small diameter (1/4 in OD) inlet and outlet tubes in the top section of the vessel. The location and proximity of these tubes mean that the gas flow to the bottom of the vessel was not direct and occurred mainly by diffusion and convection.

III. 3. Preparation of Glass Samples

III. 3.1 Casting

After melting the furnace temperature was lowered to the casting temperature (~650°C for ZBL and HBL, ~750°C for ZBLA and HBLA, ~850°C for BZnYbT). The melts were then taken out of the reactor and cast into

rectangular glass pieces a few mm thick by pouring them into brass molds at room temperature. The molds were formed by placing separate brass bars together on a brass plate. Two styles of mold were used. The first type was formed by arranging four brass bars on a brass plate (Fig. 11(a)). With this mold the thickness of the glass pieces are fixed and the other two dimensions can be varied. This style can also be used to produce several glass pieces in one quenching operation as shown in Fig. 11 (a). The other style of mold is shown in Fig. 11 (b), where two movable "L" shaped bars can be used to vary the thickness of the glass pieces while keeping the other two dimensions fixed. After filling the mold with the melt, the surface was quenched by quickly placing a brass block on top. In cases where the melt devitrified during this casting procedure, an attempt was made to form very thin glass sheets by rapid quenching. A small amount of melt was poured onto a brass plate, and a second plate quickly placed on top. For very good glass-forming compositions, thicker glass samples could be cast in molds preheated to about 300°C (up to 9 mm thick for $58ZrF_4$-$33BaF_2$-$5LaF_3$-$4AlF_3$). In some cases, to prevent reaction of the melt with any ambient moisture or oxygen, the melt was cast into a mold covered by an upside down aluminum pie pan with a hole on top. The pan was flushed with Ar or CCl_4 saturated N_2 just before casting the glass.

III. 3.2. Annealing

After casting glass specimens were immediately placed in a muffle furnace preset to an appropriate annealing temperature (slightly lower

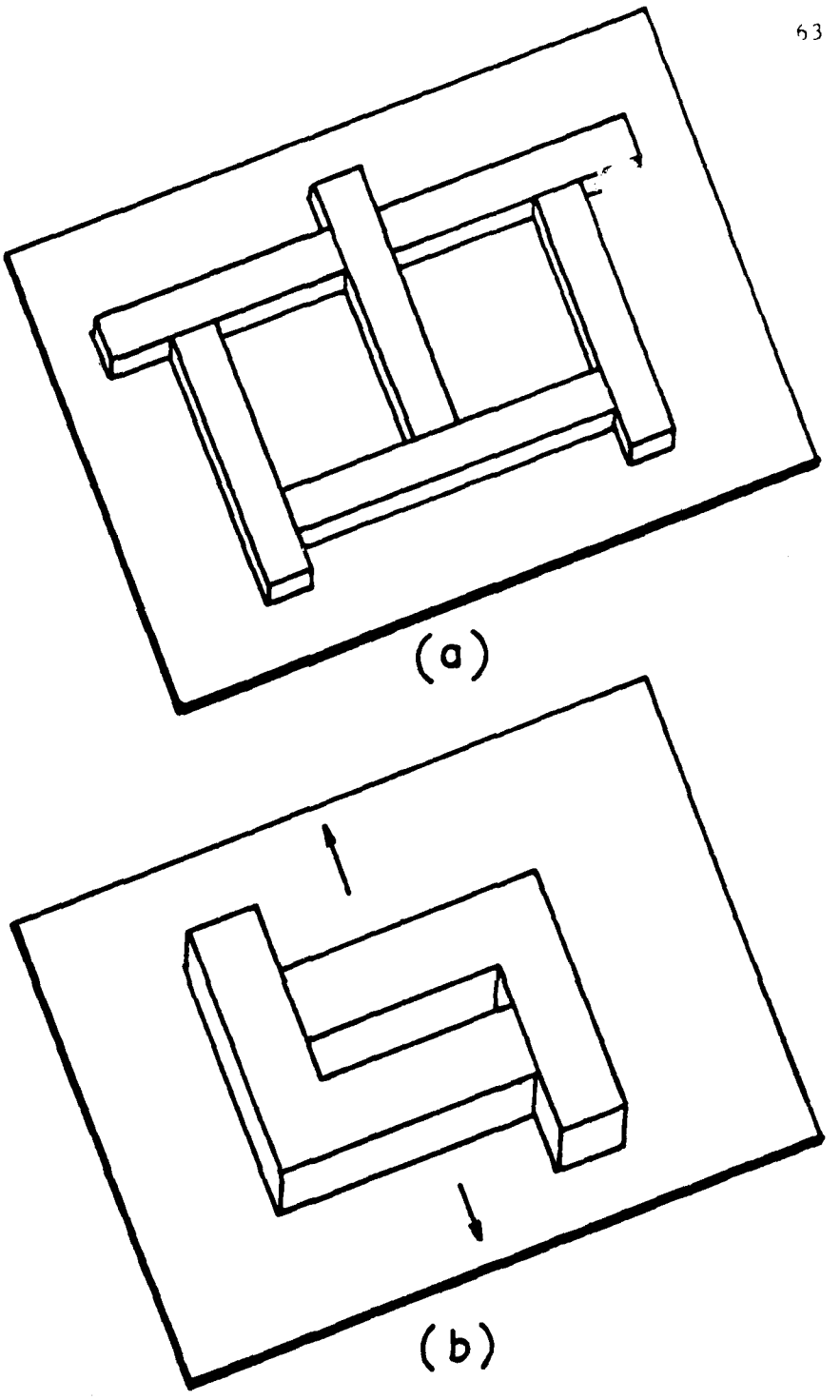

FIG. 11

than the glass transition temperature). The annealing furnace used was a Blue M (Model M 15A-2A) muffle furnace controlled with an Omega Model 52 temperature controller. After isothermal annealing for a brief time (~5 min) the furnace was turned off, and the glasses were allowed to cool to room temperature inside the furnace.

III. 3.3. Polishing

The glasses were polished in order to provide smooth parallel faces for microscopy and IR spectroscopy. Polishing was done on a Buehler 69-1000 Minimet polisher/grinder. Sample plates were mounted on the mount (1 in D, 1 1/4 in D or 1 1/2 in D x 1/2 in H aluminum disc) with cellophane tape with adhesive on both sides or with wax. Samples were fixed to the mount using wax by heating the mount on a hot plate, melting some wax on its surface, and then sticking the sample onto the wax and allowing to cool. Rough grinding was done with 180 grit SiC paper disc using lapping oil as a lubricant. Final grinding was done with 320 grit and 600 grit SiC paper discs, again using lapping oil as lubricant. Rough and final polishing was done with 5 μm and 0.05 μm Al_2O_3 on polishing cloths (Texmet and Microcloth) using water or ethylene glycol as a lubricant. There was no difference between samples polished with water and with ethylene glycol lubricants in terms of their surface smoothness and IR spectra. However, when ethylene glycol was used pieces of Al_2O_3 were occasionally found embeded in the sample near the surface. This happened less often when water was used as lubricant, so that water was preferred. In general, water plays the part of coolant on the polishing grains and at the same time reacts with the glass

surface; oil acts as coolant, causing no chemical reaction. It has been found that the chemical reaction between the glass and the polishing liquid plays an important role in the polishing process [90]. Usually in a water polishing process a soft hydrated layer is formed on the surface, and the smoothing is due to removal of the soft hydrated layer by the polishing grain. After polishing, samples were wiped clean with lens tissue (Kimwipe) moistened with methanol.

III. 4. Characterization of the Glass

III. 4.1. Microscopic Study

A Bausch & Lomb Stereozoom 7 stereo-microscope (10X to 140X) equipped with polarizer was used to examine the samples. All samples were examined using transmitted polarized light. For some samples a Polaroid camers was used to photograph the sample at various magnifications.

Many of the glasses produced appeared to contain a few small crystallites (typically 10-50 μm in size) distributed more or less randomly throughout the volume of glass. Some of these crystals may have been starting materials which did not melt because of too low a temperature or too short a melting time, and some were produced by devitrification during casting. Occasionally tiny bubbles could be observed in the bulk.

III. 4.2. IR Analysis

Samples for IR absorption measurements were prepared by polishing the opposite faces plane parallel, and ranged from 0.05 to 0.4 cm in

thickness. IR spectra over the range 250-4000 cm^{-1} (40-2.5 μm) were measured at ambient temperature on a Perkin-Elmer Model 467 double beam spectrometer with a variable comb attenuator in the reference beam. In later studies (since September 1, 1981) a Perkin-Elmer Model 298 spectrometer was used. Prior to recording the spectrum the attenuator was set to give a reading of 100% transmission at 1250 cm^{-1} with no sample in the sample beam. The spectrometer was set to read 0% transmission with the light beam to the sample blocked by adjusting the position of the pen on the pen drive. The sample mount had a 9 mm diameter hole at the center.

The absorption coefficient α at a given wavelength was obtained from the transmission T and the sample thickness X by the equation

$$\alpha = -(1/X)\ \ln\left[\{-(1-R)^2 + \sqrt{(1-R)^4 + 4R^2T^2}\} / 2R^2T\right] \quad \text{(III.1)}$$

which is valid for normal incidence of the light beam on the sample surface in regions in which $\alpha\lambda << 1$, where λ is wavelength. The reflectivity R in Eq. (III.1) was calculated from the transmission T_o measured on the same spectrum in regions of negligible absorption (the flat regions of the spectrum of Fig. 20) via the equation

$$R = (1 - T_o)/(1 + T_o) \quad \text{(III.2)}$$

If $R^2 << 1$, as is the case for heavy metal fluoride glasses, Eq. (III.1) can be written in the following approximate form:

$$\alpha = (1/X)\ \ln(T_o/T) \qquad \text{(III.3)}$$

This equation leads to the following expression for the error in the absorption coefficient, $\Delta\alpha$:

$$\Delta\alpha = (1/X)(\Delta T/T) + (1/X)(\Delta T_o/T_o) + (\Delta X/X^2)\ \ln\ (T_o/T) \qquad \text{(III.4)}$$

where ΔX, ΔT and ΔT_o are the uncertainties in X, T and T_o. The sample thickness was measured with a micrometer, and the error in the measurement was estimated to be half of the smallest division of the micrometer ($\Delta X = 0.005$ cm). The error in the measurement of the transmissions T and T_o was estimated to be half of a small division of the chart paper used to record the IR spectra ($\Delta T = \Delta T_o = 0.005$).

III. 4.3. DSC Measurements

DSC scans were carried out using either a Perkin-Elmer Model DSC-2 or Dupont Model 990 differential scanning calorimeter (DSC) to determine the glass transition temperature, Tg, and the temperature of onset of crystallization, Tx, during heating. Glass samples were contained in sealed gold or aluminum DSC sample pans, and a heating rate of 10^oC/min was employed.

Measurements of heat capacity C_p were obtained using the Perkin-Elmer DSC-2 interfaced with a Cromemco Z-2 Computer by means of a digital voltmeter. The heat capacity was measured from -23^oC to above Tg, and a

heating rate of 10^{o}C/min was employed. Thirty readings of the DSC output per degree were taken. An average was taken of every six consecutive readings to give data points every 0.2^{o}C. Each twenty fifth data point was used to calculate the heat capacity at 5^{o}C intervals. Prior to C_p measurements each sample was given a prior thermal history by heating to $\sim 50^{o}$C above Tg and then cooling at 40^{o}C/min. A minimum of four DSC measurements on each of two different samples of each glass were carried out.

CHAPTER IV

GLASS-FORMING COMPOSITIONS, GLASS TRANSITION AND CRYSTALLIZATION TEMPERATURES

IV. 1. Glass Formation in the HfF_4-BaF_2-LaF_3 System

The glass-forming region in the system HfF_4-BaF_2-LaF_3 determined in our most recent set of studies is shown in Table XI and Fig. 12. The comments in the "Results" column of Table XI (and in the remainder of this thesis) indicate the following:

"very good glass" - glasses of good quality, inclusion-free to the eye, could be cast in thicknesses up to 3.5 mm.

"glass" - glasses containing a few crystalline inclusions or with slight surface devitrification, could be cast in thicknesses up to 3.5 mm.

"glass on fast quenching" - only thin glass specimens (< 1 mm) could be prepared by quenching between two brass plates; thicker samples showed substantial devitrification.

"not a glass" - even melts subjected to fast quenching were largely or wholly devitrified.

The compositions (as in the remainder of this thesis) are given in mole percent metal fluorides calculated from the masses of materials used in the batch. The glass-forming region shown in Fig. 12 encloses those compositions designated as "very good glass" in Table XI. All the glasses

Table XI. Compositions Tested For Glass Formation In The HfF_4-BaF_2-LaF_3 System.

Sample No.	mol % HfF_4	mol % BaF_2	mol % LaF_3	Results
29-8-80	75	20	5	not a glass
1-9-80	75	15	10	not a glass
30-8-80	72.5	22.5	5	glass on fast quenching
2-9-80	72.5	17.5	10	glass
1-8-80	70	30	0	glass on fast quenching
4-9-80	70	27.5	2.5	glass on fast quenching
31-7-80	70	25	5	glass
30-7-80	70	20	10	glass
3-9-80	70	17.5	12.5	glass
5-9-80	67.5	30	2.5	glass
13-8-80	67.5	27.5	5	glass
11-8-80	67.5	22.5	10	glass on fast quenching
16-7-80	65	35	0	glass on fast quenching
14-8-80	65	32.5	2.5	very good glass
19-7-80	65	30	5	very good glass
22-8-80	65	27.5	7.5	very good glass
20-8-80A	65	25	10	glass
27-8-80	65	22.5	12.5	glass
29-7-80	65	20	15	glass on fast quenching
21-8-80	62.5	27.5	10	glass
19-8-80	62.5	25	12.5	glass on fast quenching
4-8-80	62	33	5	very good glass
17-7-80	60	40	0	glass on fast quenching
8-8-80	60	37.5	2.5	glass
5-8-80	60	35	5	very good glass
24-7-80	60	30	10	very good glass
25-7-80	60	25	15	glass on fast quenching
28-8-80	57.5	37.5	5	glass
19-8-80A	57.5	35	7.5	glass
25-8-80	57.5	32.5	10	very good glass
15-8-80	57.5	30	12.5	glass
18-7-80	55	45	0	not a glass
22-7-80	55	40	5	not a glass
23-7-80B	55	35	10	not a glass
28-7-80	55	30	15	not a glass

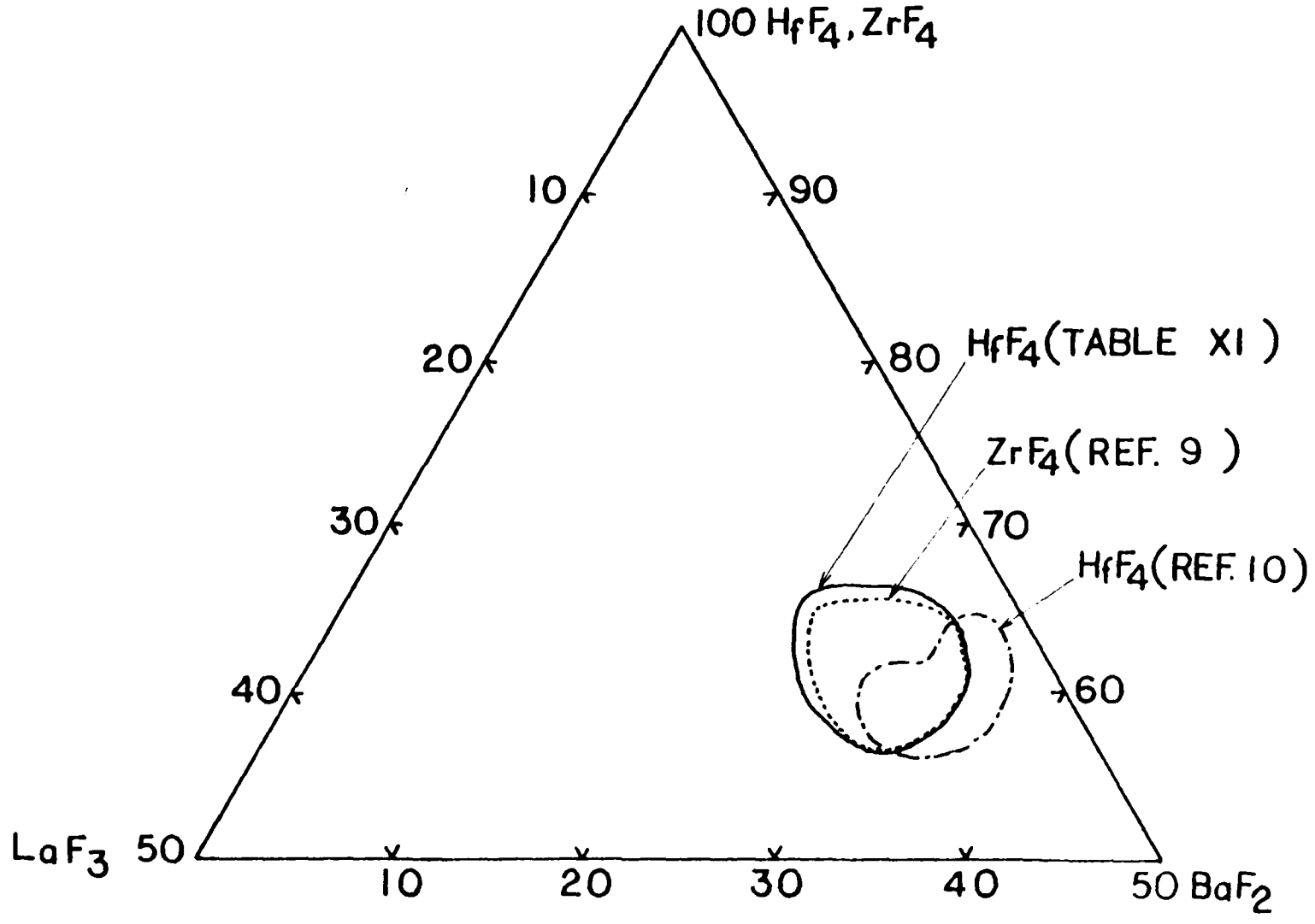
100 HfF4, ZrF4
10
90
20
80
30
70
40
60
50
LaF3
50 BaF2
10
20
30
40
HfF4 (TABLE XI)
ZrF4 (REF. 9)
HfF4 (REF. 10)

FIG. 12

in Table XI were melted in the open reactor under a N_2 atmosphere using oxides as starting materials. Fig. 12 also shows for comparison the glass-forming region in the ZrF_4-BaF_2-LaF_3 system, as reported by Lecoq, Poulain and Lucas [8]. The chemistries of Zr and Hf, which are both group IVB elements and both of which exhibit most commonly the +4 oxidation state, are virtually identical. This is due to the lanthanide contraction which makes the atomic radii (0.157 nm for both) and ionic radii (0.087 nm for Zr^{4+} vs. 0.084 nm for Hf^{4+}) nearly the same. Moreover, the single bond strengths (86 kcal/mol for HfF_4 and 85 kcal/mol for ZrF_4, Table II) and field strengths (0.78 for both, Table I) are also nearly equivalent. As expected from these chemical and physical similarities, the two glass-forming regions for the corresponding ZrF_4- and HfF_4-based glasses are also very similar.

IV. 2. Determination of Glass Formation for Other Compositions

Glass formation in other heavy metal fluoride glasses based on HfF_4 or on BaF_2/ThF_4 is reported in Tables XII and XIII. The results reported for HfF_4-BaF_2-LaF_3 compositions are from our earlier sutdies reported in Ref. 10 and are in agreement with the more extensive and definitive results of Table XI. The melts in Table XII were all prepared in the open reactor under a N_2 atmosphere using oxide starting materials. Those in Table XIII were prepared in the closed reactor under either inert or reactive atmosphere with fluoride starting materials. Recall, with regard to the reactive atmospheres, that "CCl_4" means CCl_4 entrained in a N_2 gas stream with the CCl_4 partial pressure approximately equal to the vapor pressure of liquid CCL_4 at ambient temperature, while "Cl_2"

Table XII. Compositions Tested For Glass Formation In HfF_4- and ZrF_4-Containing Systems

Sample No.	Composition (mol %)								Results
	HfF_4	ZrF_4	BaF_2	LaF_3	AlF_3	GdF_3	PbF_2	CsF	
6-12-79	65		30	5					glass on fast quenching
27-3-80	65		12			5	10	8	glass on fast quenching
26-3-80	65		10	5			12	8	very good glass
6-6-80	62		38						glass
11-12-79	62		35	3					glass
17-4-80	62		33	5					very good glass
12-12-79	62		30	8					glass
21-1-80	62		30	5				3	very good glass
12-6-80	62		30					8	glass
5-6-80	62		28	10					very good glass
7-1-80	62		28	5				5	very good glass
23-1-80	62		27	5			1	5	very good glass
16-1-80	62		26	5				7	very good glass
6-3-80	62		25			8		5	glass on fast quenching
17-1-80	62		25	5			3	5	very good glass
15-1-80	62		23	5				10	very good glass
20-3-80	62		15	5			10	8	very good glass
2-4-80	62		15	5	2		10	6	very good glass
3-4-80	62		15	5			18		glass
8-4-80	62		15				15	8	very good glass
9-4-80	62		15		2		15	6	not a glass
10-4-80	62		15	5			10	8	very good glass
3-6-80	62		10	10			10	8	glass on fast quenching
1-4-80	62		10	5	5		10	8	not a glass
31-3-80	62		10	5	15			8	not a glass
21-3-80	62			5			23	10	glass
16-6-80	62			5			23	10	glass
17-6-80	62			5			25	8	not a glass
9-6-80	60.3		27.2					12.5	glass on fast quenching

Table XII. Continued

Sample No.	Composition (mol %)								Results
	HfF_4	ZrF_4	BaF_2	LaF_3	AlF_3	GdF_3	PbF_2	CsF	
5-12-79	60		40						glass on fast quenching
30-11-79	60		35	5					glass
28-11-79	60		30	10					glass
29-11-79	57.5		33.75	8.75					glass
4-12-79	55		40	5					not a glass
16-5-80		62	33	5					very good glass

Table XIII. Compositions tested for glass formation in BaF_2/ThF_4-based systems

Sample No.	Composition (mol %)									Results
	BaF_2	ThF_4	ZnF_2	YbF_3	YF_3	LaF_3	GdF_3	MF	Atmosphere	
20-10-81	20	32	24	24					CCl_4	glass
27-10-81	20	32	24			24			CCl_4	not a glass
18-11-81	19	27	27	27					CCl_4	glass
30-10-81	19	27	27	27					CCl_4	glass
29-10-81	19	27	27	27					Ar	not a glass
9-11-81	19	27	27	13.5	13.5				CCl_4	glass
2-11-81	19	27	27	13.5		13.5			CCl_4	not a glass
10-11-81	19	27	27	20		7			CCl_4	not a glass
12-11-81	19	27	27	24		3			Cl_2	glass
17-11-81	19	27	27	22			5		Cl_2	glass
14-10-81	19	27	27		27				CCl_4	glass on fast quenching
5-11-81	19	27	27		27				CCl_4	not a glass
26-10-81	19	27	27			27			CCl_4	not a glass
16-11-81	19	27	27				27		Cl_2	not a glass
13-11-81	19	27	27		13.5	13.5			Cl_2	not a glass
20-11-81	19	27	27		13.5		13.5		Cl_2	not a glass
23-11-81	19	27	27		17		10		Cl_2	glass on fast quenching
24-11-81	19	27	27		22		5		Cl_2	glass on fast quenching
21-10-81	19	25	25		31				CCl_4	glass on fast quenching
28-1-82	18.05	25.65	25.65	25.65				5(Cs)	Cl_2	glass on fast quenching
2-2-82	18.05	25.65	25.65	25.65				5(K)	CCl_4	glass on fast quenching
8-3-82	15	25	25	25				10(Na)	Cl_2	glass
4-2-82	14	27	27	27				5(K)	CCl_4	glass on fast quenching
4-3-82	14	27	27	27				5(Na)	Cl_2	very good glass
24-3-82	14	27	27	27				5(Li)	Cl_2	very good glass
1-4-82	14	27	27	27				2.5(Li) 2.5(Na)	Cl_2	very good glass
9-3-82	10	27	27	27				9(Na)	Cl_2	very good glass
12-3-82	5	27	27	27				14(Na)	Cl_2	glass

means a Cl_2-N_2 mixture containing 3.5% Cl_2.

The optimum composition for glass formation in the HfF_4-BaF_2-LaF_3 system is roughly $62HfF_4$-$33BaF_2$-$5LaF_3$. As shown in Table XII, up to 10 mol% of the BaF_2 may be replaced by CsF and up to 18 mol% of the BaF_2 may be replaced by PbF_2 with no great sacrifice in glass forming ability. Replacement of BaF_2 by both CsF and PbF_2 is also possible. Addition of small amounts of AlF_3 into this system appears to aid glass formation; these melts during casting appear to be more viscous than the melts without AlF_3 and show a decreased tendency toward devitrification during casting. Assuming that $58HfF_4$- or $58ZrF_4$-$33BaF_2$-$5LaF_3$-$4AlF_3$ are the optimum compositions for glass formation in these systems, since they lie in the center of the HfF_4- or ZrF_4-BaF_3-LaF_3-AlF_3 glass forming region [36], many samples of this were prepared and used for studying glass properties.

In the nonfluorozirconate BaF_2/ThF_4-based system the $19\ BaF_2$-$27ZnF_2$-$27YbF_3$-$27ThF_4$ composition was taken as the optimum composition, again since it lies in the center of the glass forming region [17]. These melts are not as viscous as ZrF_4-containing fluoride melts at the liquidus temperature and show a greater tendency toward devitrification while casting. From Table XIII it can be seen that for the optimum BZnYbT glass some YbF_3 may be replaced by GdF_3 (up to 5 mol%), LaF_3 (up to 3 mol%) or YF_3 (up to 13.5 mol%). Addition of small amounts (5 mol%) of CsF or KF to this system prevented glass formation, however, substitution of BaF_2 by moderate amounts of NaF and/or LiF was possible. Replacement of BaF_2 by ~5 mol% NaF, LiF or $Na_{0.5}Li_{0.5}F$ improved

glass-forming ability and gave glasses of exceptional quality in terms of their clarity and freedom from inclusions.

IV. 3. Thermal Analysis

DSC scans for typical HfF_4- or ZrF_4-based and BaF_2/ThF_4-based glasses are shown in Figs. 2 and 13 respectively. The heating rate used in the DSC runs was $10^{\circ}C$/min. In Fig. 13 two traces are indicated for the glass. These were obtained simultaneously by monitoring the DSC output on two channels of a 2-pen recorder; the sensitivities of the two channels differed by a factor of 10. On the more sensitive channel (X10) a sizeable deviation is observed at the glass transition, while the peak of the crystallization exotherm is off scale. On the less sensitive channel (X1), the deviation at Tg is barely discernible, but the crystallization exotherm is entirely on scale. The glass transition temperature, Tg ($\sim 300^{\circ}C$ for most ZrF_4- and HfF_4-based glasses and $\sim 350^{\circ}C$ for BaF_2/ThF_4-based glasses) marks the temperature region in which the glass begins to exhibit liquid-like properties. The glass annealing temperature should be chosen to be a few degrees below Tg. All values of Tg reported in this study were taken as the extrapolated onset of the heat capacity change, as shown in Figs. 2 and 13.

The onset temperature, Tx, of the crystallization exotherm is of interest for two reasons: (1) it defines a safe upper limit for processing of the melt if devitrification is to be avoided, (2) the quantity (Tx - Tg) has frequently been used as a rough measure of the glass-forming ability of the melt, i.e., of resistance to devitrification during casting.

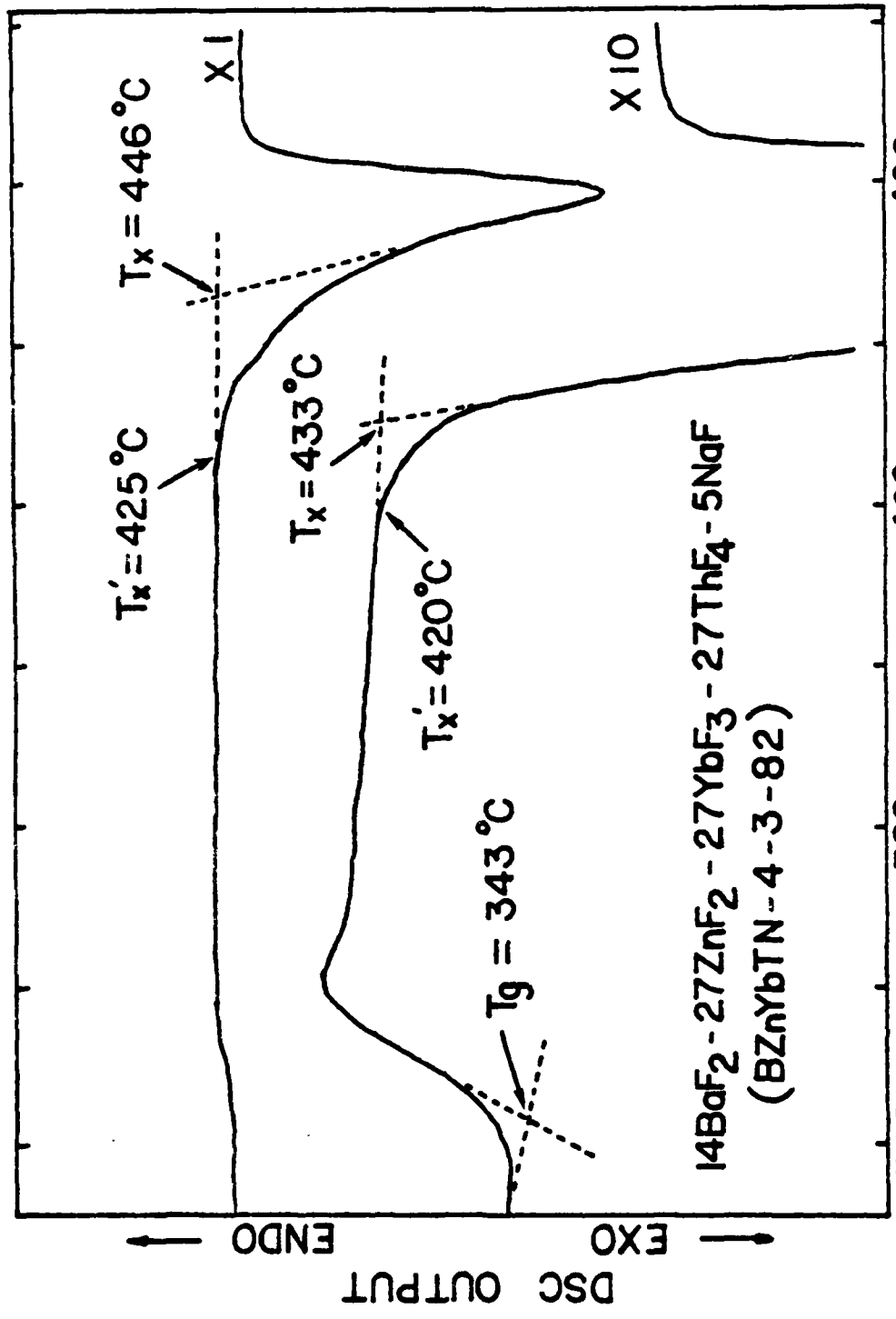
X1
X10
$T_x = 446°C$
$T_x' = 425°C$
$T_x = 433°C$
$T_x' = 420°C$
$T_g = 343°C$
$14BaF_2 - 27ZnF_2 - 27YbF_3 - 27ThF_4 - 5NaF$
(BZnYbTN-4-3-82)
ENDO
EXO
DSC OUTPUT
340
380
420
460
TEMPERATURE [°C]

FIG. 13

(Note that Tx is a temperature generally well below the liquidus at which the rate of crystallization becomes sizeable.) To achieve a large working range during operations such as fiber fabrication or the preparation of bulk glass articles it is desirable to have (Tx - Tg) as large as possible. (It is also desirable to have the liquidus temperature as low as possible.)

For a given DSC trace, there are two operationally significant definitions of the crystallization temperature; Tx' is the temperature at which the exotherm just commences, while Tx is the extrapolated onset (intercept of the leading edge of the crystallization exotherm and the base line). The measured values of Tx and Tx' for a given glass depend on the size of the crystallization exotherm as displayed on the DSC trace. Displaying the DSC trace on a larger scale plot will make the onset of the exotherm more perceptible. For example, in Fig. 13, Tx is 446°C measured using the X1 plot and 433°C when measured on the X 10 trace; similar variations arise in the determination of Tx'. The size of the displayed crystallization exotherm will increase with increases in the sensitivity settings on the DSC and the recorder, the heating rate, and the sample size. Note also that a change in heating rate alters the time scale allowed for crystallization at a given temperature. Since crystallization is a kinetic process, this will in itself change the measured value of Tx or Tx' [58]. In this study we report crystallization temperatures at the extrapolated onset, Tx, measured at a heating rate of 10°C/min and with other factors adjusted so as to keep the exotherm entirely on scale in the DSC display.

Values of Tg and Tx are listed in Tables XIV-XVI for a large number of glasses. The glasses in Tables XIV and XVI were included in Tables XII and XIII, while those in Table XV were melted at RADC. The comments in the "source of glass" column of Table XVI indicate the following:

"RADC" - glasses melted at Rome Air Development Center, Hanscom Air Force Base, MA.

"CUA/RPI" - glasses melted at the Catholic University of America (before September 1, 1981) and at Rensselaer Polytechnic Institute (after September 2, 1981)

"U.Rennes" - glasses melted at the University of Rennes, France

In Table XIV samples numbered 20-3-80, 22-4-80 and 23-4-80 are separately melted glass batches of the same composition; sample 20-3-80 was melted by using 97% HfO_2, the others using 99.999% HfO_2. Samples numbered 16-5-80, 20-5-80 and 21-5-80 are separately melted glasses of the same composition and same starting materials. In these two cases there is excellent agreement in the Tg and Tx values measured for samples of the same composition from different batches.

All of the fluorozirconate and fluorohafnate glasses in Table XIV exhibit Tg's of $\sim 300^{\circ}C$. Addition of CsF and/or PbF_2 at the expense of BaF_2 to a HfF_4-BaF_2-LaF_3 glass appears to lead to small decreases in Tg. From Tables XII and XIV there seems to be a fair correlation, such that melts which form a "very good glass" tend to have the larger (Tx - Tg)

Table XIV. Glass transition temperature Tg and temperatures of onset crystallization Tx measured at 10°C/min heating rate for ZrF_4- and HfF_4-based glasses.

	composition (mol %)										
Sample No.	HfF_4	ZrF_4	BaF_2	LaF_3	AlF_3	GdF_3	PbF_2	CsF	Tg(°C)	Tx(°C)	Tx-Tg (°C)
27-3-80	65		12			5	10	8	286	349	63
26-3-80	65		10	5			12	8	296	390	94
11-12-79	62		35	3					319	391	72
17-4-80	62		33	5					312	395	83
21-1-80	62		30	5				3	311	382	71
7-1-80	62		28	5				5	316	390	74
23-1-80	62		27	5			1	5	313	393	80
16-1-80	62		26	5				7	313	398	85
6-3-80	62		25			8		5	304	377	73
15-1-80	62		23	5				10	306	391	85
3-4-80	62		15	5			18		292	362	70
2-4-80	62		15	5	2		10	6	309	427	118
22-4-80	62		15	5			10	8	295	393	98
23-4-80	62		15	5			10	8	295	393	98
20-3-80	62		15	5			10	8	295	392	97
8-4-80	62		15				15	8	277	340	63
30-11-79	60		35	5					315	389	74
16-5-80		62	33	5					305	380	75
20-5-80		62	33	5					309	372	63
21-5-80		62	33	5					304	379	75

Table XV. Glass Transition Temperatures and Temperatures of Onset of Crystallization Measured at 10°C/min Heating Rate for Fluoride Glasses Melted at RADC.

	composition (mol %)													
Sample No.	ZrF_4	HfF_4	BaF_2	ThF_4	LaF_3	LuF_3	LiF	NaF	KF	RbF	CsF	Tg(°C)	Tx(°C)	Tx-Tg(°C)
063	53		22	7.7	4.2			4.37		4.37	4.37	296	384	88
045	53		22	7.7		4.2			4.37	4.37	4.37	300	376	76
058	53		22	7.7	4.2				4.37	4.37	4.37	304	382	78
046	57.37		22	7.7	4.2					4.37	4.37	303	402	99
033	60		27.5		7.5						5	300	374	74
062		53	22	7.7	4.2		2.62	2.62	2.62	2.62	2.62	298	397	99
059		53	22	7.7	4.2				4.37	4.37	4.37	312	389	77
065		53	22	7.7	4.2			4.37		4.37	4.37	302	403	101
029		56	22.5		6.5						15	295	375	80
028		56	22.5		6.5					15		299	367	68

Table XVI (a). Glass transition Temperatures and Temperatures of Onset of Crystalization Measured at 10°C/min Heating Rate For BaF_2/ThF_4-based glasses.
* Data from Fig. 15 of Ref. 17.

	Composition (mol %)											
Sample No.	BaF_2	ThF_4	ZnF_2	YbF_3	YF_3	LaF_3	GdF_3	LuF_3	Tg(°C)	Tx(°C)	Tx-Tg(°C)	Source of Glass
14-4-82	25	25	25	25					368	415	47	CUA/RPI
*5F	20.0	26.7	26.7	26.7					344	428	84	U. Rennes
265	19	27	27	27					364	440	76	RADC
21-1-82	19	27	27	27					356	455	99	CUA/RPI
17-11-81	19	27	27	22			5		359	435	76	CUA/RPI
12-11-81	19	27	27	24		3			357	411	54	CUA/RPI
6-11-81	19	27	27	13.5	13.5				365	429	64	CUA/RPI
314	19	26	26	26			3		359	414	55	RADC
318	19	26	26	26		3			358	416	58	RADC
2-4-82	16	28	28	28					349	454	105	CUA/RPI
6F	15.0	28.33	28.33	28.33					338	394	56	U. Rennes
6-4-82	14.0	28.7	28.7	28.7					349	446	97	CUA/RPI
13-4-82	10	30	30	30					345	448	103	CUA/RPI
161	17.5	30.0	26.5		26.0				348	408	60	RADC
274	19	27	27					27	353	452	99	RADC
296	19	25	25				6	25	357	443	86	RADC

AD-A122 359 METALLIC HALIDE OPTICAL GLASSES: SYNTHESIS AND CHARACTERIZATION OF IR TRA..(U) CATHOLIC UNIV OF AMERICA WASHINGTON DC C T MOYNIHAN ET AL. OCT 82 2/3

UNCLASSIFIED RADC-TR-82-264 F19628-81-K-0010 F/G 11/2 NL

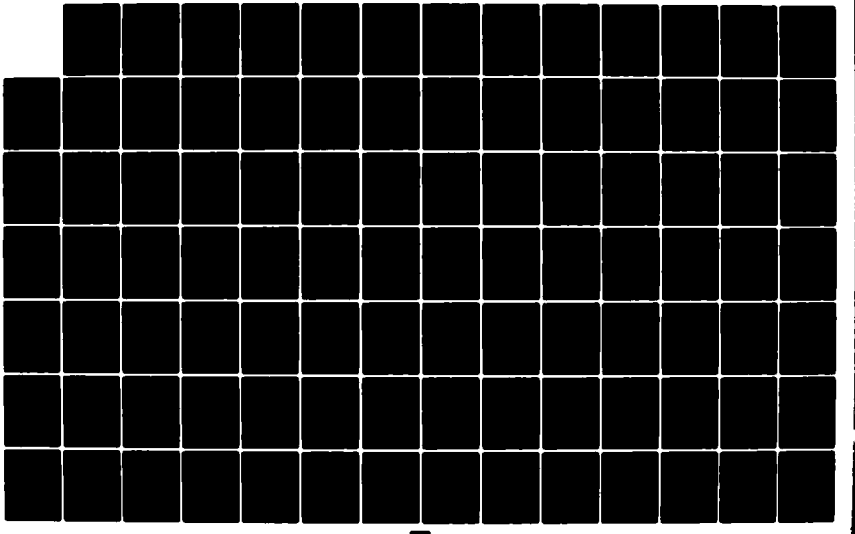

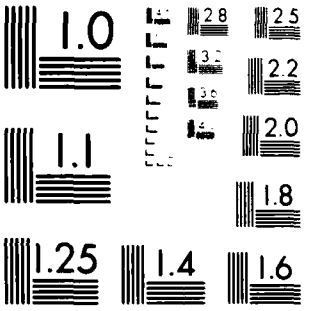

Table XVI (b). Glass Transition Temperatures and Temperatures of Onset of Crystallization Measured at 10°C/min heating rate for BaF_2ThF_4-based glasses.

	Composition (mol %)											
Sample No.	BaF_2	ThF_4	ZnF_2	YbF_3	YF_3	AlF_3	BiF_3	MF	Tg(°C)	Tx(°C)	Tx-Tg(°C)	Source of glass
15-6-82	20	25	25	25				5(Li)	338	424	86	CUA/RPI
17-6-82	20	25	25	25				5(Na)	350	412	62	CUA/RPI
15-6-82A	20	25	25	25				5(K)	358	408	50	CUA/RPI
16-6-82	20	25	25	25				2.5(Li) 2.5(Na)	341	424	83	CUA/RPI
169	20.0	22.5	28.75		14.38	14.38			354	494	140	RADC
163	20.0	22.5			28.75	28.75			449	525	76	RADC
307	19	26	26	26			3		354	445	91	RADC
28-1-82	18.05	25.65	25.65	25.65				5(Cs)	-	368	< 20	CUA/RPI
7F	14.42	27.24	27.24	27.24		3.85			350	459	109	U. Rennes
24-3-82	14	27	27	27				5(Li)	331	409	78	CUA/RPI
4-3-82	14	27	27	27				5(Na)	343	446	103	CUA/RPI
4-2-82	14	27	27	27				5(K)	347	414	67	CUA/RPI
1-4-82	14	27	27	27				2.5(Li) 2.5(Na)	333	437	104	CUA/RPI
9-3-82	10	27	27	27				9(Na)	337	426	89	CUA/RPI
12-3-82	5	27	27	27				14(Na)	320	394	74	CUA/RPI

values. Addition of CsF and PbF_2 to HfF_4-BaF_2-LaF_3 glasses increases (Tx - Tg). This is as expected, i.e., an improvement in glass-forming ability on increasing the number of melt components. The largest value of (Tx - Tg) in Table XIV is for sample 2-4-80 containing 2 mol% AlF_3; as noted before, small AlF_3 additions appear to enhance glass formation in these melts. The two glasses (6-3-80 and 27-3-80) in which LaF_3 has been replaced by GdF_3 have fairly low (Tx - Tg) values and form glasses only on fast quenching, suggesting that GdF_3 is deliterious to glass formation in these systems. The glasses in Table XV were melted at RADC using a technique very similar to that of open reactor melting described in Chapter III (Experimental Procedure) of this thesis. The Tg and (Tx - Tg) values are comparable to those for the glasses listed in Table XIV. From Table XV it appears that one reaches a point of diminishing returns in enhancement of glass-forming ability by going to a very large number of components, particularly if these are different alkali fluorides.

Tg and Tx for the BaF_2/ThF_4-based glasses are higher than those observed for fluorozirconate and fluorohafnate glasses (see Tables XIV-XVI). The quantity (Tx - Tg),however, is comparable to the ZrF_4/HfF_4-based glasses ($\sim 80^{\circ}C$) for several of the compositions in Table XVI. The glasses numbered 265, 21-1-82, 5F in Table XVI (a) are all of virtually the same nominal batch composition (which is close to the optimum glass-forming composition), but were prepared in three different laboratories. The Tg values for the three glasses cover a range of $20^{\circ}C$ while the (Tx - Tg) values cover a range of $23^{\circ}C$. Similarly glasses 2-4-82 and 6F

are of virtually identical compositions but they differ by 11°C in Tg and by 49°C in (Tx - Tg). The differences in Tg values are outside experimental error and probably reflect compositional differences (Recall that batch compositions are reported for all glasses). The scatter in (Tx - Tg) probably may be due to compositional differences or also to microscopic differences affecting crystal growth rates, e.g., the presence of small crystals or crystal nuclei formed on casting or undissolved raw materials, any of which could serve as sites for crystal growth on reheating.

As noted by Lucas et al. [14] in their study of the ternary systems, the glass-forming ability of BaF_2/ThF_4 glasses containing rare earth fluorides appears to increase with a decrease in the trivalent lanthanide cationic radius. Accordingly, since Yb and Lu lie next to one another in the lanthanide series and differ little in ionic radii (Yb^{3+} = 0.0858 nm, Lu^{3+} = 0.0850 nm), the quality of glasses of otherwise identical composition prepared with LuF_3 was very similar to those containing YbF_3 (Compare glasses numbered 265, 21-1-82 and 274). Similarly, it was not possible to replace YbF_3 with lighter lanthanides (e.g., LaF_3 or GdF_3) in concentrations greater than 3 or 5 mol% respectively and still form glasses. Even such small replacements reduced (Tx - Tg) (glasses 12-11-81 and 17-11-81), although the effect on (Tx - Tg) was not as pronounced in the corresponding LuF_3 containing glass (296).

CHAPTER V

HEAT CAPACITIES OF HEAVY METAL FLUORIDE GLASSES

V. 1. Experimental Results

Heat capacity measurements were carried out for five glass compositions given in Table XVII. Figs. 14-18 show the results of one heat capacity run for each of these glasses. The heat capacities were measured every 0.2 K (cf. section III. 4.3.), so a virtually continuous record of Cp as a function of temperature is obtained. Recall that the temperature range was covered in two DSC scans, one from 250 K to about 450 K and the other from 450 K to above the glass transition region. A small discontinuity or change of slope at 450 K in Figs. 14-18 marks the point where the low temperature DSC scan stopped and the high temperature scan started.

The abrupt rises in Cp which commence at ∿570-610 K mark the glass transitions for the various compositions. The glass transition temperatures Tg were taken at the extrapolated onset of this rise in Cp and are listed in Table XVIII. The glass heat capacity below Tg increased gradually with temperature and was in all cases described well by the expression:

$$Cp = A + BT + C/T^2 \qquad (V.1)$$

where A, B and C are constants. The liquid heat capacity was assumed to

Table XVII. Parameters For Fits Of Fluoride Glass And Liquid Heat Capacity To Equation: $Cp(cal/g.K) = A + BT(K) + C/T^2\ (K^2)$

Glass	Composition (mol %)	Temperature Range (K)	A	10^5B	10^{-2}C	Std. Dev. of Cp
ZBL	$62ZrF_4$-$33BaF_2$-$5LaF_3$ (glass)	250-530	0.1245	5.76	-11.7	0.0017
	(liquid)	605-615	0.239	——	——	0.0013
HBL	$62HfF_4$-$33BaF_2$-$5LaF_3$ (glass)	250-550	0.0974	3.97	- 9.1	0.0014
	(liquid)	620-630	0.179	——	——	0.0019
ZBLA	$58ZrF_4$-$33BaF_2$-$5LaF_3$-$4AlF_3$ (glass)	250-530	0.1185	6.66	- 9.8	0.0020
	(liquid)	620-630	0.235	——	——	0.0026
HBLA	$58HfF_4$-$33BaF_2$-$5LaF_3$-$4AlF_3$ (glass)	250-550	0.1002	3.57	-10.5	0.0012
	(liquid)	620-530	0.183	——	——	0.0014
BZnYbT	$15BaF_2$-$28.33ZnF_2$-$28.33YbF_3$-$28.33ThF_4$ (glass)	250-570	0.0945	3.89	- 6.6	0.0023
	(liquid)	645-655	0.174	——	——	0.0031

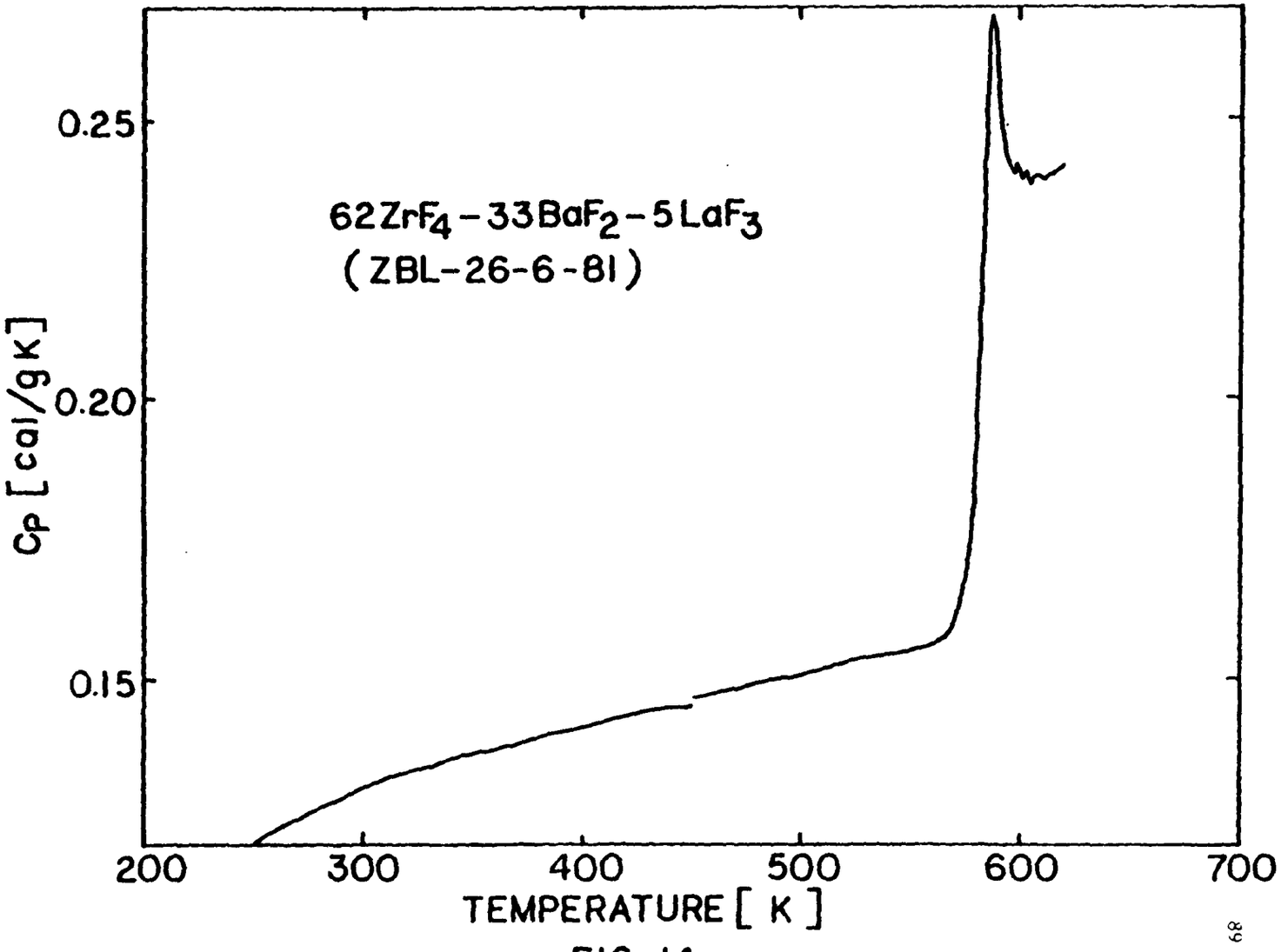
62ZrF4 – 33BaF2 – 5LaF3
(ZBL-26-6-81)
0.25
0.20
0.15
Cp [cal/g K]
200
300
400
500
600
700
TEMPERATURE [K]

FIG. 14

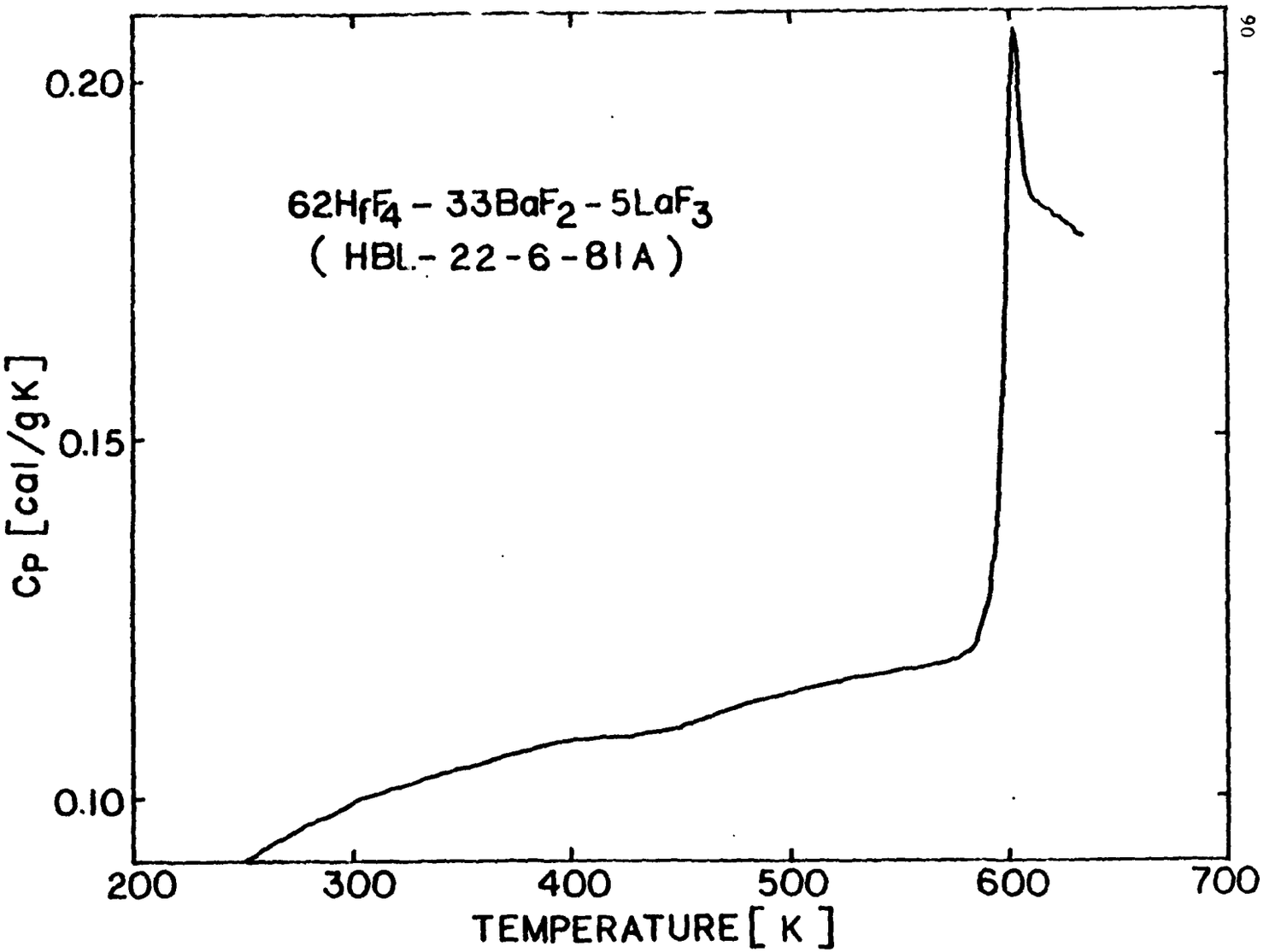
90
0.20
0.15
0.10
$62HfF_4 - 33BaF_2 - 5LaF_3$
(HBL.- 22-6-81A)
C_P [cal/g K]
200
300
400
500
600
700
TEMPERATURE [K]

FIG. 15

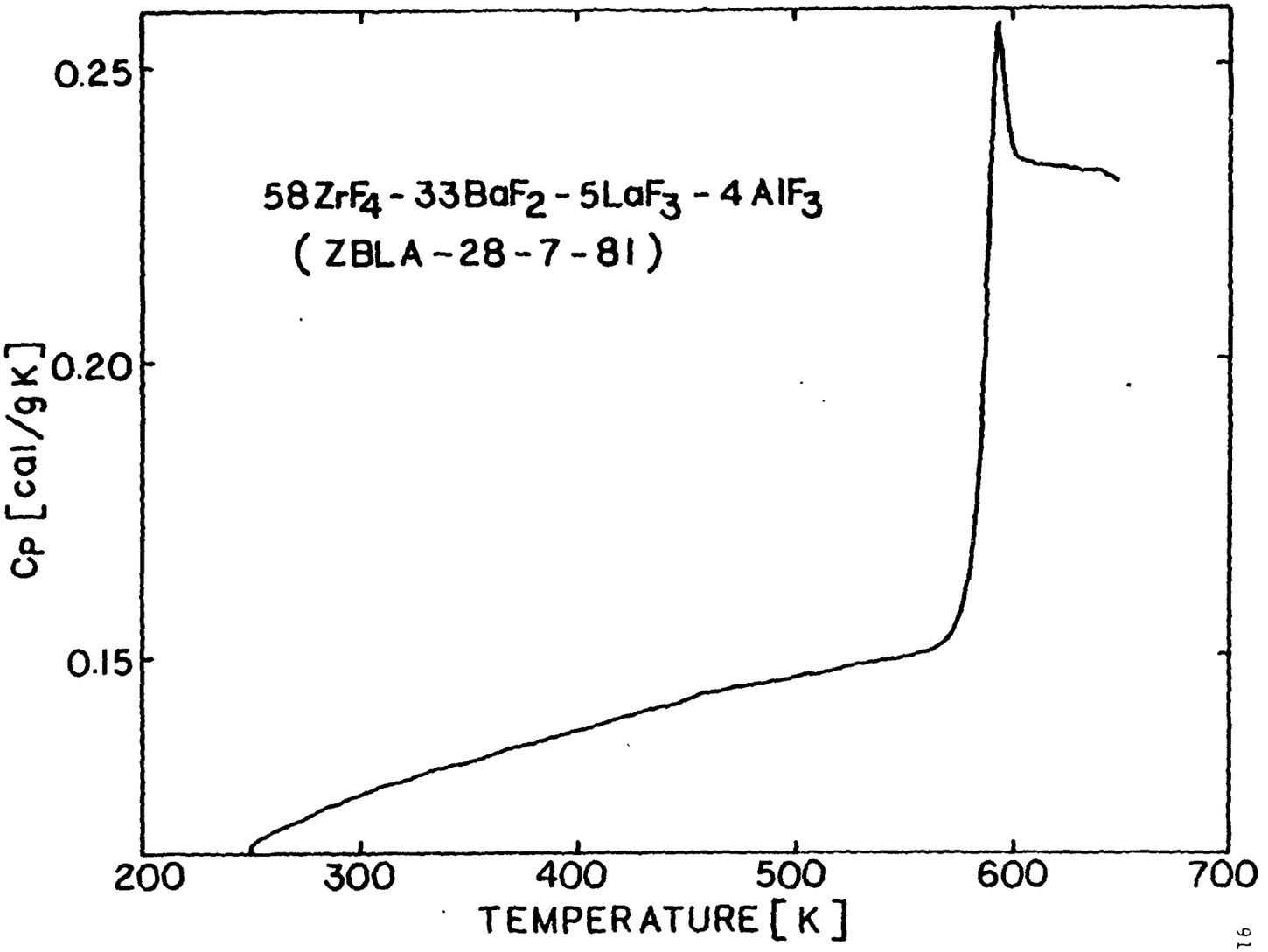
0.25
0.20
0.15
C_P [cal/g K]
$58ZrF_4 - 33BaF_2 - 5LaF_3 - 4AlF_3$
(ZBLA-28-7-81)
200
300
400
500
600
700
TEMPERATURE [K]

FIG. 16

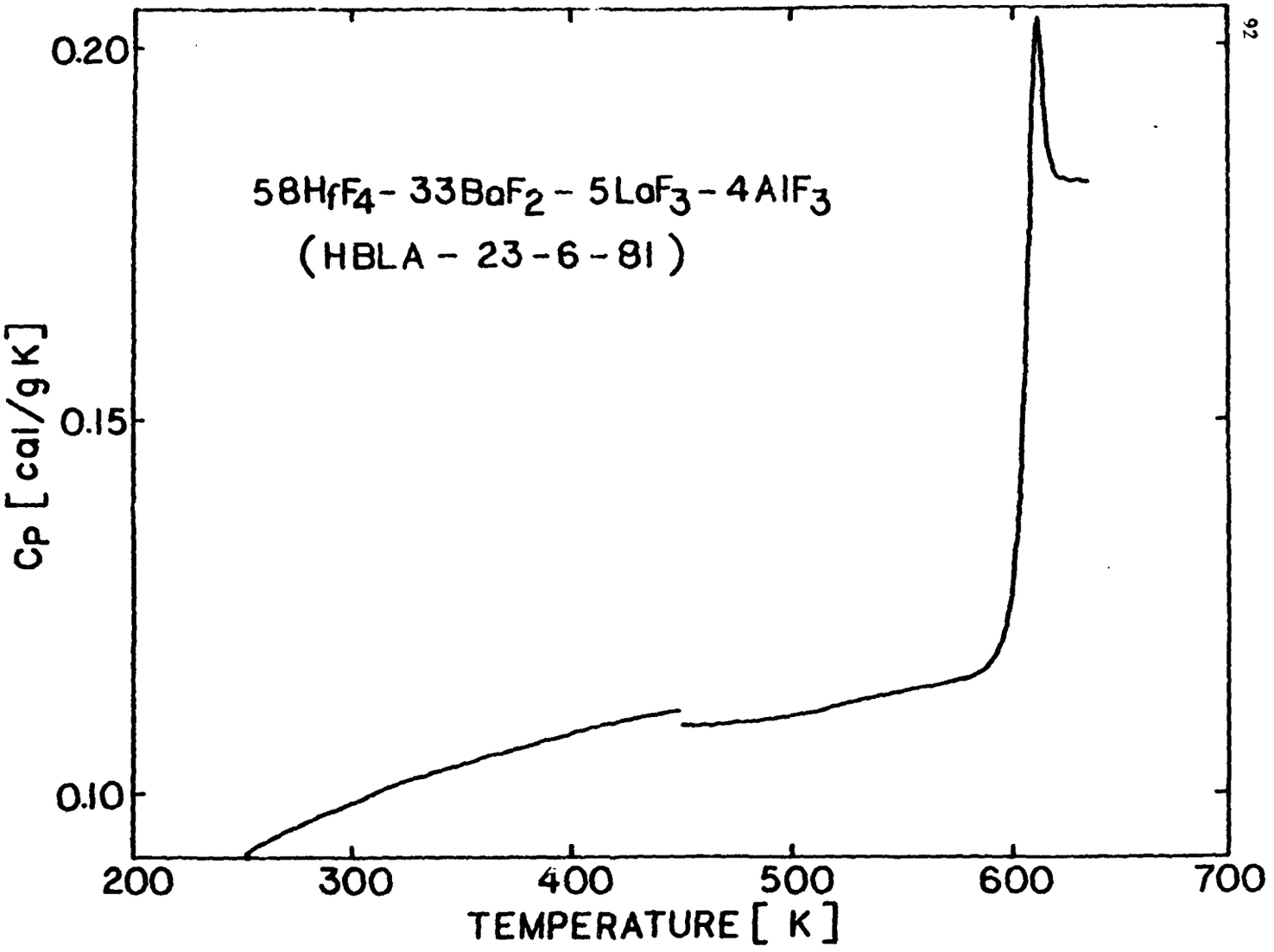
92
0.20
0.15
0.10
$58HfF_4 - 33BaF_2 - 5LaF_3 - 4AlF_3$
(HBLA - 23-6-81)
C_P [cal/g K]
200
300
400
500
600
700
TEMPERATURE [K]

FIG. 17

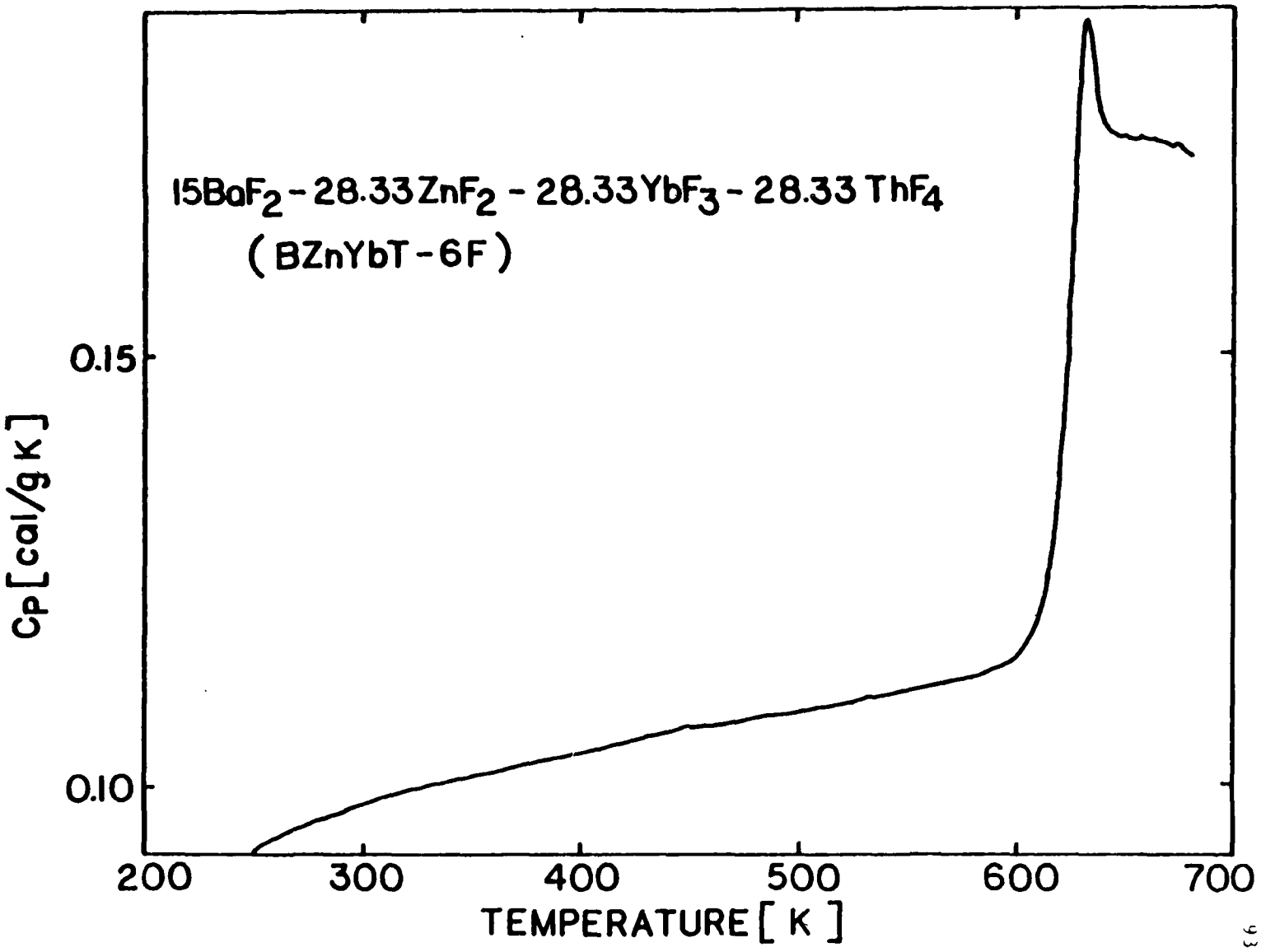
15BaF2 - 28.33ZnF2 - 28.33YbF3 - 28.33 ThF4
(BZnYbT-6F)
0.15
0.10
Cp [cal/g K]
200
300
400
500
600
700
TEMPERATURE [K]

FIG. 18

Table XVIII. Values of M, Tg, $\bar{C}p$ at 25°C and Tg-35°C θ_D, ν_D and $\Delta\bar{C}p$ for Fluoride Classes

Glass	M(g/g-at)	Tg(°C)	$\bar{C}p$(cal/g-at·K) at 25°C	$\bar{C}p$(cal/g-at·K) at Tg - 35°C	θ_D(K)	ν_D(cm^{-1})	$\Delta\bar{C}p$(cal/g-at·K)
ZBL	39.94	306	5.15	6.07	540	375	3.47
HBL	52.55	312	5.22	6.10	510	354	3.29
ZBLA	39.53	310	5.05	5.96	580	403	3.33
HBLA	51.44	312	5.11	5.99	550	382	3.41
BZnYbT	54.04	344	5.35	6.12	430	298	3.26

be temperature independent over the short interval above the glass transition in which it could be measured. The parameters of Eq. (V.1) characterizing the glass and liquid heat capcities were obtained from least square fits to the combined results from all the DSC measurements for each composition and are listed in Table XVII. The standard deviations from the least square fits indicate an accuracy of 1-2% in the Cp values.

The heat capacity per gram-atom $\bar{C}p$ is related to the heat capacity per gram Cp by

$$\bar{C}p = M\ Cp \qquad (V.2)$$

where M, given in Table XVIII, is the average atomic weight of the glass. Heat capacities of glasses are best compared on a "per gram-atom" basis, and $\bar{C}p$ values at 25°C and just below the transition region (at Tg - 35°C) are given in Table XVIII.

The $\bar{C}p$ values at 25°C for the ZrF_4- and HfF_4- containing glasses are all quite close, approximately 5.1 cal/g-at.K. This is in reasonable agreement with respective $\bar{C}p$ values of 5.0 and 5.5 cal/g-at.K reported for $60ZrF_4$-$7ThF_4$-$33BaF_2$ and $60HfF_4$-$7ThF_4$-$33BaF_2$ glasses at 45°C by Robinson et al. [31]. $\bar{C}p$ at 25°C for the BZnYbT glass is a bit higher than that for the other glasses in Table XVII. For engineering purposes, however, it appears that a $\bar{C}p$ value of 5.2 cal/g-at.K may be used to estimate within a few percent the ambient temperature heat capacity of any heavy metal fluoride glass of the general type studied here.

V. 2. Vibrational Contributions to Glass Heat Capacities

Near Tg the glass $\bar{C}p$ values approach but do not exceed, within experimental error, the Dulong-Petit limit of 3R(= 5.97 cal/g-at.K) for the vibrational heat capacity of solids where R is the ideal gas constant. This has also been found to be the case for other inorganic glasses in which the bonding is predominantly of one type [34,91-94]. Vibrational contributions to the heat capacity should be discussed in terms of the constant volume heat capacity, $\bar{C}v$, which is related to $\bar{C}p$ by the expression:

$$\bar{C}p/\bar{C}v = 1 + (\alpha_v^2 T/\rho \kappa_s Cp) \qquad (V.3)$$

where α_v is the volume coefficient of thermal expansion, ρ the density and κ_s the adiabatic compressibility. Values of these last quantities (Table XIX) were obtained or estimated from previous reports [17,26,43] and used to calculate $\bar{C}v$ for the present glasses. $\bar{C}v$ was only about 3% less than $\bar{C}p$ near Tg and correspondingly closer to $\bar{C}p$ at lower temperatures. A plot of $\bar{C}v$ versus temperature is shown in Fig. 19 for the ZBLA glass.

$\bar{C}v$ values for the various glasses were fitted to the Debye heat capacity function, using the characteristic Debye temperature, θ_D, as a variable:

$$\bar{C}_v = 9R(T/\theta_D)^3 \int_0^{\theta_D/T} \left[x^4 \exp(-x)/(1-\exp(-x))^2 \right] dx \qquad (V.4)$$

Table XIX. Density, Thermal Expansion Coefficient And Adiabatic Compressibility Data For Heavy Metal Fluoride Glasses. Values in Parentheses Are Estimated From Data On Glasses Of Similar Composition.

Composition	$\rho(g/cm^3)$	$10^7 \alpha_v(K^{-1})$	$10^{11} \kappa_s(Pa^{-1})$
ZBL	4.79	564	(2.08)
HBL	5.78	546	(2.08)
ZBLA	(4.61)	(582)	2.08
HBLA	(5.88)	(552)	2.08
BZnYbT	(6.43)	(453)	(2.08)

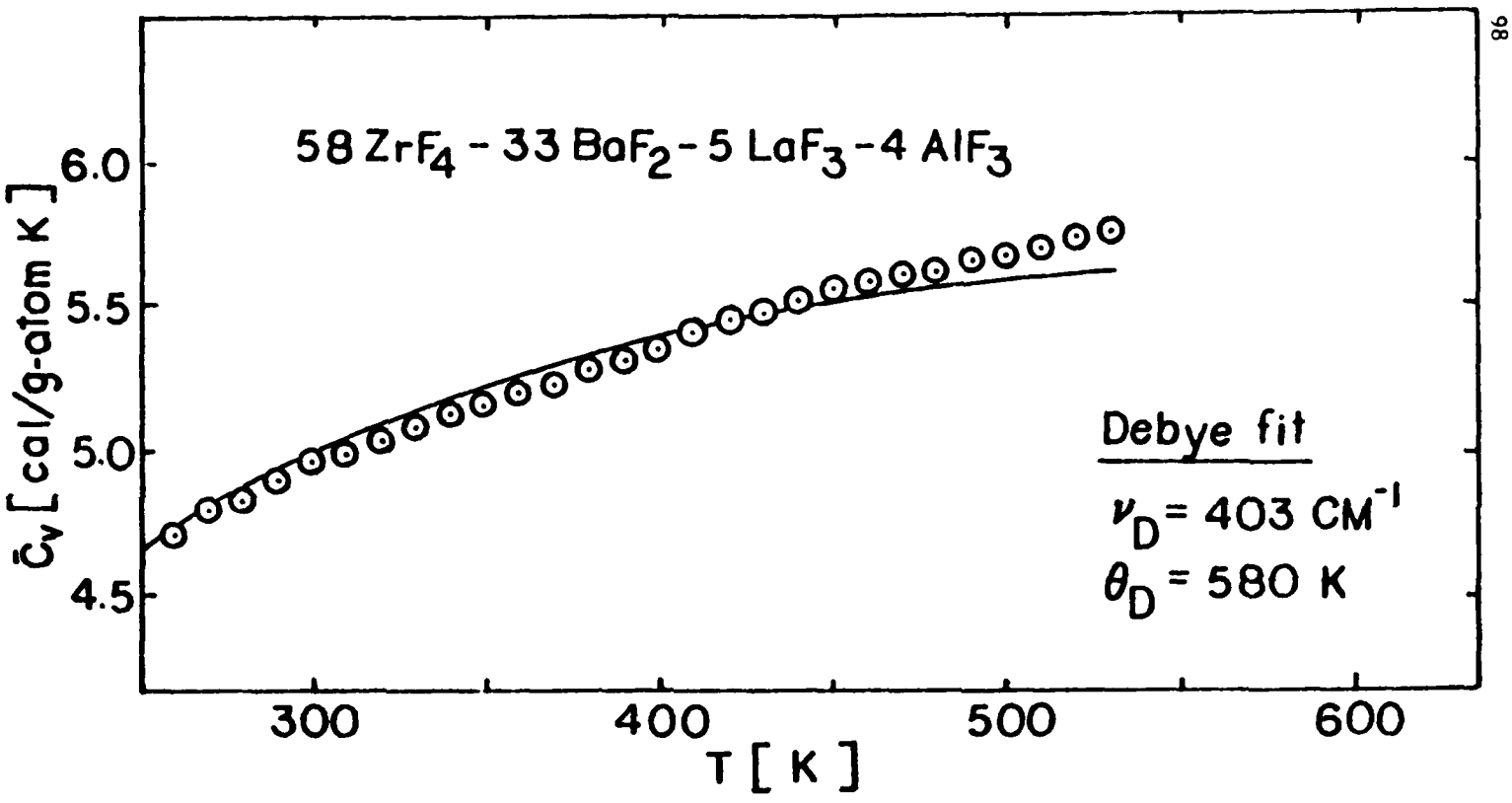
58 ZrF4 - 33 BaF2 - 5 LaF3 - 4 AlF3
Debye fit
νD = 403 CM-1
θD = 580 K
C̄v [cal/g-atom K]
6.0
5.5
5.0
4.5
300
400
500
600
T [K]

FIG. 19

Θ_D values, along with the values of the corresponding Debye-frequency

$$\nu_D = k\,\Theta_D/h \qquad (V.5)$$

where k and h are respectively the Boltzmann and Planck constants, are listed in the Table XVIII. The solid line in Fig. 19 is the best fit Debye curve for the ZBLA glass; corresponding curves for the other glasses were similar in appearance. Standard deviations of the data from the Debye curves were about 2%, i.e., very nearly within experimental error, but in all cases the Debye curves underestimated $\bar{C}v$ slightly at the higher temperatures near Tg. This may be because the Debye density of vibrational states is only a crude approximation to the real density of states in these glasses or, equally likely, $\bar{C}v$ at higher temperatures contains contributions from sub-Tg secondary structural relaxations.

The Debye frequencies for the ZBL, HBL, ZBLA and HBLA glasses are all the same within experimental error, about 380 cm^{-1}. This is, as expected, lower than the high frequency fundamental Zr-F or Hf-F stretching vibration at about 500 cm^{-1} which dominates the IR spectra of these glasses [76], since other nearest neighbor vibrations (e.g., Ba-F, La-F) of lower frequency will also contribute to this heat capacity. The Debye frequency of the BZnYbT glass, 298 cm^{-1}, is lower than those for the ZrF_4- and HfF_4- containing glasses, in line with the correspondingly lower value (about 400 cm^{-1}) of the frequency of the strong IR fundamental and the extended IR transparency at long wavelengths of the BZnYbT

glass [95]. The Debye frequencies and temperatures of all of the glasses are sufficiently low (compared to, e.g., oxide glasses) that even the ambient temperature heat capacities are not far from the 3R per gram-atom limit, which accounts for the close agreement of the 25°C $\bar{C}p$ values in Table XVIII.

V. 3. Structural Contribution to the Heat Capacity

$\Delta\bar{C}p$, the difference between the liquid and glass heat capacities at Tg, is listed in Table XVIII and is roughly the same for all the glasses, about 3.4 cal/g-at.K. This is much larger than $\Delta\bar{C}p$ for typical network oxide glasses (1.1 to 1.8 cal/g-at.K) [34,91,93] and comparable in size to $\Delta\bar{C}p$ observed for chalogenide glasses [91,93,94]. $\bar{C}p$ is generally thought to reflect the energy required to effect changes in the liquid structure (e.g., bond breaking) with increasing temperature above Tg. The larger values of $\Delta\bar{C}p$ for the heavy metal fluoride glasses thus presumably indicate that substantial changes in the melt structure are occurring in the temperature range just above Tg.

CHAPTER VI

INFRARED ABSORPTION, PROCESSING CONDITIONS AND GLASS QUALITY-PRELIMINARY DISCUSSION

VI. 1. General Features of IR Spectra

IR absorption spectra were recorded for most of glasses in the region of 250-4000 cm^{-1}. Typical results for a fluorohafnate glass are shown in Fig. 20. The flat, upper spectrum (close to the 100% transmission level) was recorded with no sample in the beam and is used to assess the degree to which the 100% transmission line changes with wavelength. (Recall that the open beam transmission is set to read 100% at 1250 cm^{-1}.) The discontinuity at about 2000 cm^{-1} is due to a grating change. The lower spectrum was taken with the sample in the beam and also shows the discontinuity at 2000 cm^{-1}.

In Fig. 20 T_o is the transmission in a flat region of the spectrum where apparent losses are due only to reflection. Note that because of the grating change different values of T_o need to be used above and below 2000 cm^{-1}. The prominant broad absorption peak in the sample at about 3400 cm^{-1} (2.7 - 3.4 μm) is due to -OH, and the gradual decrease in transmission below about 1800 cm^{-1} is due first to surface H_2O and oxide impurity and later to intrinsic multiphonon absorption [8,10,74]. Multiphonon absorption causes the sample to become opaque (0% transmission) below about 1000 cm^{-1}. The multiphonon edge tends to be fairly featureless, although shoulders are found around $\sim$1400 cm^{-1} and $\sim$1600 cm^{-1} in many specimens. The shoulder at $\sim$1400 cm^{-1} is thought to be caused

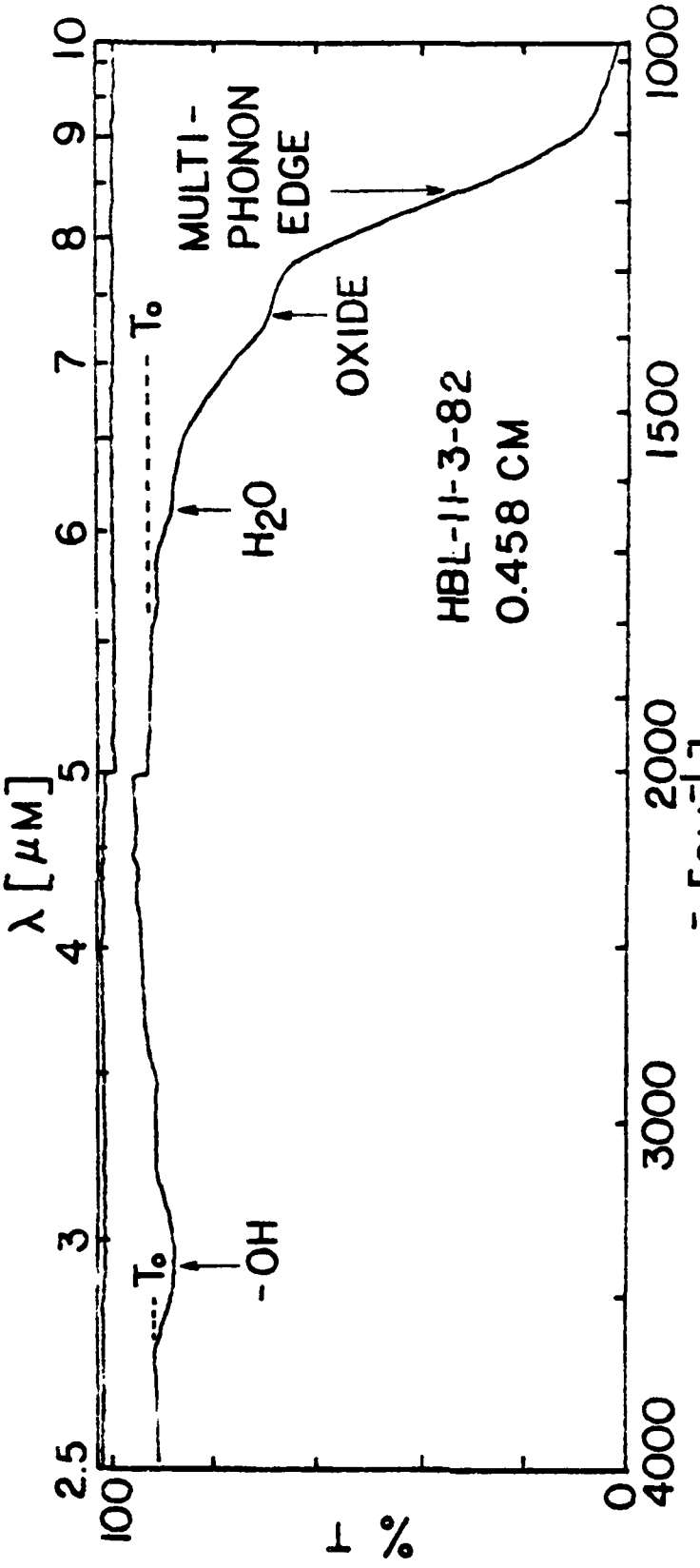
λ [μM]
2.5
3
4
5
6
7
8
9
10
T %
100
0
4000
3000
2000
1500
1000
ν̃ [CM⁻¹]
T₀
-OH
T₀
H₂O
MULTI-
PHONON
EDGE
OXIDE
HBL-11-3-82
0.458 CM

FIG. 20

by oxide impurities, while the one at ~1600 cm^{-1} corresponds to the bending vibration of water molecules. In addition to the above absorptions, weak, poorly resolved absorption bands are sometimes observed at ~2900 cm^{-1} due to C-H vibrations of organic surface contaminants.

The remainder of this thesis will mainly be concerned with effects of glass composition and processing conditions on the IR spectra, with particular attention being paid to the features noted above.

VI. 2. Study of Processing Conditions

Three standard compositions of ZBL ($62ZrF_4$-$33BaF_2$-$5LaF_3$), HBL ($62HfF_4$-$33BaF_2$-$5LaF_3$) and ZBLA ($58ZrF_4$-$33BaF_2$-$5LaF_3$-$4AlF_3$) glasses were selected in order to investigate the effect of processing conditions on the quality of glass and especially on the IR spectrum. Tables XX-XXII contain data on the glass quality for the standard ZBL, HBL and ZBLA glasses prepared under different processing conditions. The glasses designated 074, 080, 081 and 083 were prepared at RADC. The starting materials were the metal fluorides, except for the glasses marked "oxide" in the "Remarks" column of the tables, which were prepared from the oxides (e.g., ZBL-25-9-80). The crucible and lid materials used are also given, together with the type of atmosphere ("Atmos.") used for melting and the corresponding gas flow rates in L/min. Glasses prefluorinated with $NH_4F{\cdot}HF$ are indicated with an "X" in the "$NH_4F{\cdot}HF$" column, and temperatures listed are the final melting temperatures. Thicknesses were measured at the center of the samples through which the spectrometer beam passed, and the values of T_o listed were those for the flat region of the IR spectrum below 2000 cm^{-1} (cf. Fig. 20),

Table XX. Values of Thickness, T_o, α at 1400 cm^{-1}, $\ln(T_o/T)$ at 3400 cm^{-1} and appearance of $62ZrF_4$-$33BaF_2$-$5LaF_3$ Glasses Prepared Under Various Processing Conditions.
(Appearance; C-clear, B-black, G-gray, P-pink, W-white, Y-yellow, S-slight, I-inclusion)

Sample No.	Crucible + lid	Temp. (°C)	Atmos. (L/min)	NH_4F·HF	Reactor	Thickness (cm)	T_o	$\alpha(cm^{-1})_{-1}$ @ 1400cm	$\ln(T_o/T)_{-1}$ @ 3400 cm	Remarks
2-10-80	pt,pt	760	N_2(2.0)	X	open	0.351	0.895	—	0.029	C, oxide, ZBL-1 [96]
16-5-80	pt,pt	760	N_2(2.0)	X	open	0.244	0.93	1.26 ± 0.1	0.008	C, oxide, ZBL-2 [96]
12-9-80	pt,pt	760	N_2(2.0)	X	open	0.259	0.94	1.48 ± 0.09	0.013	C, oxide, ZBL-4 [96]
25-9-80	pt,pt	760	N_2(2.0)	X	open	0.254	0.92	1.38 ± 0.09	0.034	C, oxide, ZBL-5 [97]
29-1-81	pt,pt	750	N_2(0.5)		open	0.415	0.93	1.4 ± 0.06	0.027	C, WI
4-2-81	pt,pt	730	N_2(0.5)		open	0.395	0.908	1.56 ± 0.06	0.036	SP, WI
13-7-81	vc,pt	800	N_2(0.2)		open	0.229	0.925	1.34 ± 0.09	0.028	WI, BI
14-7-81	vc,pt	800	N_2(0.2)	X	open	0.398	0.93	1.12 ± 0.06	0.030	SWI, SBI
083	pt,pt	800	CCl_4(0.1)	X	open	0.333	0.92	1.13 ± 0.07	0.01	Y, oxide, ZBL-3 [96,97]
29-1-81A	pt,pt	750	CCl_4(0.5)		open	0.381	0.867	1.13 ± 0.06	0.01	SP, SWI
30-1-81	pt,pt	750	CCl_4(0.5)		open	0.396	0.912	1.46 ± 0.07	0.043	C, (melting finished under N_2)
21-7-81	vc,pt	800	CCl_4(0.1)	X	open	0.347	0.925	1.01 ± 0.06	0.025	SWI
27-1-81	vc,pt	800	CCl_4(0.2)	X	open	0.223	0.874	0.87 ± 0.09	0.006	BI
24-7-81	vc,pt	800	Cl_2(0.2)		open	0.268	0.97	1.03 ± 0.07	0.017	SWI
27-7-81	vc,pt	800	Cl_2(0.2)	X	open	0.382	0.92	0.97 ± 0.06	0.017	SY
7-7-81	vc,vc	800	N_2(0.5)		closed	0.234	0.842	1.35 ± 0.1	0.010	G
7-7-81A	vc,vc	800	N_2(1.0)		closed	0.223	0.92	1.45 ± 0.1	0.017	SWI
18-2-82	vc,vc	850	N_2(0.2)	X	closed	0.249	0.69	0.9 ± 0.1	0.018	PG, BI
23-2-82	vc,vc	850	N_2(0.2)	X	closed	0.248	0.75	1.29 ± 0.1	0.008	WI
8-10-81	vc,vc	800	CCl_4(0.2)	X	closed	0.329	0.87	0.86 ± 0.06	0.021	Y, WI, BI, CCl_4 bubble
9-2-82	vc,vc	850	CCl_4(0.2)	X	closed	0.219	0.90	1.05 ± 0.09	0.005	C
3-3-82	vc,vc	800	CCl_4(0.2)		closed	0.261	0.85	0.87 ± 0.08	0.006	SWI
15-6-81	vc,vc	850	Cl_2(0.2)		closed	0.249	0.915	1.38 ± 0.09	0.016	SWI
26-6-81	vc,vc	800	Cl_2(0.5)		closed	0.234	0.92	1.35 ± 0.09	0.016	C
4-8-81	vc,vc	800	Cl_2(0.2)	X	closed	0.375	0.87	1.47 ± 0.07	0.025	SWI
11-8-81	vc,vc	800	Cl_2(0.2)	X	closed	0.342	0.875	1.43 ± 0.08	0.023	SWI
14-12-81	vc,vc	850	Cl_2(0.2)	X	closed	0.632	0.805	1.35 ± 0.05	0.030	C, unpolished
16-12-81	vc,vc	870	Cl_2(0.2)	X	closed	0.658	0.88	1.19 ± 0.04	0.031	SY, unpolished

Table XXI. Values of Thickness, T_o, α at 1400 cm^{-1}, $\ln(T_o/T)$ at 3400 cm^{-1} and Appearance of $62HfF_4$-$33BaF_2$-$5LaF_3$ Glasses Prepared Under Various Processing Conditions. *Composition is $60HfF_4$-$35BaF_2$-$5LaF_3$. (Appearance; C-clear, Y-yellow, G-gray)

Sample No.	Crucible + lid	Temp. (°C)	Atmos. (L/min)	$NH_4F{\cdot}HF$	Reactor	Thickness (cm)	T_o	$\alpha(cm^{-1})$ @ 1400 cm^{-1}	$\ln(T_o/T)_{-1}$ @ 3400 cm^{-1}	Remarks
*5-8-80A	pt,pt	800	N_2(2.0)	X	open	0.226	0.965	1.42 ± 0.1	0.039	C, oxide, HBL-1 [96]
11-9-80	pt,pt	800	N_2(2.0)	X	open	0.152	0.944	1.25 ± 0.13	0.016	C, oxide, HBL-5 [97]
11-9-80B	pt,pt	800	N_2(2.0)	X	open	0.245	0.90	0.94 ± 0.8	0.0371	C, oxide
080	pt,pt	800	CCl_4(0.1)	X	open	0.058	0.93	1.09 ± 0.25	0.016	Y, oxide, HBL-3 [97]
081	pt,pt	800	CCl_4(0.1)	X	open	0.236	0.935	1.05 ± 0.09	0.027	Y, oxide, HBL-2 [96]
074	pt,pt	800	CCl_4(0.2)	X	open	0.243	0.90	0.64 ± 0.08	—	Y, oxide, HBL-4 [97]
6-4-82	vc,pt	850	CCl_4(0.2)	X	open	0.318	0.875	0.83 ± 0.07	0.030	C
22-6-81	vc,vc	800	CCl_4(1.0)	X	open	0.381	0.88	1.09 ± 0.06	0.095	G, CCl_4 from bottom
9-4-82	vc,pt	880	CCl_4(0.5)	X	open	0.302	0.895	1.29 ± 0.08	0.006	C
25-3-82	vc,pt	850	Cl_2(0.2)	X	open	0.353	0.88	1.22 ± 0.07	0.008	C
3-12-81	vc,vc	870	Cl_2(0.2)	X	closed	0.456	0.88	0.99 ± 0.05	0.008	C
11-3-82	vc,vc	880	Cl_2(0.2)	X	closed	0.458	0.89	1.05 ± 0.05	0.045	C

Table XXII. Values of Thickness, T_o, α at 1400 cm^{-1}, $\ln(T_o/T)$ at 3400 cm^{-1} and Appearance of $58ZrF_4$-$33BaF_2$-$5LaF_3$-$4AlF_3$ Glasses Prepared Under Various Processing Conditions.
(Appearance; C-clear, B-black, G-gray, P-pink, W-white, Y-yellow, S-slight, I-inclusion)

Sample No.	Crucible + lid	Temp. (°C)	Atmos. (L/min)	$NH_4F \cdot HF$	Reactor	Thickness (cm)	T_o	$\alpha(cm^{-1})$ @ 1400 cm^{-1}	$\ln(T_o/T)$ @ 3400 cm^{-1}	Remarks
13-7-81	vc,pt	800	N_2(0.5)		open	0.156	0.855	2.15 ± 0.16	0.025	WI
14-7-81	vc,pt	775	N_2(0.2)	X	open	0.256	0.92	1.8 ± 0.09	0.062	SWI
21-7-81	vc,pt	800	CCl_4(0.1)	X	open	0.383	0.935	1.61 ± 0.06	0.031	SWI
22-7-81	vc,pt	800	CCl_4(0.1)		open	0.289	0.88	1.59 ± 0.08	0.035	SP, BI
8-2-82	vc,pt	850	CCl_4(0.2)	X	open	0.194	0.779	1.46 ± 0.13	0.003	WI
10-2-82	vc,pt	860	CCl_4(0.2)	X	open	0.237	0.855	1.28 ± 0.1	0.010	C
27-7-81	vc,pt	800	Cl_2(0.2)		open	0.387	0.76	1.86 ± 0.08	0.035	WI
28-7-81	vc,pt	800	Cl_2(0.2)	X	open	0.405	0.93	1.74 ± 0.06	0.055	SY, WI
5-2-81	vc,pt	850	Cl_2(0.2)	X	open	0.204	0.894	1.72 ± 0.12	0.009	C
6-7-81	vc,vc	800	N_2(1.0)		closed	0.226	0.885	1.82 ± 0.11	0.008	G, BI
9-7-81	vc,vc	800	N_2(1.0)		closed	0.224	0.885	1.8 ± 0.11	0.011	G, BI
19-11-81	vc,vc	880	N_2(0.2)	X	closed	0.127	0.508	1.46 ± 0.29	0.011	G, SBI
22-2-82	vc,vc	880	N_2(0.2)	X	closed	0.243	0.86	1.86 ± 0.1	0.007	SG
26-5-81	vc,vc	800	CCl_4(0.2)		closed	0.199	0.854	1.65 ± 0.12	0.018	P, CCl_4 bubble
28-5-81	vc,vc	800	CCl_4(0.2)		closed	0.158	0.895	1.68 ± 0.14	0.012	SP, CCl_4 bubble
16-2-82	vc,vc	850	CCl_4(0.2)	X	closed	0.226	0.865	1.95 ± 0.11	0.003	SY
25-6-81	vc,vc	800	Cl_2(0.2)		closed	0.250	0.895	1.9 ± 0.1	0.022	SWI
3-8-81	vc,vc	800	Cl_2(0.2)	X	closed	0.248	0.87	2.02 ± 0.11	0.039	C
12-8-81	vc,vc	800	Cl_2(0.2)	X	closed	0.318	0.865	1.94 ± 0.09	0.024	SWI
22-12-81	vc,vc	880	Cl_2(0.2)	X	closed	0.658	0.88	1.73 ± 0.11	0.065	SY, unpolished
11-2-82	vc,vc	860	Cl_2(1.0)	X	closed	0.230	0.87	1.75 ± 0.11	0.007	Y, SWI

since the 100% transmission was set on the spectrometer scale in this region. The values of absorption coefficient ϵ at 1400 cm^{-1} and $\ln(T_o/T)$ at 3400 cm^{-1} are useful for comparing the respective oxide and -OH impurities in the glasses. Properties of some of glasses have been reported in earlier publications on bulk and surface -OH absorption [96] and influence of processing conditions on IR edge absorption [97]; the glass sample designations ("ZBL-1", "HBL-5", etc.) used in these papers are given in the "Remarks" column.

VI. 3. Effect of Processing Conditions on Glass Quality and Appearance

The appearances of the glasses listed in Tables XX-XXII are described in terms of their color and whether or not inclusions are present using the acronyms given at the top of tables. For example, "SWI" means "slight (amounts of) white inclusions", "BI" means "black inclusions", and "SP" means "slight pink (color)". For ZrF_4-containing glasses melted under inert atmosphere (N_2), the melts which were kept for lengthy periods at the melting temperatures contained many black inclusions or were gray in color, possibly due to the reduction of zirconium (IV) to zirconium (II) [32]. When appropriate amounts of a reactive atmosphere (CCl_4 or Cl_2) were introduced during melting, no black inclusions were formed. Presumably chlorine reoxidizes any reduced zirconium (II) which may be formed. With larger amounts of reactive gas the glasses turned yellow in color, and at high flow rates of CCl_4 vapor black inclusions again appeared. This latter feature is possibly due to carbon produced by thermal cracking of CCl_4.

Some of the fluorides used (e.g., ZrF_4) sublime at high

temperatures and white materials evolved from the melt were found condensed on the cooler parts of the melting chamber, especially when a reactive atmosphere was used. With an inert or Cl_2 atmosphere the sublimed material was soluble in water. When CCl_4 was used larger amounts of white material were evolved, and this adhered to the inside of the reactor vessel at temperatures above 600°C. This substance was not soluble in the melt, and if pieces flaked off the reactor wall and dropped into the melt, the extent of devitrification on casting the glass was increased. The substance was apparently insoluble in water, but was soluble in methanol, and may therefore be a polymeric material derived from CCl_4.

For HfF_4-containing glasses no yellow color usually developed in the glasses even with high flow rates of Cl_2 or CCl_4 in either the open or closed reactor. However, when extremely large amounts of reactive gases (1.0 L/min Cl_2 or 0.3 L/min CCl_4 bubbling vapor) were used in the modified open reactor (Fig. 8), the HBL melts rapidly crystallized on casting. Some ZrF_4- and HfF_4-containing glasses were pink in color, and this may be due to the presence of transition metal impurities in the particular glasses.

VI. 4. Reflectivity From IR Spectra

Recall that the reflectivity R is related to the transmission, T_o, in a spectral region where only reflectivity losses occur by

$$R = (1 - T_o)/(1 + T_o) \qquad \text{(III.2)}$$

and to the index of refraction by

$$R = (n-1)^2/(n+1)^2 \qquad \text{(VI.1)}$$

Since $n \sim 1.52$ (cf. Tables III and IV) for ZrF_4- and HfF_4-based glasses, T_o should be ~ 0.92. Slight differences between the T_o values obtained from the IR spectrum (Tables XX-XXII) and from Eqs. (III.2) and (VI.1) may arise because of (1) slight deviations from normal light incidence due to a convex sample surface (perhaps the result of bad polishing) or (2) light scattering from small surface imperfections or inhomogeneities in the sample (e.g., crystallites or foreign material inclusions).

CHAPTER VII

EFFECT OF PROCESSING CONDITIONS ON 3400 cm^{-1} -OH PEAK

VII. 1. Bulk and Surface Contributions to -OH Absorption in ZrF_4- and HfF_4-Glasses

The data presented in this section are mostly derived from a preliminary study [96] of the bulk and surface contributions to the -OH absorption in ZBL and HBL glasses. Six glasses included in Tables XX and XXI were studied. (These glasses were designated as HBL-1, HBL-2 and ZBL-1 to ZBL-4 in our published work [96]). After polishing the glass plates, the IR spectra were recorded both on a normal transmission scale (from 1000 to 4000 cm^{-1}) and on a transmission scale expanded X5 (from 2000 to 4000 cm^{-1})(cf. Fig. 21). Following this, one of the glass plates (ZBL-12-9-80) was left mounted on the IR spectrometer specimen holder, and its spectrum was measured periodically over one month. During this time, the glass was covered loosely, so that it was protected from dust, but otherwise exposed to the ambient laboratory atmosphere. The other five glass plates were reduced in thickness in several stages, using the polisher, and the IR spectrum was recorded for each thickness. For one of these glasses(HBL-5-8-80A), water and lapping oil were used alternatively as lubricants during the final stage of polishing to assess the effect of the lubricant on the intensity of the -OH absorption.

Fig. 22 shows expanded scale IR spectra in the vicinity of the -OH peak for different thicknesses, X, of two glasses. The intensity of

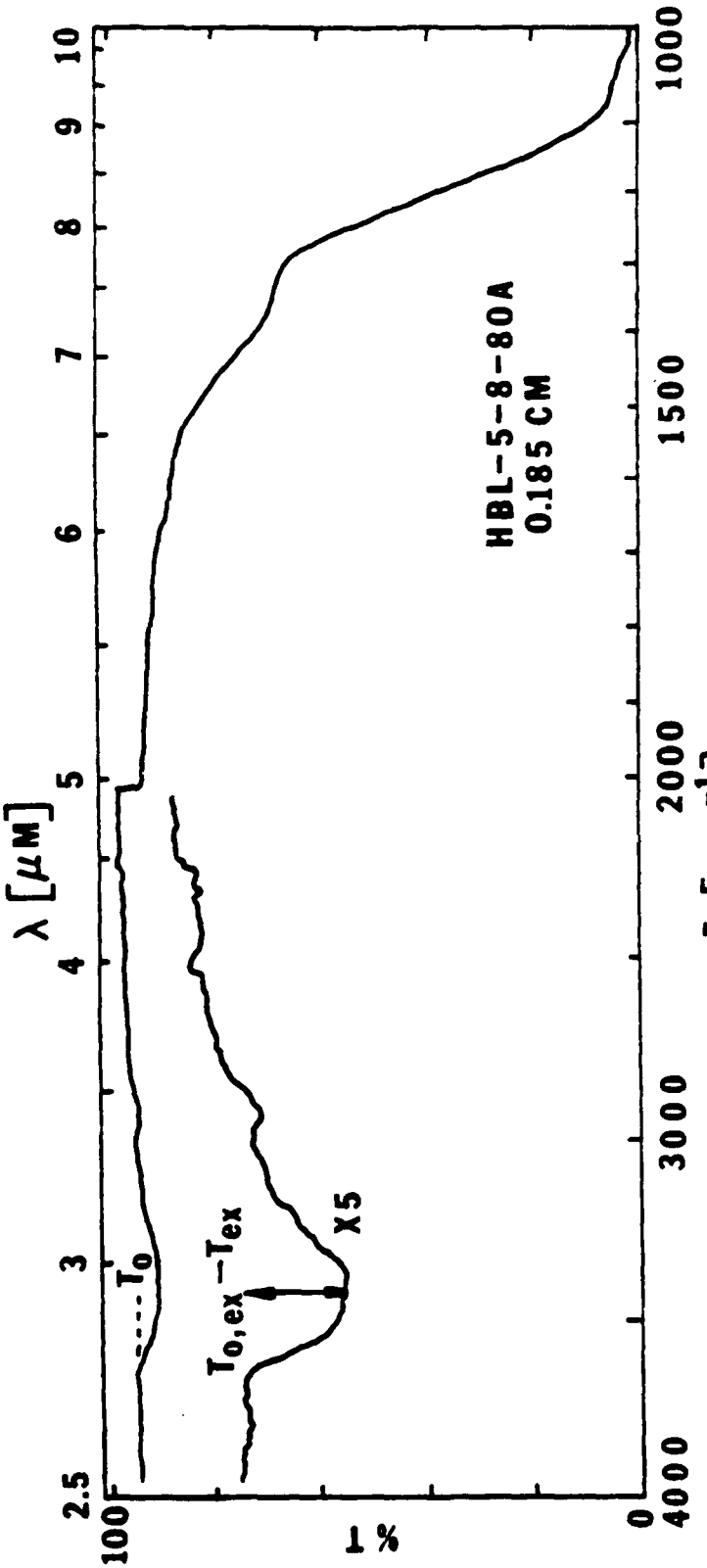
λ [μM]
2.5
3
4
5
6
7
8
9
10
100
T
0
$T_{o,ex} - T_{ex}$
X5
HBL-5-8-80A
0.185 CM
4000
3000
2000
1500
1000
$\bar{\nu}$ [cm^{-1}]

FIG. 21

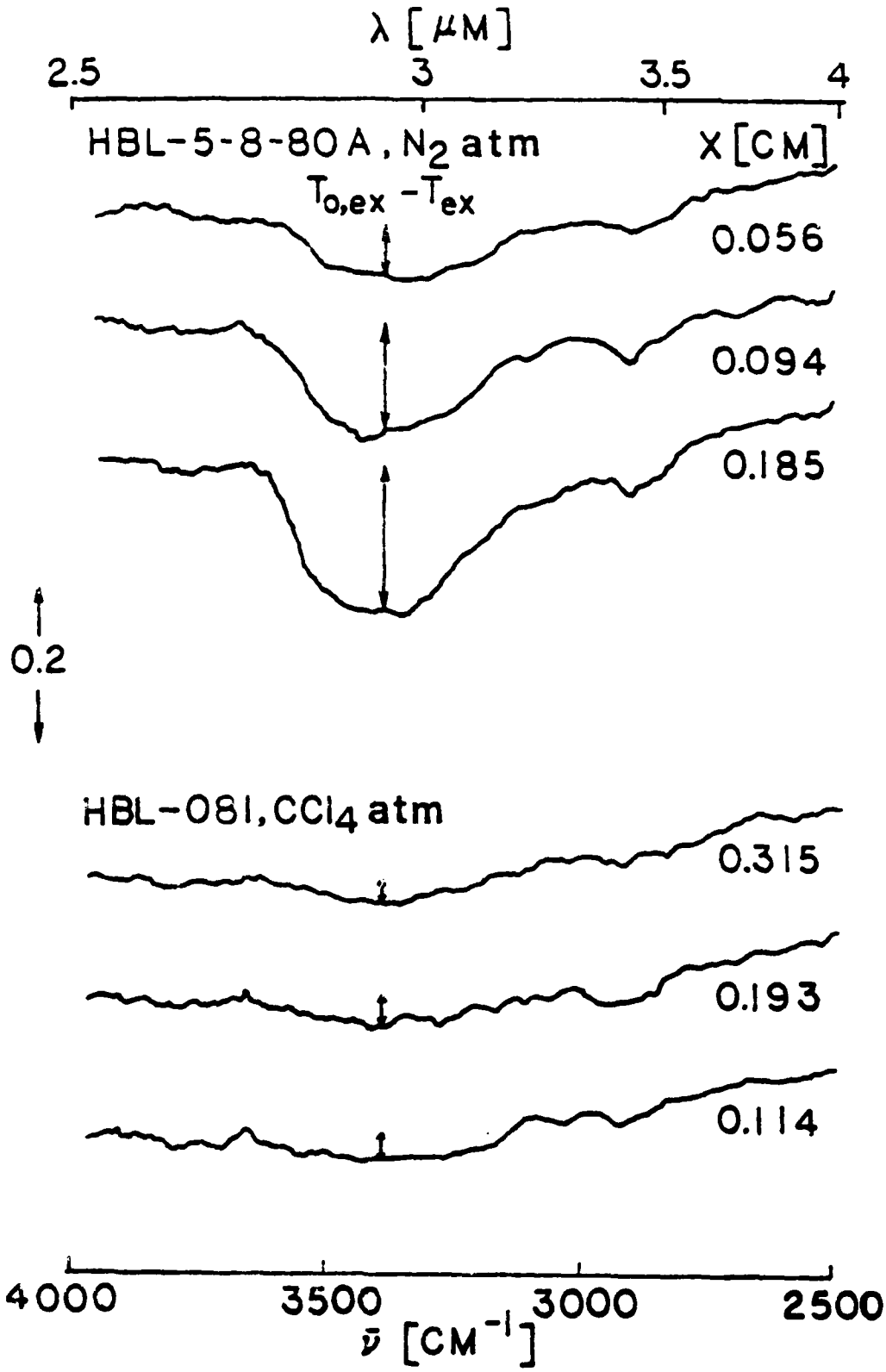
λ [μM]
2.5
3
3.5
4
HBL-5-8-80A, N2 atm
X [CM]
To,ex - Tex
0.056
0.094
0.185
0.2
HBL-081, CCl4 atm
0.315
0.193
0.114
4000
3500
3000
2500
ν̄ [CM-1]

FIG. 22

the -OH absorption on the expanded scale is designated by $(T_{o,\,ex} - T_{ex})$, where $T_{o,ex}$ is the measured transmission in a flat region of the spectrum, where the apparent losses are due only to reflection, and T_{ex} the measured transmission at the 3400 cm^{-1} peak. For the HBL-5-8-80A glass, melted only under N_2 atmosphere, $(T_{o,ex} - T_{ex})$ decreases with decreasing thickness, indicating that a substantial amount of the -OH responsible for the 3400 cm^{-1} peak is contained in the bulk of the glass. For the HBL-081 glass, melted under CCl_4 atmosphere, $(T_{o,ex} - T_{ex})$ is much smaller than for the HBL-5-8-80A glass and independent of thickness within experimental error. Hence, the amount of -OH in the HBL-081 glass is much smaller than in the HBL-5-8-80A glass and is situated primarily on the surface.

In a case in which both surface and bulk components contribute to a weak absorption band, the dependence of the band intensity on sample thickness, X, should be given to a good approximation by

$$\ln (T_o/T) = \alpha_{bulk} X + B \qquad \text{(VII.1)}$$

where T is the transmission at the absorption peak measured on the normal spectrometer scale, T_o the normal scale transmission in an adjacent spectral region where only reflectivity losses occur (cf. Fig. 21), α_{bulk} the absorption coefficient at the peak due to material in the bulk of the specimen, and B the contribution to $\ln (T_o/T)$ from surface material. For our glasses, T at the 3400 cm^{-1} peak was evaluated from the X5 expanded scale spectra via the expression:

$$T = T_o - (T_{o,ex} - T_{ex})/5 \qquad \text{(VII.2)}$$

In Figs. 23 and 24, $\ln (T_o/T)$ is plotted versus glass thickness for two HBL and three ZBL glass specimens. The lines are least squares fits to Eq. (VII.1), and the corresponding least squares parameters are given in Table XXIII. Standard deviations from the fits are of the order of the estimated experimental uncertainty in $\ln(T_o/T)$, $\pm$ 0.004. The uncertainty in the 3400 cm^{-1} bulk -OH absorption coefficient, α_{bulk}, evaluated by this method is roughly $\pm$ 0.01 cm^{-1}.

For the glasses (HBL-5-8-80A, ZBL-2-10-80, ZBL-16-5-80) melted only under N_2 atmosphere, α_{bulk} is of variable magnitude, ranging from zero within experimental error to 0.19 cm^{-1}. Melting under an inert atmosphere thus leaves a varied and uncontrolled amount of -OH in the bulk glass. On the other hand, α_{bulk} at 3400 cm^{-1} for the glasses HBL-081 and ZBL-083 melted under CCl_4 atmosphere is zero within $\pm$ 0.01 cm^{-1}. Robinson et al. [32] reported an absorption coefficient of 0.006 cm^{-1}, measured calorimetrically with an HF laser at 2.8 μm (3600 cm^{-1}), for a $60ZrF_4$-$33BaF_2$-$7ThF_4$ glass melted under CCl_4. The intensity of the -OH peak at 3600 cm^{-1} is about half its value at 3400 cm^{-1}, so that our results ($\pm$ 0.01 cm^{-1} at 3400 cm^{-1}) for ZrF_4- or HfF_4-based glasses melted under CCl_4 would give an upper limit of $\sim$0.005 cm^{-1} for the bulk -OH abosrption coefficient at 3600 cm^{-1}. This is in good agreement with the results of Robinson et al. [32], presuming that their calorimetric method is sensitive primarily to bulk absorption.

Knowing the band shape of the -OH peak for glasses containing

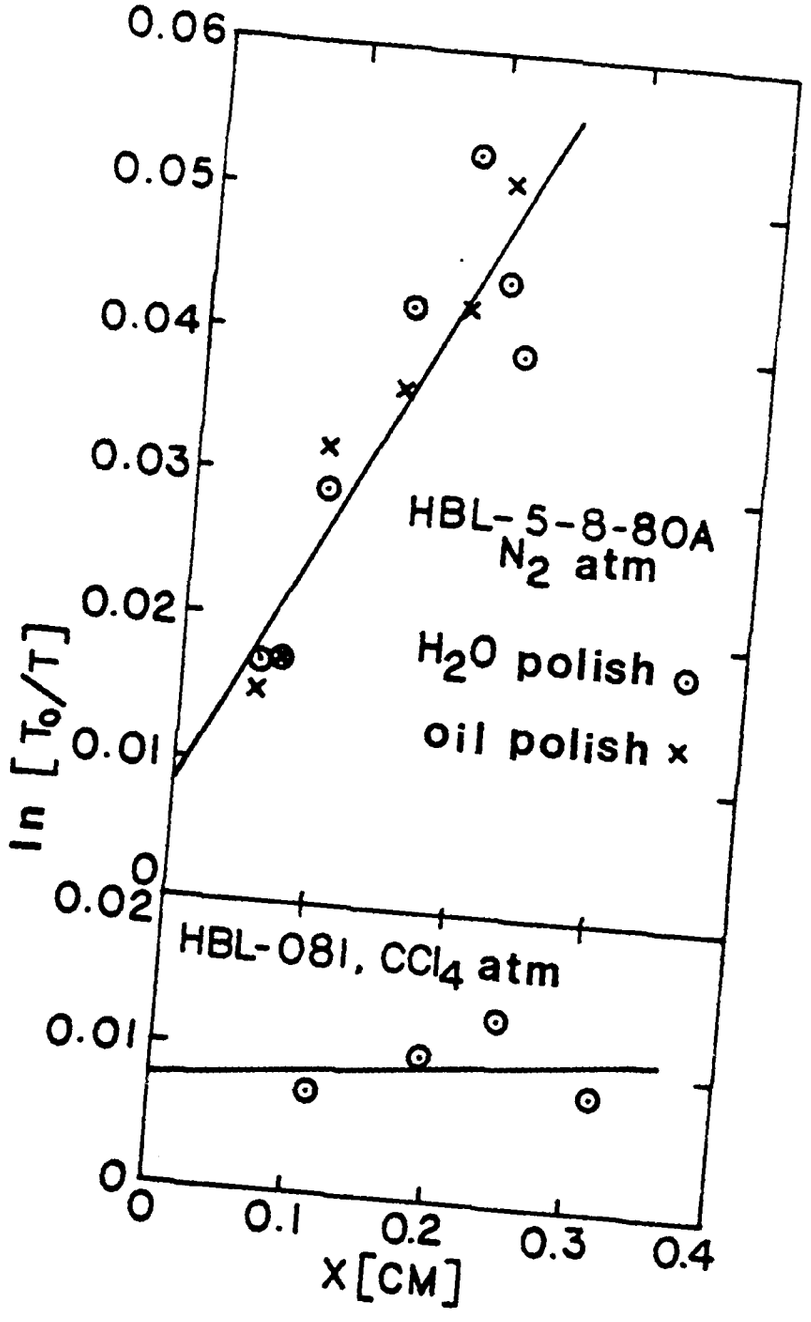
0.06
0.05
0.04
0.03
0.02
0.01
0
ln [T₀/T]
HBL-5-8-80A
N₂ atm
H₂O polish ⊙
oil polish ×
0.02
0.01
0
HBL-081, CCl₄ atm
0
0.1
0.2
0.3
0.4
X[CM]

FIG. 23

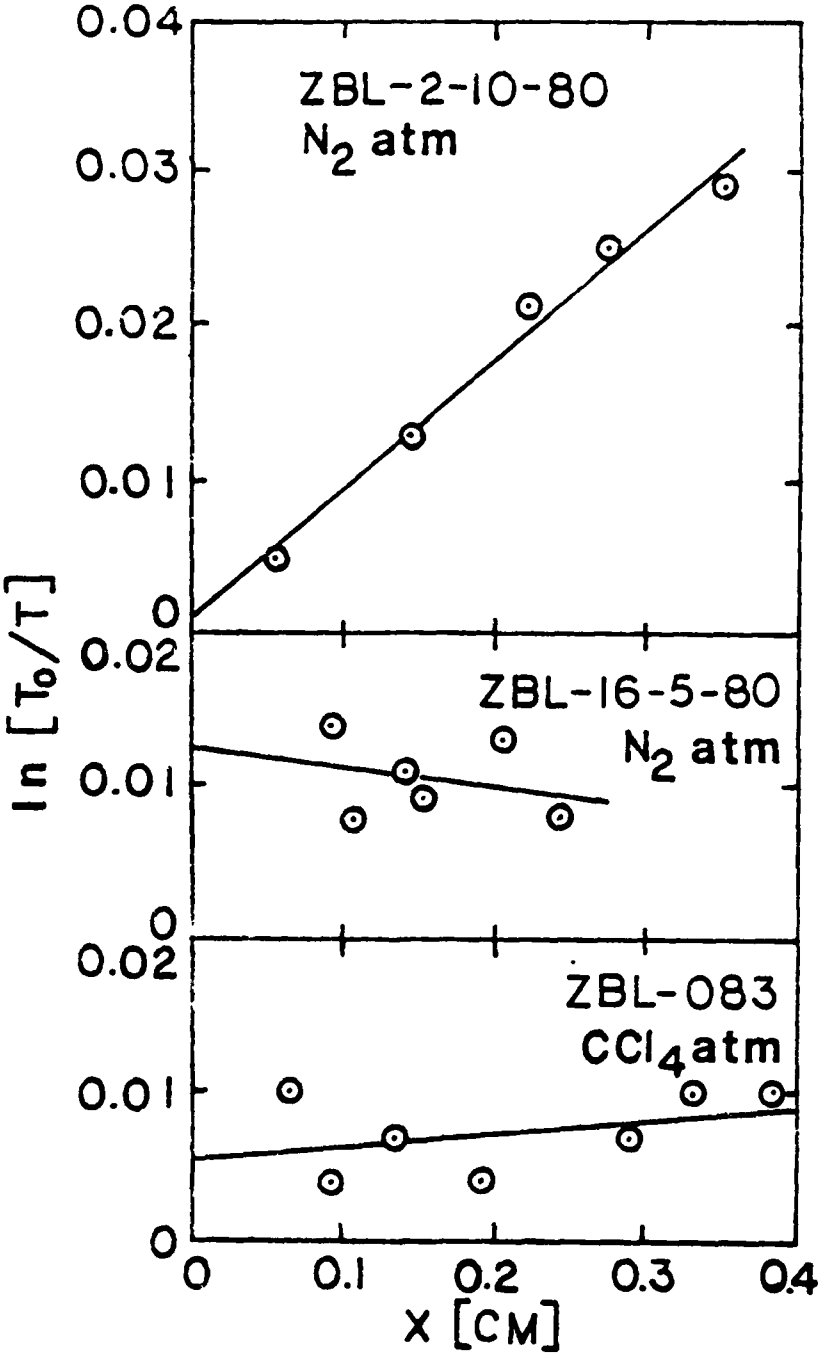
0.04
0.03
0.02
0.01
0
ZBL-2-10-80
N2 atm
0.02
0.01
0
ZBL-16-5-80
N2 atm
0.02
0.01
0
ZBL-083
CCl4 atm
ln [To/T]
0
0.1
0.2
0.3
0.4
X [CM]

FIG. 24

Table XXIII. Melting Conditions and Thickness Dependence of Absorption Loss at 3400 cm^{-1} for Fluorohafnate and Fluorozirconate.

Sample No.	Reactor	Melting atm.	α_{bulk} (cm^{-1})	B	Std. deviation
HBL-5-8-80A	open	N_2	0.19	0.008	0.006
HBL-081	open	CCl_4	0.01	0.008	0.003
ZBL-2-10-80	open	N_2	0.08	0.001	0.001
ZBL-16-5-80	open	N_2	-0.01	0.012	0.003
ZBL-083	open	CCl_4	0.01	0.006	0.002
ZBL-12-9-80	open	N_2	—	--	--

large amounts of -OH, our upper limit of $\sim$0.01 cm^{-1} at 3400 cm^{-1} for the bulk -OH absorption coefficient in glasses melted under CCl_4 can be used to estimate the bulk -OH absorption coefficients at other wavelengths for the latter glasses. For example, the intensity of the -OH band has dropped to 10% of its peak value by 3000 cm^{-1}, so that at this frequency, an upper limit of $\sim 1.0^{-3}$ cm^{-1} can be set for the bulk -OH absorption coefficient of glasses melted under CCl_4. This is in good agreement to the optical loss values ($0.7 - 1.12 \times 10^{-3}$ cm^{-1} at 2950 cm^{-1}) reported for several ZrF_4-BaF_2-CdF_3 and ZrF_4-BaF_2-GdF_3-AlF_3 glass fibers [37,39, 59,66].

As shown in Fig. 23 for the HBL-5-8-80A glass, the intensity of the -OH absorption band for a given thickness is independent of whether the final stages of polishing are done with lapping oil or with pure water as a lubricant. Consequently, no special precautions need to be taken to protect these glasses from water during polishing. Rather, it appears that the surface -OH observed in the IR spectrum is produced by the attack of environmental water on the fresh surface after polishing.

Fig. 25 shows the time dependence of $\ln(T_o/T)$ at the 3400 cm^{-1} -OH peak for the ZBL-12-9-80 glass exposed to the ambient laboratory atmosphere over a 30 day period. The mean value of $\ln (T_o/T)$, as shown by the dashed line, is 0.015 ± 0.004 cm^{-1}, and only one point in Fig. 4 departs by more than two standard deviations from this mean. Since the estimated experimental accuracy of $\ln(T_o/T)$ is also ± 0.004, there is no evidence of increase in thickness of the surface -OH layer due to attack by atmospheric water over this time period. This underlines the

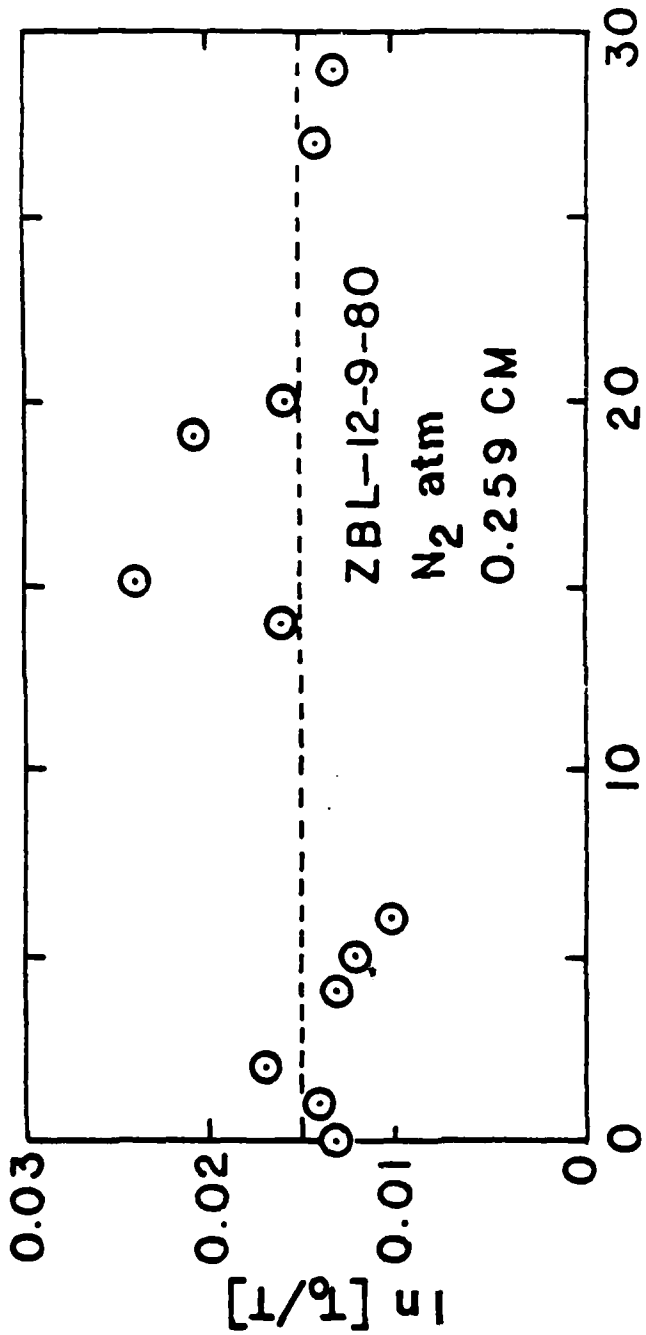

FIG. 25

previously reported [7, 32] chemical inertness of these glasses in a neutral or basic aqueous environment.

Table XXIII shows that the value of B in Eq. (VII.1), i.e., the contribution to $\ln(T_o/T)$ at 3400 cm^{-1} from surface -OH, is of the order of 0.01 for the five glasses studied. This corresponds to a thickness independent loss in transmitted light intensity of ~1% at 3400 cm^{-1}, with correspondingly lower losses at frequencies removed from -OH band maximum. Losses of this magnitude are generally not important for applications involving low to medium light intensities, e.g., fiber optic waveguides, but might be objectionable for high power applications such as high-energy laser windows.

VII. 2. Extensive Study of Effect of Processing Conditions on -OH Peak Intensity

Tables XX-XXII include the values of $\ln(T_o/T)$ at 3400 cm^{-1} for glasses melted under various processing conditions. The $\ln(T_o/T)$ results for both the ZBL (Table XX) and HBL (Table XXI) glasses are relatively comparable, while the high -OH contents (large $\ln(T_o/T)$ values at 3400 cm^{-1}) of ZBLA (Table XXII) glasses could be substantially reduced by increasing their melting temperatures from 800°C to 850°C. For the glasses melted under N_2 atmosphere in the open reactor the $\ln(T_o/T)$ values at 3400 cm^{-1} are relatively high and of variable magnitude. However, glasses melted in the closed reactor (under N_2 atmosphere) exhibit lower and less variable $\ln(T_o/T)$ values. The values of $\ln(T_o/T)$ for the glasses melted under reactive atmospheres (CCl_4 or Cl_2) both in the open and closed reactors

also show some variation, but are usually of the order of 0.01 for sample thickness ≥ 2 mm. This indicates that most of the -OH is on the surface of the glasses, if we recall that the $\ln(T_o/T)$ values include both bulk (α_{bulk}) and surface (B) absorptions (cf. Eq. VII.1) and that the contribution to $\ln(T_o/T)$ values at 3400 cm^{-1} from surface -OH was found to be of the order of 0.01 in the preliminary study of the previous section.

Generally, glasses prepared under CCl_4 atmospheres were found to have lower -OH contents than those prepared under Cl_2 atmospheres, and the most effective removal of -OH was achieved by using the closed reactor. However, in order to compare the effectiveness of CCl_4 and Cl_2 atmospheres both their concentrations and flow rates should be considered. Recall the CCl_4 concentration was roughly 13% (CCl_4 vapor pressure at 23°C = 100 mmHg, (100/760) x 100 = 13%) while that of Cl_2 was 3.5% in N_2. When a reactive atmosphere was used, some glasses melted in the closed reactor showed higher -OH contents than those prepared in the open reactor. This could be due to the fact that the amount of reactive gas diffusing into a melt in the closed reactor is less than in the open reactor. Such behavior may conceivably occur because of (1) the bad design of the gas inlet of the closed reactor (Fig. 10), and (2) the formation of heavy vapor layers between the melt surface and the gas inlet due to the volatilization of fluoride materials. These would create a diffusion barrier for the reactive gases.

VII. 3. -OH Absorption in BaF_2/ThF_4 Glasses

Table XXIV contains the $\ln(T_o/T)$ values at 3400 cm^{-1} for some

Table XXIV. Values of Thickness, T_o and $\ln(T_o/T)$ at 3400 cm^{-1} of BaF_2/ThF_4-based Glasses in Tables XIII and XIV (b).

Glass	Melting Atmos.	Thickness X(cm)	T_o	$\ln(T_o/T)$ @3400 cm^{-1}	Remarks
BZnYbT-6F	inert gas	0.325	0.86	0.192	
BZnYbT-20-10-81	CCl_4	0.246	0.90	0.008	
BZnYbT-30-10-81	CCl_4	0.216	0.905	0.002	
BZnYbLT-12-11-81	Cl_2	0.258	0.865	0.002	
BZnYbYT-9-11-81	CCl_4	0.209	0.885	0	
BZnYbGdT-17-11-81	Cl_2	0.238	0.89	0.006	
BZnYbTN-4-3-82	Cl_2	0.315	0.895	0.006	
BZnYbTN-9-3-82	Cl_2	0.254	0.90	0.028	
BZnYbTLi-24-3-82	Cl_2	0.260	0.905	0.025	
BZnYbTNLi-1-4-82	Cl_2	0.278	0.895	0.008	

glasses given in Tables XIII and XIV (b). All the glasses were melted in the closed reactor except BZnYbT-6F, which was melted at University of Rennes in an open furnace. BZnYbT glasses exhibit values of $\ln(T_o/T)$ less than 0.01, and this is also true for glasses in which the YbF_3 was partially replaced by LaF_3, GdF_3 or YF_3. However, when alkali fluoride (e.g., NaF or LiF) is added to the BZnYbT glasses, the $\ln(T_o/T)$ values at 3400 cm^{-1} and presumably the -OH contents of the glasses tend to be higher in some specimens.

In general, the -OH absorptions of the BaF_2/ThF_4 based glasses are not so intense as those based on ZrF_4 or HfF_4. However, this may simply be due to the higher melting temperatures used for these glasses (950°C for the BaF_2/ThF_4 glasses as opposed to 800-850°C for the ZrF_4 and HfF_4 glasses).

CHAPTER VIII

EFFECT OF PROCESSING CONDITIONS ON OXIDE ABSORPTION (1100 - 1400 cm^{-1})

VIII. 1. IR Edge Transmission Spectra of Heavy Metal Fluoride Glasses

Figs. 26-29 show typical transmission spectra for ZBL, HBL, ZBLA and BZnYbT glasses in the region of IR edge, with the transmission scales of the spectra being displaced for clarity. The spectrum in Fig. 26 for ZBL-25-9-80 glass melted under N_2, shows a weak shoulder around 1400 cm^{-1}. This shoulder is much less pronounced for the ZBL-27-1-82 and ZBL-083 glasses prepared under reactive atmospheres (CCl_4). Similar behavior is evident in Fig. 1 of the study by Robinson et al. [32], in which they compare the IR spectra of ZrF_4 glasses melted under inert gas, HF and CCl_4 atmospheres.

Similar comparisons are also made in Fig. 27 for the IR spectra of the HBL glasses. Again the 1400 cm^{-1} shoulder decreases in intensity when the flow rate of the reactive gas is increased during melting. For the HBL glasses, however, most of the samples with thickness $X \geq 2$ mm prepared even under reactive atmospheres still showed a well defined shoulder at 1400 cm^{-1}. The 1400 cm^{-1} shoulder also appears in the ZBLA glasses of Fig. 28, but not as clearly as in Figs. 26 and 27. For the BZnYbT glasses prepared under an inert atmosphere (BZnYbT-6F of Fig. 29) a strong peak is observed at ~1100 cm^{-1} in the IR spectra. Samples prepared under a reactive atmospheres show much reduced or no contribution from this peak. Drexhage et al. [8,10] have speculated that oxide impurities may be

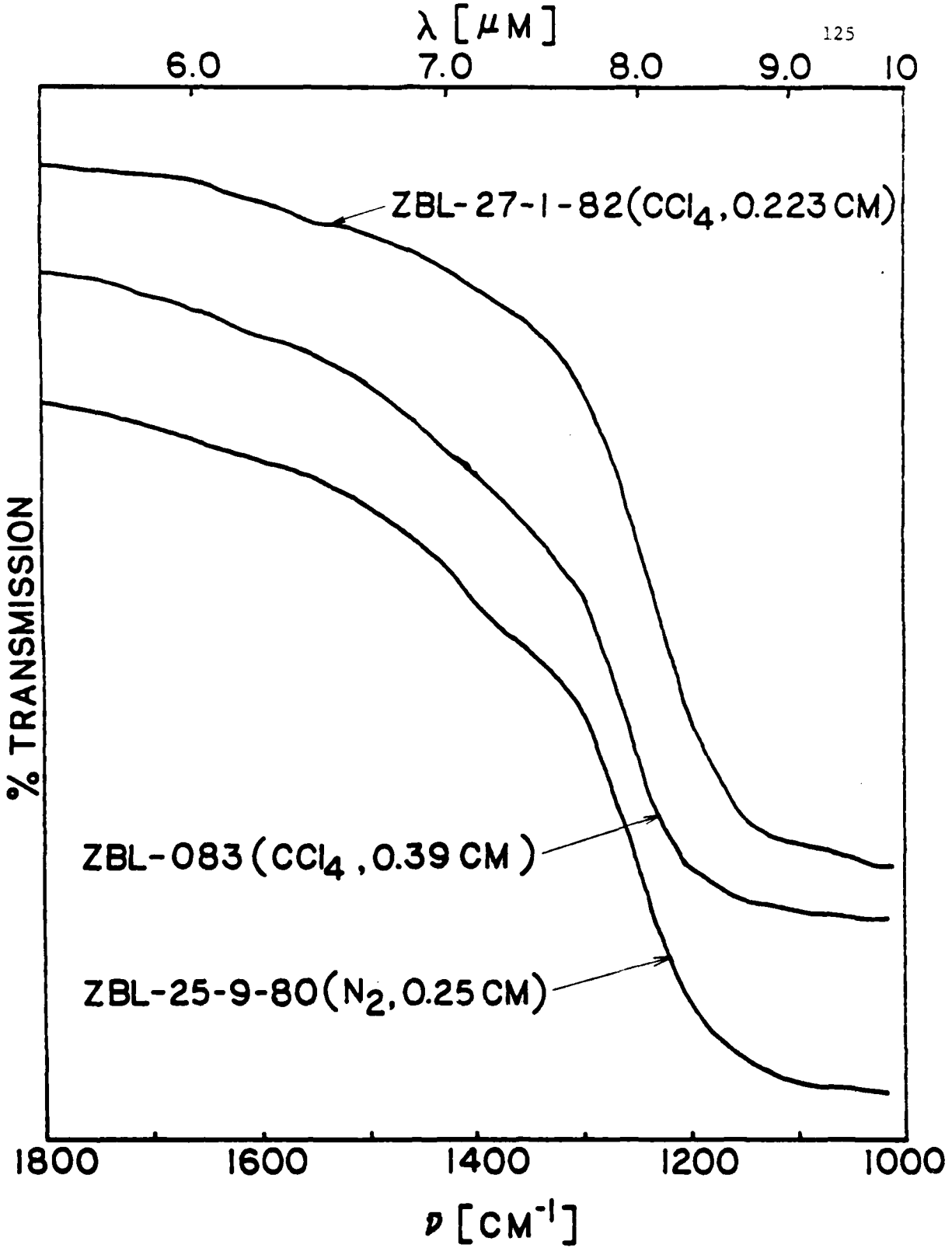
λ [μM]
6.0
7.0
8.0
9.0
10
ZBL-27-1-82(CCl4, 0.223 CM)
ZBL-083 (CCl4, 0.39 CM)
ZBL-25-9-80(N2, 0.25 CM)
% TRANSMISSION
1800
1600
1400
1200
1000
ν [CM-1]

FIG. 26

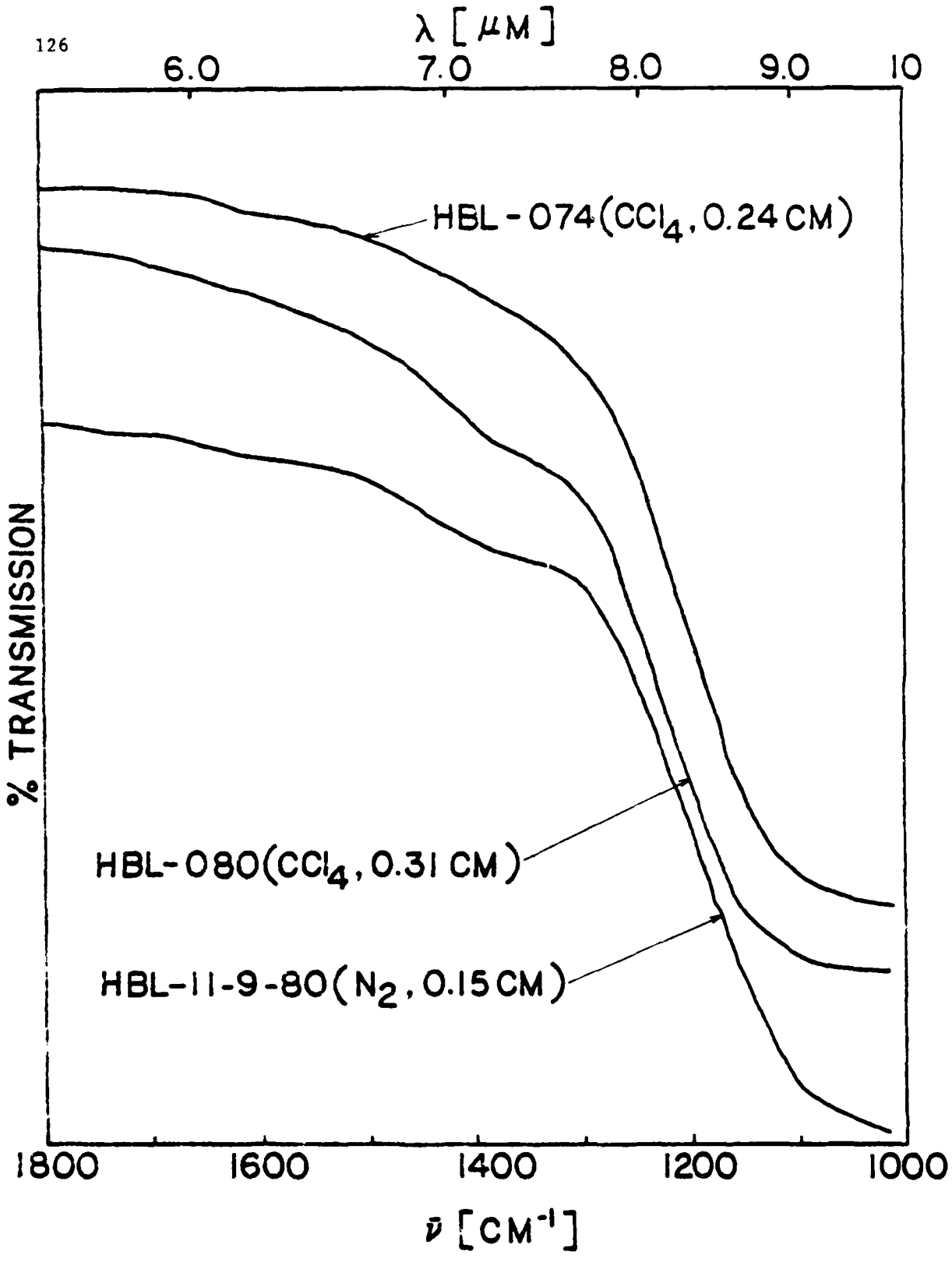
λ [μM]
6.0
7.0
8.0
9.0
10
HBL-074(CCl4, 0.24 CM)
HBL-080(CCl4, 0.31 CM)
HBL-11-9-80(N2, 0.15 CM)
% TRANSMISSION
1800
1600
1400
1200
1000
ν̄ [CM-1]

FIG. 27

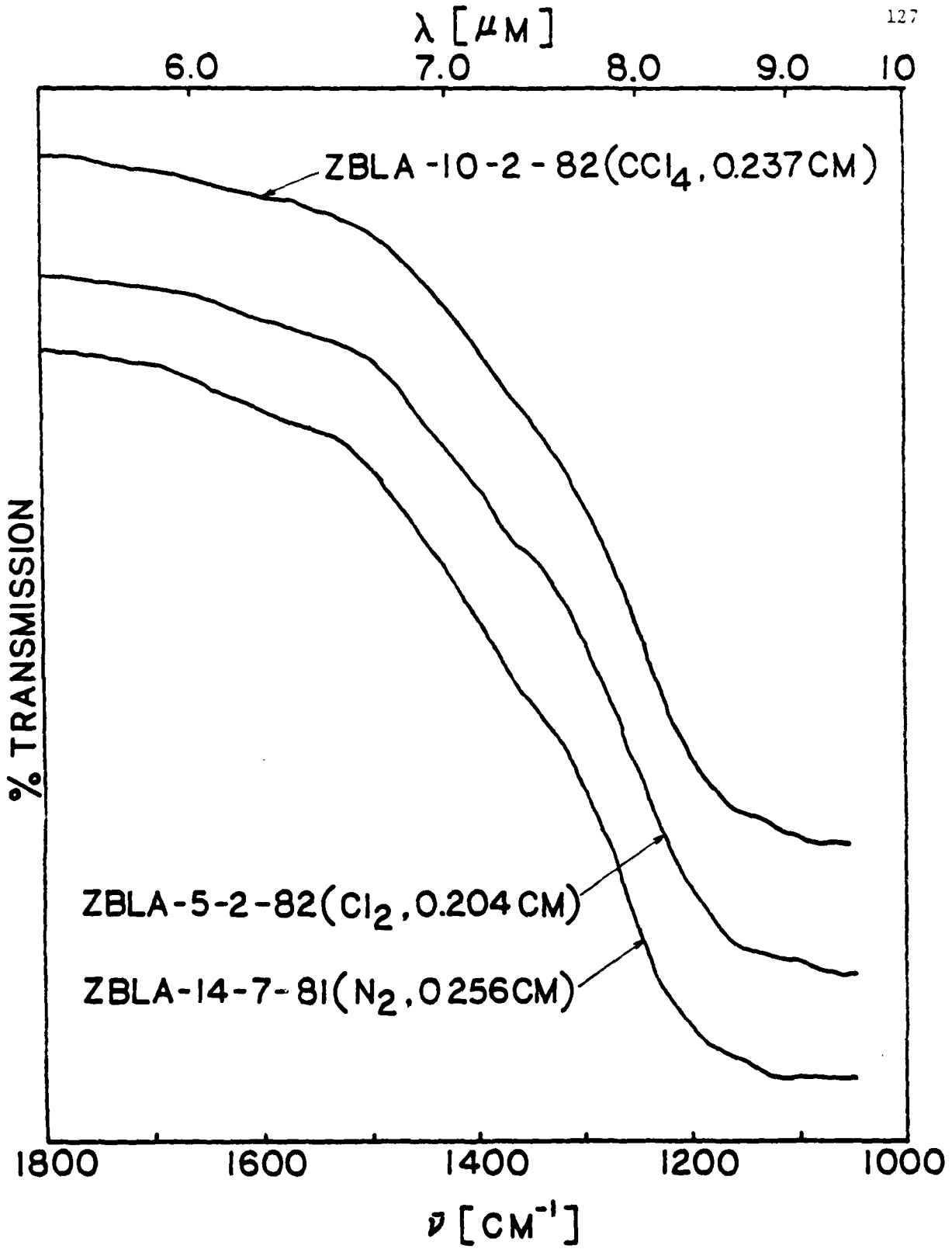
λ [μM]
6.0
7.0
8.0
9.0
10
ZBLA -10-2 - 82(CCl4, 0.237CM)
% TRANSMISSION
ZBLA-5-2-82(Cl2, 0.204 CM)
ZBLA-14-7-81(N2, 0256CM)
1800
1600
1400
1200
1000
ν̄ [CM⁻¹]

FIG. 28

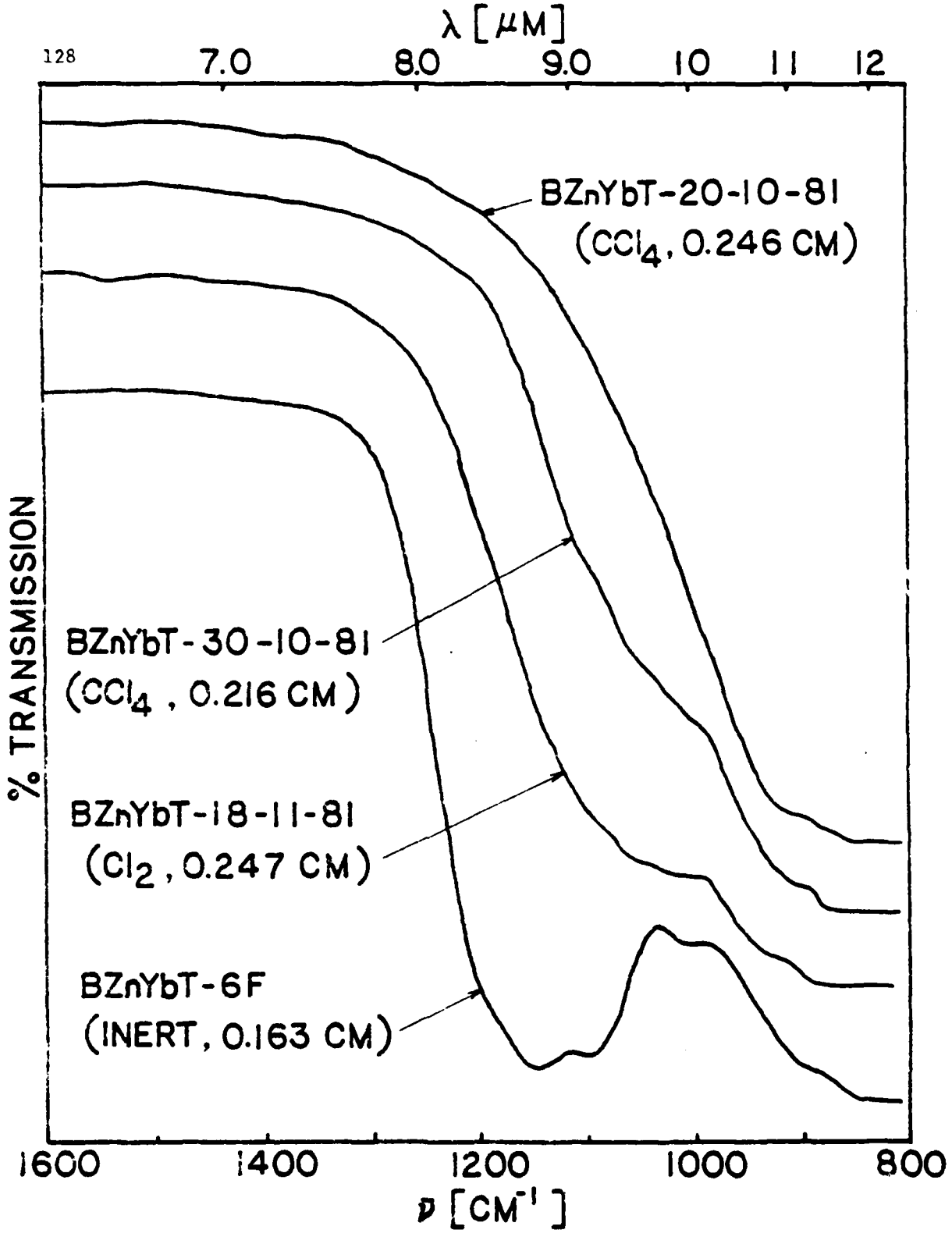
λ [μM]
7.0
8.0
9.0
10
11
12
BZnYbT-20-10-81
(CCl4, 0.246 CM)
BZnYbT-30-10-81
(CCl4, 0.216 CM)
BZnYbT-18-11-81
(Cl2, 0.247 CM)
BZnYbT-6F
(INERT, 0.163 CM)
% TRANSMISSION
1600
1400
1200
1000
800
ν [CM-1]

FIG. 29

contributing to the absorption on the IR edge and, in particular, be responsible for the shoulders observed in many ZrF_4- and HfF_4- based glass specimens at ∿1400 cm^{-1}. The peak at ∿1100 cm^{-1} in the IR spectra of BZnYbT glasses is probably also due to oxide impurities.

All the ZrF_4- and HfF_4-based glasses in Figs. 26-28 exhibit very weak shoulders at ∿1600 cm^{-1} (∿6.3 μm), which may be attributed to the bending vibration of water molecules. Careful examination of the spectrometer traces, taken after successive thinnings of the glasses, showed that the intensities of these shoulders were independent of sample thickness. This indicates that the 1600 cm^{-1} shoulders are probably due to H_2O in thin hydrated layers formed on the sample surfaces after polishing and that H_2O is not present in the glass interior. Surface hydration has also been indicated in the study of the 3400 cm^{-1} -OH band (cf. Chapter VII of this thesis).

VIII. 2. Absorption Coefficient-Frequency Plots For Heavy Metal Fluoride Glasses

Figs. 30-33 depict semi-logarithmic plots of the absorption coefficients (α) versus frequency ($\bar{\nu}$) for the glasses whose IR spectra are shown in Figs. 26-29. In most cases for HBL and ZBL, the spectra for a number of thicknesses of each specimen were used in constructing the plots. Tables of α and T vs. $\bar{\nu}$ are given in Appendix I for all these samples. These data are representative of all the samples characterized and show the extremes of the α values measured at each frequency in each case.

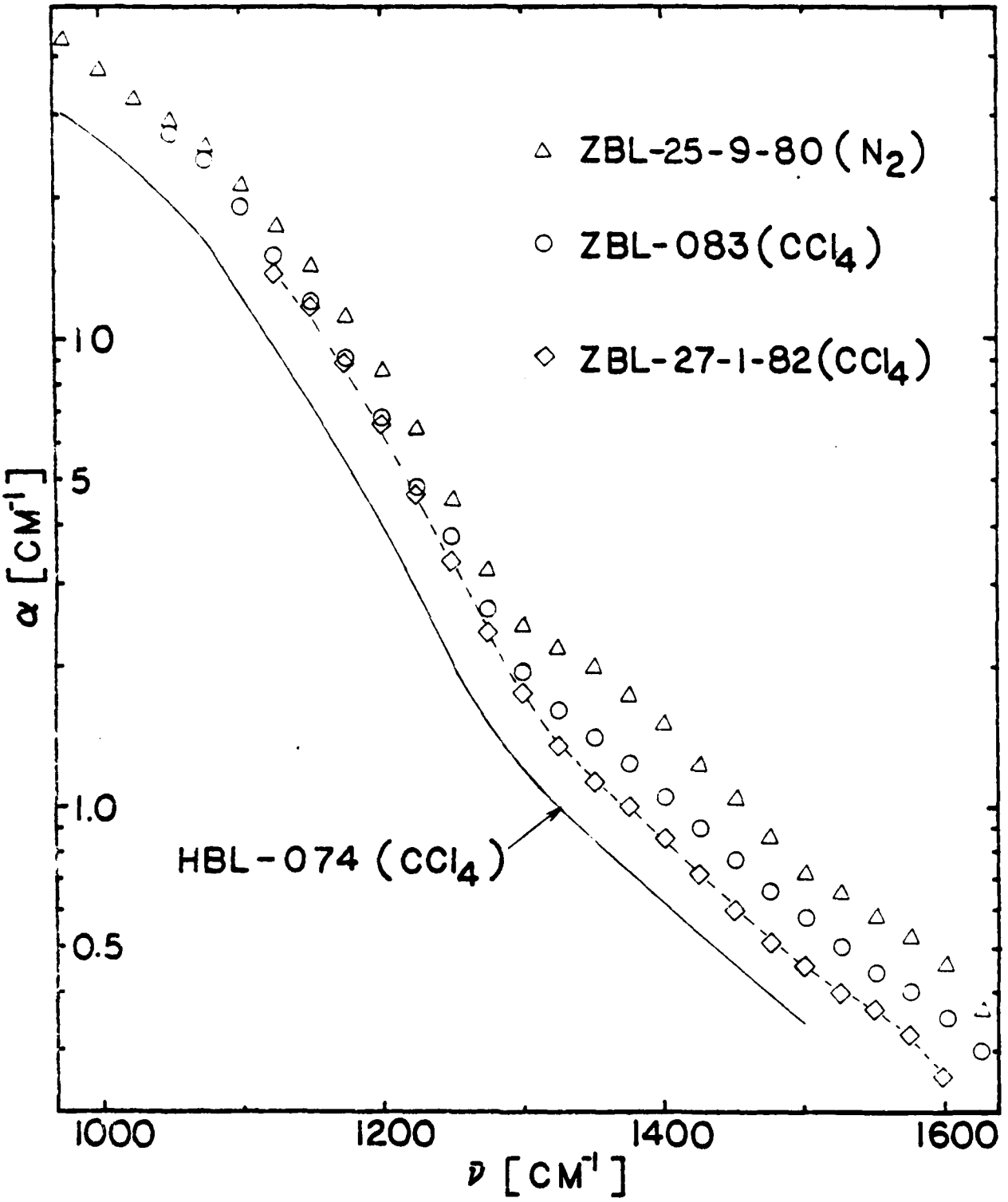
ZBL-25-9-80 (N_2)
ZBL-083(CCl_4)
ZBL-27-1-82(CCl_4)
HBL-074 (CCl_4)
10
5
1.0
0.5
α [CM^{-1}]
1000
1200
1400
1600
$\bar{\nu}$ [CM^{-1}]

FIG.30

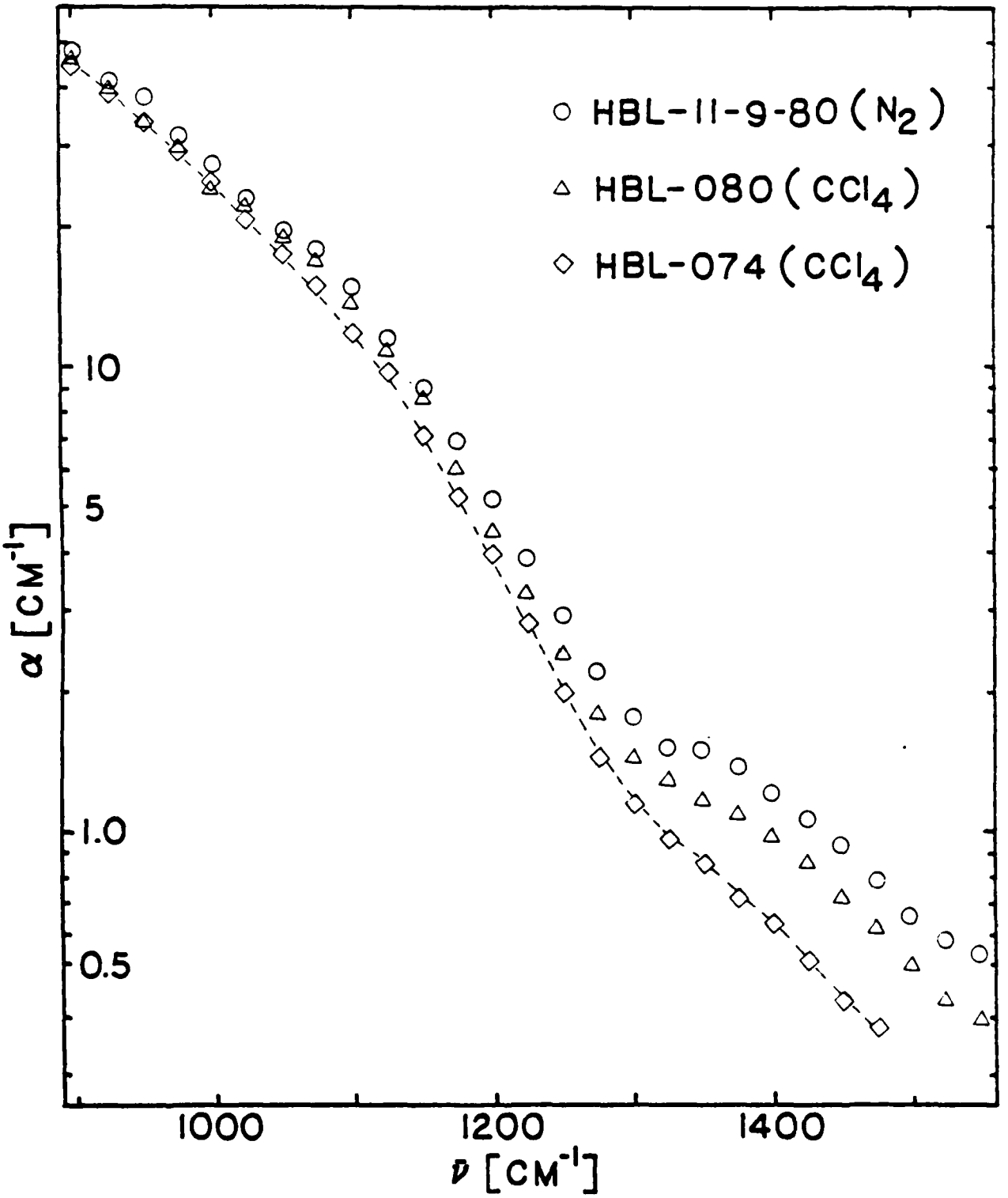
HBL-11-9-80 (N_2)
HBL-080 (CCl_4)
HBL-074 (CCl_4)
10
5
1.0
0.5
α [CM^{-1}]
1000
1200
1400
ν [CM^{-1}]

FIG. 31

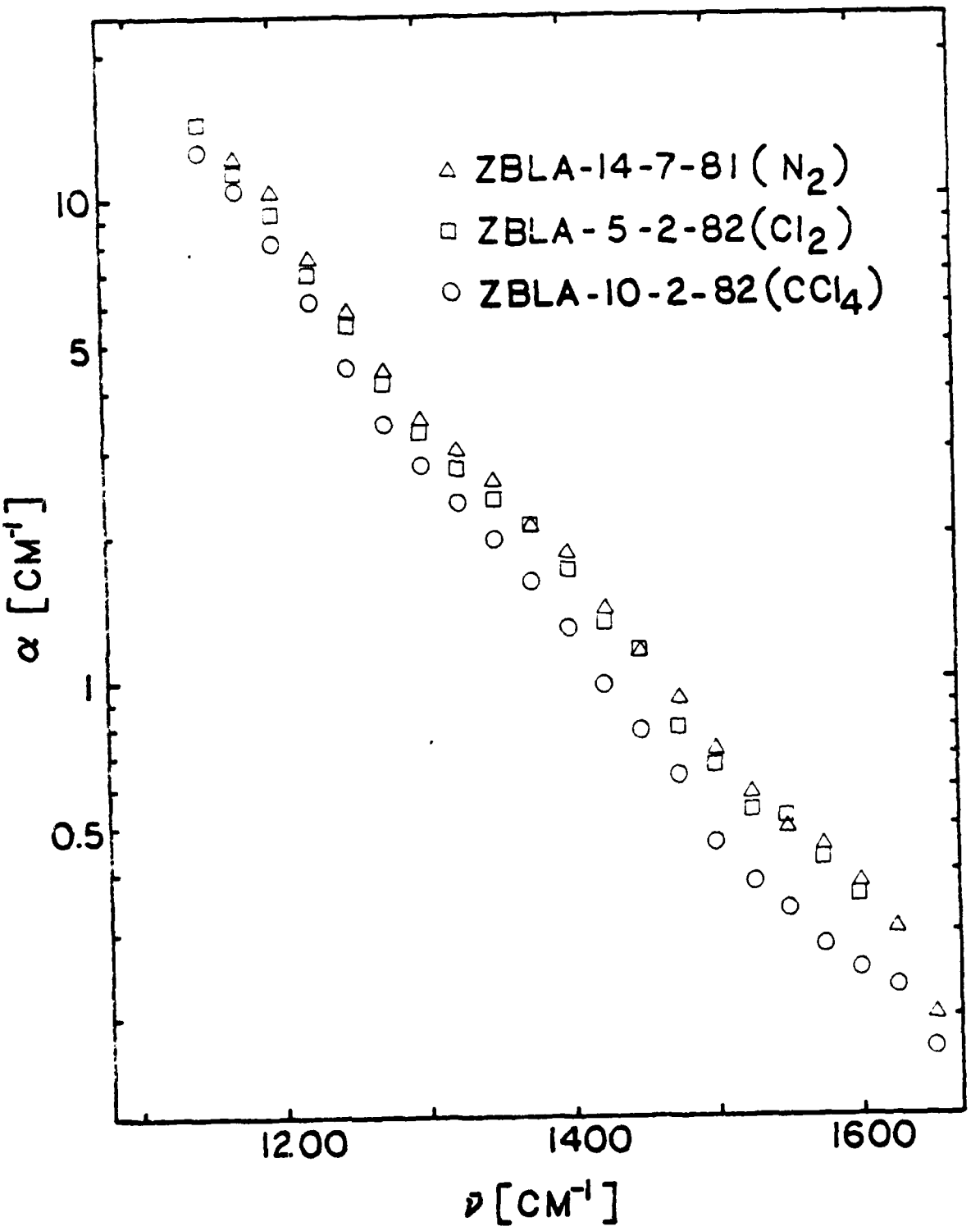
ZBLA-14-7-81 (N_2)
ZBLA-5-2-82(Cl_2)
ZBLA-10-2-82(CCl_4)
10
5
1
0.5
α [CM⁻¹]
1200
1400
1600
ν [CM⁻¹]

FIG. 32

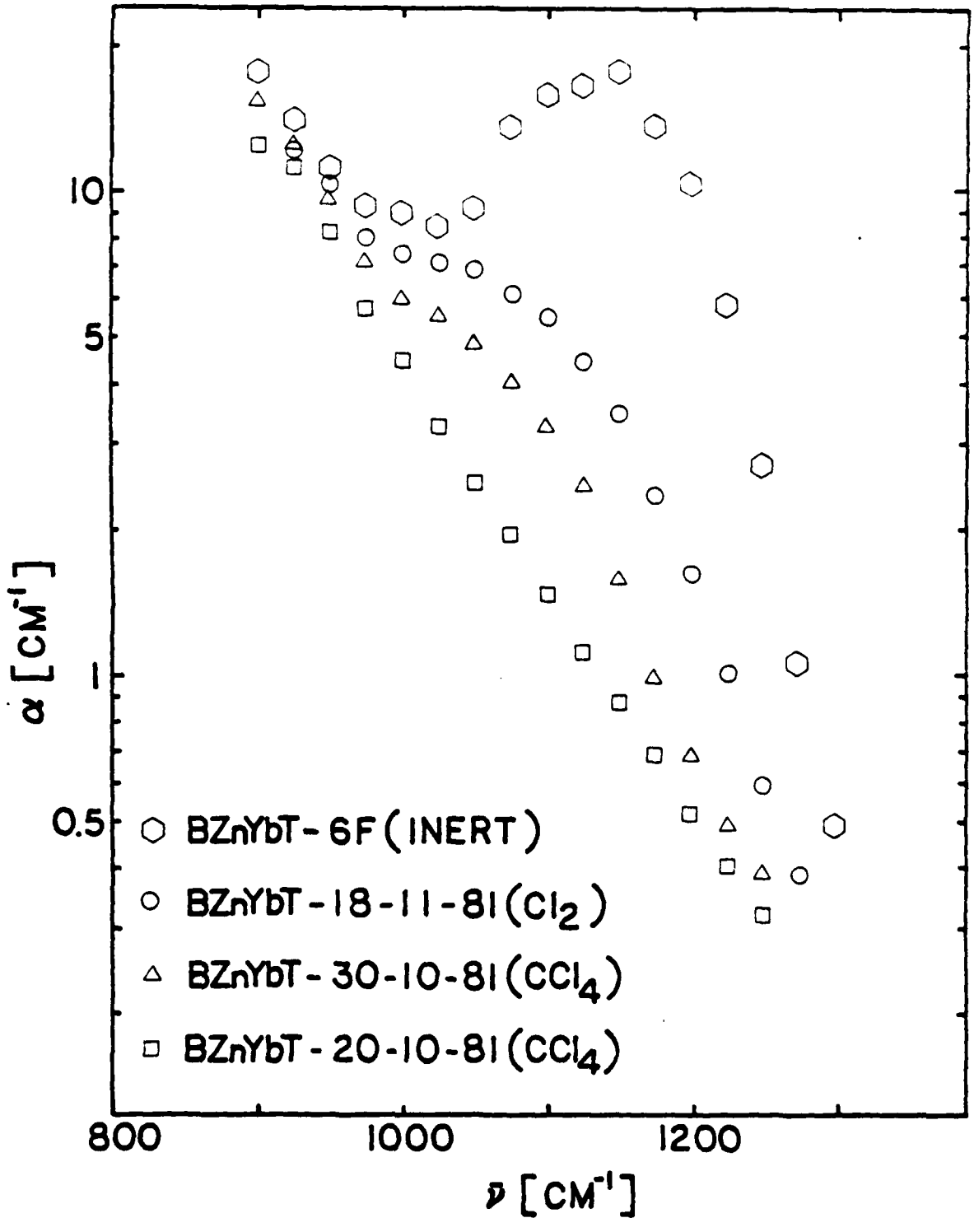
10
5
1
0.5
α [CM⁻¹]
800
1000
1200
ν [CM⁻¹]
BZnYbT-6F(INERT)
BZnYbT-18-11-81(Cl2)
BZnYbT-30-10-81(CCl4)
BZnYbT-20-10-81(CCl4)

FIG. 33

At the lower frequencies (<1100 cm^{-1}) the data for the various ZBL, HBL and ZBLA samples are in good agreement, indicating that intrinsic behavior is being observed. Above 1100 cm^{-1}, however, there are variations in the α values, suggesting that there are extrinsic contributions. In particular, the specimens showing the most pronounced shoulders at 1400 cm^{-1} (Figs. 26-28) exhibit the largest α values in this frequency range. The observation that the 1400 cm^{-1} absorptions are lowest for the samples subjected to the most rigorous procedures designed to remove oxide and -OH (i.e., high flow rate of reactive atmosphere) again suggests the assignment of the shoulder to oxide impurities.

Similarly, in the semi-logarithmic plots of α vs. $\bar{\nu}$ for the BZnYbT glasses (Fig. 33) at the lower frequencies (<950 cm^{-1}) the data for the various samples are in good agreement, again indicating that intrinsic behavior is being observed. Above 950 cm^{-1} there are variations in the α values, especially around the 1100 cm^{-1} region, suggesting that there are extrinsic contributions - probably oxide impurities.

At present, it is not possible to say how close the absorption coefficients of those glasses with the lowest α values in the high frequency region are to the intrinsic limit, and it may be possible to lower the absorption further by using more stringent processing conditions to remove oxide species from the melt. For comparison purposes, however, we can use the α vs. $\bar{\nu}$ curves of our "best" glasses (i.e., those with the lowest α values at a given frequency) as upper limit estimates of the intrinsic IR edges. Differences in the intrinsic, multiphonon IR edge absorption resulting from changes in glass composition will be discussed in detail and from a fundamental standpoint in Chapter

IX. In what follows in the present chapter we will evaluate our current estimates of the intrinsic edges of the ZBL and HBL glasses from an experimental standpoint. These estimated intrinsic edges are shown as dashed lines in Figs. 30 and 31 and correspond to the lowest measured α vs. $\bar{\nu}$ plots in the high frequency region ($\bar{\nu} \geq 1100$ cm^{-1}). The dashed line of Fig. 31 is also shown as a solid line in Fig. 30 for comparison.

First, although we cannot say with absolute certainty that improvements in processing would not lower α further in the frequency region where oxide contamination is suspected, the use of reactive atmosphere processing usually leads to decreases of only about a factor of two in α at 1400 cm^{-1} for ZBL or HBL glasses, moreover, the 1400 cm^{-1} α values obtained after reactive atmosphere processing are now reasonably reproducible (cf. Tables XX and XXI). This strongly suggests lowest α vs. $\bar{\nu}$ curves are probably reasonably close to intrinsic levels for ZrF_4- and HfF_4-containing glasses.

Second, the α vs. $\bar{\nu}$ curves for out best ZBL and HBL glasses in IR edge region are of a shape that is consistent in comparison with the α vs. $\bar{\nu}$ curves in the fundamental region, with the expected shape of intrinsic multiphonon absorption curves. In Fig. 34 the α vs. $\bar{\nu}$ curve for the fundamental absorption regime (200 - 600 cm^{-1}), derived from IR reflectivity measurements [77] has been plotted for ZBL glass. Shown on the same plot is the α vs. $\bar{\nu}$ curve between 900 and 1800 cm^{-1} obtained from the IR transmission spectra of our "best" ZBL glass (ZBL-27-1-82). The dashed line is the interpolated α vs. $\bar{\nu}$ curve in the 600 to 900 cm^{-1} region where data are not available.

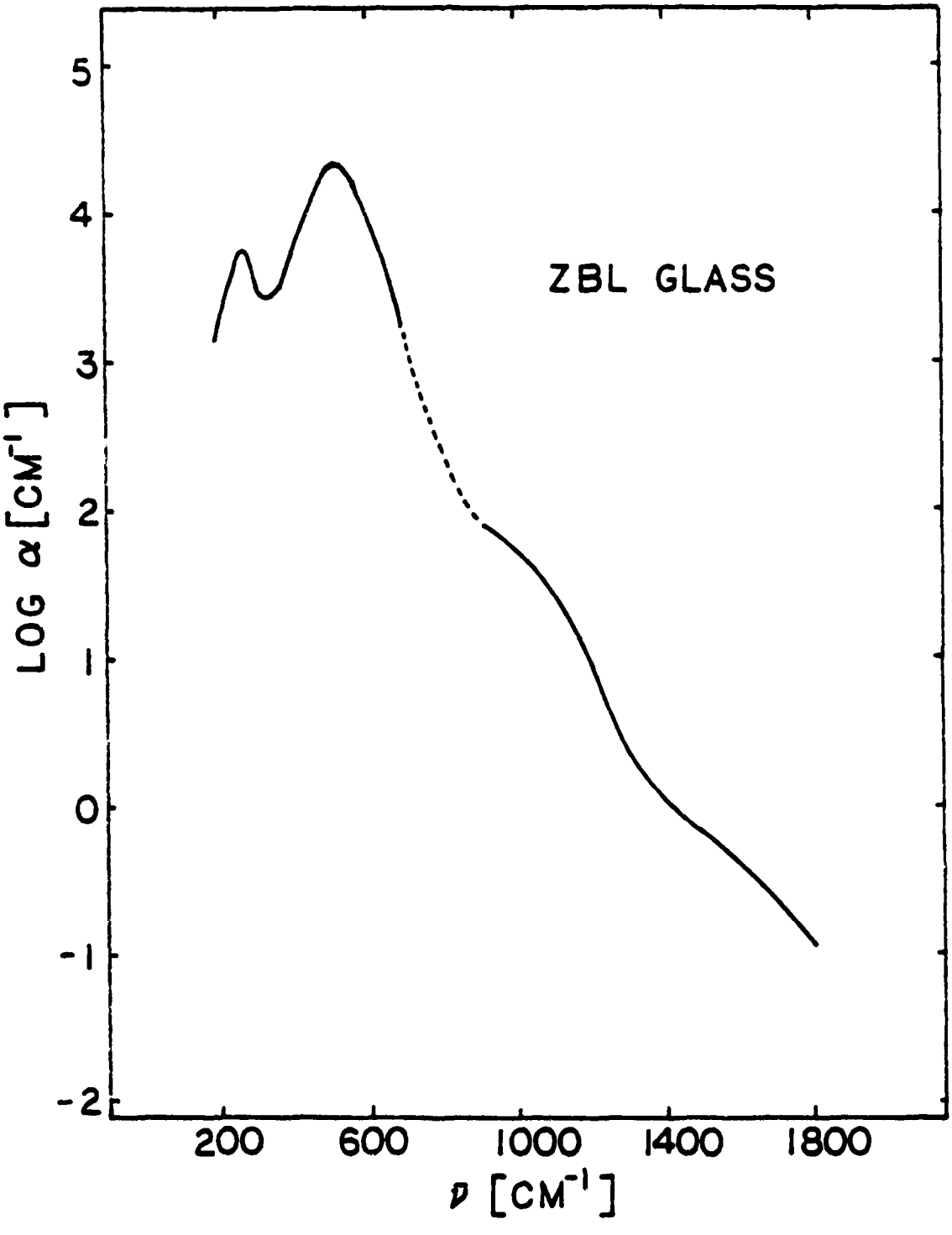

FIG. 34

Fig. 34 shows the typical decrease in structure as one moves from the fundamental to the multiphonon region. The absorption peak in the high frequency fundamental region (500 cm^{-1}) becomes a shoulder in the 2-phonon region (1000 cm^{-1}) and a change in slope in the 3-phonon region (1500 cm^{-1}). The envelope of the α vs. $\bar{\nu}$ curve beyond the fundamental region shows the exponential fall off of α with increasing $\bar{\nu}$ typical of intrinsic multiphonon absorption. The amount of structure in Fig. 34 is intermediate between that observed for covalent solids (considerable structure on the multiphonon edge) and that for ionic solids (featureless multiphonon edges).

VIII. 3. Removal of Oxide From Heavy Metal Fluoride Melts

In Tables XX-XXII for the ZBL and HBL glasses melted under CCl_4 atmosphere the values of α at 1400 cm^{-1} are lower than for those melted under N_2 or Cl_2 atmosphere. Generally CCl_4 seems better than Cl_2 for removing oxide impurities associated with the 1400 cm^{-1} peaks, and either reactive atmosphere is considerably better than an inert atmosphere. Also, whether an open or closed reactor was used did not seem to have a marked effect on the oxide impurity levels. For ZBLA glasses changes in processing conditions affected the absorption coefficient at 1400 cm^{-1} much less than with the ZBL and HBL glasses. This may be because Al-O bonds in the melt are more stable than Zr-O or Hf-O bonds, or because the intrinsic α values are larger for the AlF_3-containing glasses, giving a higher background against which the oxide peak must be observed. For the BaF_2/ThF_4 glasses the oxide absorption peak at $\sim$1100 cm^{-1} could be made

negligible by using CCl_4 atmosphere in the closed reactor.

CHAPTER IX

COMPOSITION DEPENDENCE OF INTRINSIC IR EDGE ABSORPTION IN HEAVY METAL FLUORIDE GLASSES

IX.1. Experimental IR Edge Absorption

Having discussed extrinsic contributions to the IR edge absorption of heavy metal fluoride glasses, we now turn to a consideration of the intrinsic contributions. IR edge spectra for samples of ZBL, HBL, ZBLA, HBLA and BZnYbT glasses, all of which are of comparable thickness (listed in Table XXV), are shown in Fig. 35 in the frequency range 800 to 1800 cm^{-1}. These samples have minimal oxide impurity absorption at 1400 or 1100 cm^{-1}, i.e., the spectra to a close approximation exhibit only intrinsic losses. Fig. 36 shows the corresponding semi-logarithmic plots of the absorption coefficient α versus frequency $\bar{\nu}$ for these samples. (Tables of α vs. $\bar{\nu}$ are given in Appendix I.) Trends with composition in the location of the IR edge are immediately apparent from Fig. 36. The IR edge of the HBL glass is shifted to lower frequencies relative to that of the presumably isostructural ZBL glass (see also Fig. 35), i.e., α for HBL is less than α for ZBL at a given frequency. Addition of small amounts of AlF_3 enhances absorption at a given frequency relative to the same glass without AlF_3 (compare ZBL with ZBLA and HBL with HBLA). On the other hand, a glass without ZrF_4 or HfF_4, such as BZnYbT, exhibits an extended transparency in the mid-IR range relative to that observed for fluorozirconate or fluorohafnate glasses.

Table XXV. Compositions and Processing Conditions of Some Fluoride Glasses Used to Compare IR Edges in Fig. 35.

Sample No.	Composition (mol %)	Thickness (cm)	Atmosphere	Reactor Type
HBL ——— 074	62-HfF_4-33BaF_2-5LaF_3	0.243	CCl_4	open
HBLA ——— 1-21-81	58HfF_4-33BaF_2-5LaF_3-4AlF_3	0.272	Cl_2	closed
ZBL ——— 8-10-81	62ZrF_4-33BaF_2-5LaF_3	0.329	CCl_4	closed
ZBLA ——— 22-7-81	58ZrF_4-33BaF_2-5LaF_3-4AlF_3	0.289	CCl_4	open
BZnYbT — — 20-10-81	20BaF_2-24ZnF_2-24YbF_3-32ThF_4	0.246	CCl_4	closed

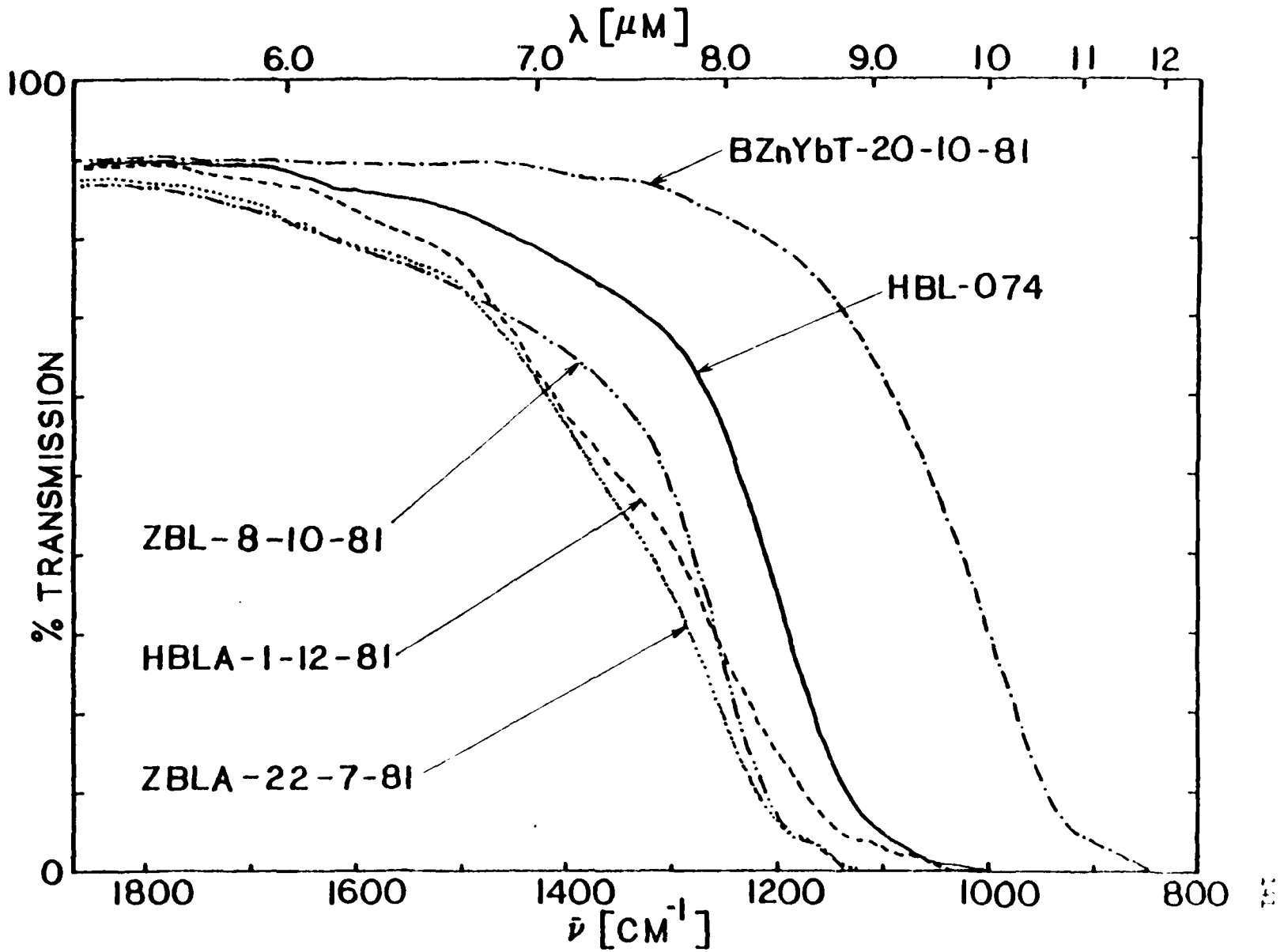
λ [μM]
6.0
7.0
8.0
9.0
10
11
12
100
0
% TRANSMISSION
BZnYbT-20-10-81
HBL-074
ZBL-8-10-81
HBLA-1-12-81
ZBLA-22-7-81
1800
1600
1400
1200
1000
800
ν̄ [CM⁻¹]

FIG. 35

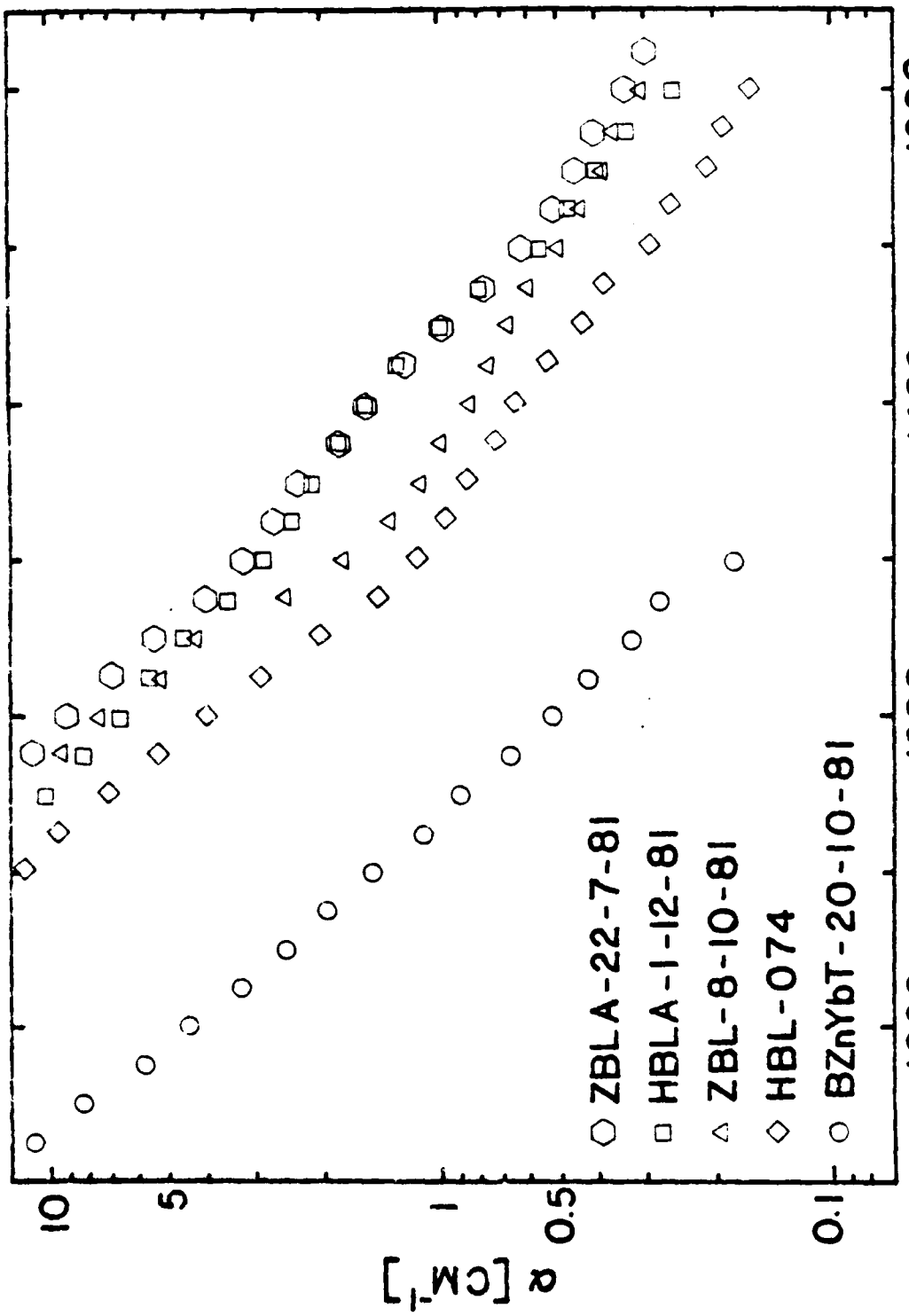
α [CM⁻¹]
10
5
1
0.5
0.1
1000
1200
1400
1600
ν [CM⁻¹]
ZBLA-22-7-81
HBLA-1-12-81
ZBL-8-10-81
HBL-074
BZnYbT-20-10-81

FIG. 36

IX. 2. Semiempirical Rules for Multiphonon Edge Absorption

There exist some semiempirical rules, reported in a publication [99] of early results from this project, which are useful for correlating and predicting multiphonon absorption behavior in crystals and glasses. These rules, given below, are illustrated in Table XXVI with some data for crystalline fluorides and typical heavy metal fluoride glasses.

(A) For a pair of binary isostructural solid compounds containing a common atom (e.g., CaF_2 and BaF_2 crystals, As_2S_3 and As_2Se_3 glasses), the member with the heavier atomic weight component will exhibit the smaller multiphonon attenuation coefficient α at a given frequency $\bar{\nu}$. Moreover, the difference in the α values increases with increasing frequency. For example, using data in Table XXVI, $\alpha_{BaF_2} < \alpha_{SrF_2} < \alpha_{CaF_2} < \alpha_{MgF_2}$ at a given frequency. As_2S_3 and As_2Se_3 glasses are another example [100]. The most important source of this correlation is probably the decrease of the fundamental vibration $\bar{\nu}_f$ which occurs with an increase in the masses of the atomic pairs in the solids. The harmonic oscillator expression for $\bar{\nu}_f$ is:

$$\bar{\nu}_f = (1/2\pi)(k/\mu)^{\frac{1}{2}} \qquad \text{(IX.1)}$$

where k is the force constant and μ the reduced mass of the atomic pair. An increase in atomic mass of one of the atoms will directly decrease $\bar{\nu}_f$ via the increase in μ and indirectly decrease $\bar{\nu}_f$ via the decrease in the force constant k due to the increase in interatomic distance which accompanies the mass increase. Since multiphonon absorption of a given

Table XXVI. Room Temperature Attenuation Coefficients In The Multiphonon Absorption Region For Fluoride Crystals and Heavy Metal Fluoride Glasses. Values in Parenthesis Are Extrapolated From The log α vs. $\tilde{\nu}$ Plots. Data From Ref. 99. (ZBL = $62ZrF_4$-$33BaF_2$-$5LaF_3$ glass, HBL = $62HfF_4$-$33BaF_2$-$5LaF_3$ and BZnYbT = $19\ BaF_2$-$27ZnF_2$-$27YbF_3$-$27ThF_4$ Glass).

	$\alpha(cm^{-1})$ AT $\tilde{\nu}$ =		
Compound	1000 cm^{-1}	1200 cm^{-1}	1400 cm^{-1}
LiF	34	10	3
NaF	2.6×10^{-1}	2.8×10^{-2}	(3×10^{-3})
KF	2.2×10^{-3}	1.0×10^{-4}	(5×10^{-6})
MgF_2	20	3.2	7.6×10^{-1}
CaF_2	2.2	2.6×10^{-1}	3.6×10^{-2}
SrF_2	3.2×10^{-1}	3.2×10^{-2}	3.2×10^{-3}
BaF_2	9×10^{-2}	(6×10^{-3})	(4×10^{-4})
LaF_3	1.5	1.9×10^{-1}	2.2×10^{-2}
ThF_4	1.2	(2×10^{-1})	——
ZBL	38	6.9	8.7×10^{-1}
HBL	25	4.0	6.4×10^{-1}
BZnYbT	4.5	5.3×10^{-1}	(7×10^{-2})

order (e.g., 2-phonon, 3-phonon, etc. absorption) occurs roughly at frequencies which are integral multiples of $\bar{\nu}_f$, a decrease in $\bar{\nu}_f$ shifts the entire IR absorption edge down in frequency and by relative amounts which increase with increasing frequency.

(B) For a pair of binary solid compounds with an atom in common and unlike atoms of comparable atomic weight (e.g., KF and CaF_2 crystals), the member with the unlike atom of lower charge will exhibit the smaller multiphonon attenuation coefficient at a given frequency. Again the difference in the α values increases with increasing frequency. For example, in Table XXVI, $\alpha_{KF} < \alpha_{CaF_2}$. The source of this correlation is the dependence of the fundamental vibration frequency on the square root of the force constant, k, for nearest neighbor atoms (cf. Eq. (IX.1)). k in turn increases with increasing electrostatic attraction of the nearest neighbor atoms.

(C) For ternary solids with a common anion (e.g., $KF \cdot MgF_2$ crystal, $GeSe_2$-As_2Se_3 glasses) the multiphonon absorption coefficients are given accurately by a volume-fraction weighted sum of the α values of the end member compounds. This additivity rule has been found to hold within experimental error for $GeSe_2$-As_2Se_3 glasses [100] and GeS_2-As_2S_3 glasses [101]. In these two cases the cations in the ternary glasses presumably retain the same local coordination as in the binary glasses, i.e., GeS_4 or $GeSe_4$ tetrahedra and AsS_3 or $AsSe_3$ pyramids. Another illustration, for high coordination number crystals, is shown in Fig. 37, which compares multiphonon α values for MgF_2, KF and $KMgF_3$ [99,102,103].

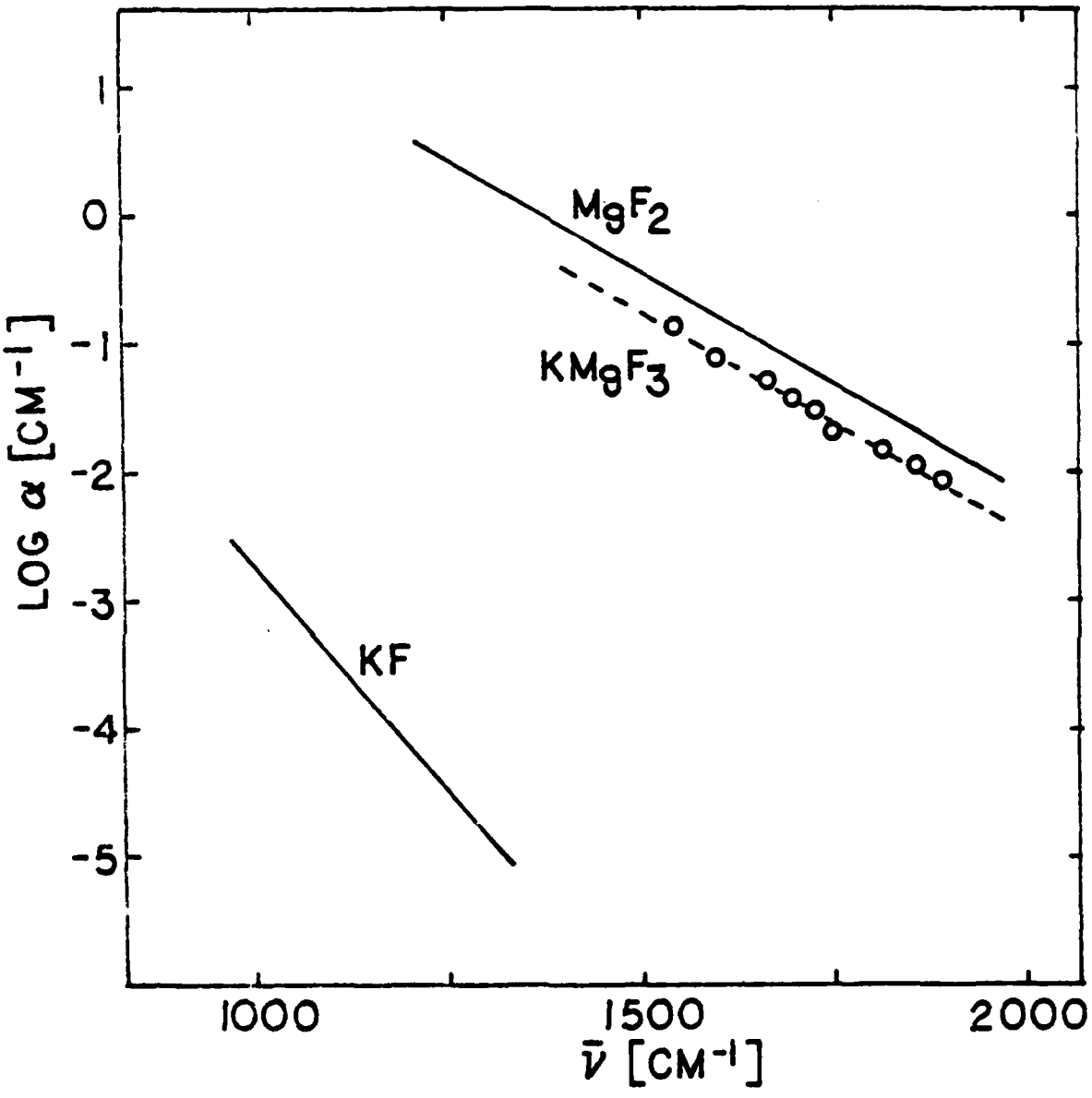

FIG. 37

Since $\alpha_{MgF_2} >> \alpha_{KF}$, only the MgF_2 component should contribute to α for the $KMgF_3$ crystal, and the α values for MgF_2 and $KMgF_3$ should be proportional to the respective Mg concentrations. From their densities (3.148 g/cm^3 for MgF_2, 3.19 g/cm^3 for $KMgF_3$) one calculates that the Mg concentration in $KMgF_3$ is 0.525 that in MgF_2; thus we expect $\alpha_{KMgF_3} = 0.525\ \alpha_{MgF_2}$. The dashed line through the $KMgF_3$ data in Fig. 37 is calculated from this relation and agrees within experimental error with the measured values. The validity of the additivity rule in this case may again depend on the fact the coordination number of 6 exhibited by Mg in MgF_2 (SnO_2 structure) is retained in $KMgF_3$ (perovskite structure).

IX.3. Multiphonon Absorption in Heavy Metal Fluoride Glasses

IX.3.1. ZrF_4- and HfF_4-Containing Glasses

By using the semiempirical rules listed in section IX.2, together with the data presented in Table XXVI, it should be possible to determine which components in the heavy metal fluoride glasses provide the main contributions to the observed IR absorption edges. For example, α values at 1000 cm^{-1} for the ZBL and HBL glasses are 38 and 25 cm^{-1} respectively (Table XXVI), well above the α values for pure crystalline BaF_2 (9×10^{-2} cm^{-1}) and LaF_3 (1.5 cm^{-1}). Although the α vs. $\bar{\nu}$ data for pure ZrF_4 and HfF_4 are not available, comparison of the masses and radii of Zr^{4+} and Hf^{4+} with that of Th^{4+} suggests that ZrF_4 and HfF_4 should be considerably more absorbing at a given frequency than the heavier ThF_4 and that α at 1000 cm^{-1} should be larger than that of ThF_4 (1.2 cm^{-1}).

Thus ZrF_4 or HfF_4 are probably the main contributors to the absorption in the region of IR edge of ZBL and HBL glasses.

Fig. 38 shows semi-logarithmic plots of α vs. $\bar{\nu}$ in the region of the IR edge for six different ZrF_4-containing glasses in Table XXVII. The α values were calculated from IR transmission spectra of polished specimens measured at CUA or reported in Ref. [32]. There are undoubtedly some extrinsic oxide contributions to α above 1300 cm^{-1}. However, the α vs. $\bar{\nu}$ curves below 1300 cm^{-1} of Fig. 38 should be very close to the intrinsic values (cf. Chapter VIII).

The ZrF_4 concentrations in all the glasses of Fig. 38 are the same to within ~14% (Table XXVII). From Table XXVII we also see that the contributions of the other glass components (ThF_4, LaF_3, BaF_2, KF, RbF and CsF) to multiphonon absorption should be negligible in this frequency range. Consequently, we expect intrinsic α versus $\bar{\nu}$ plots ($\bar{\nu} < 1300$ cm^{-1}) for all these glasses to superimpose to within 14%. As Fig. 38 demonstrates, this appears to be the case within experimental uncertainty.

In general, it appears that NaF and any monovalent cation fluorides heavier than it, CaF_2 and any divalent cation fluorides heavier than it, LaF_3 and any trivalent cation fluorides heavier than it, and ThF_4 and any quadrivalent cation fluorides heavier than it should contribute negligibly to the absorption on the IR edge of ZrF_4 glasses containing these other fluorides as components. ZrF_4 glass data have been used here as an example, but these conclusions will also hold true for the analogous HfF_4-based glasses, whose intrinsic absorption coefficients on the IR edge are of the same magnitude as those for the analogous ZrF_4

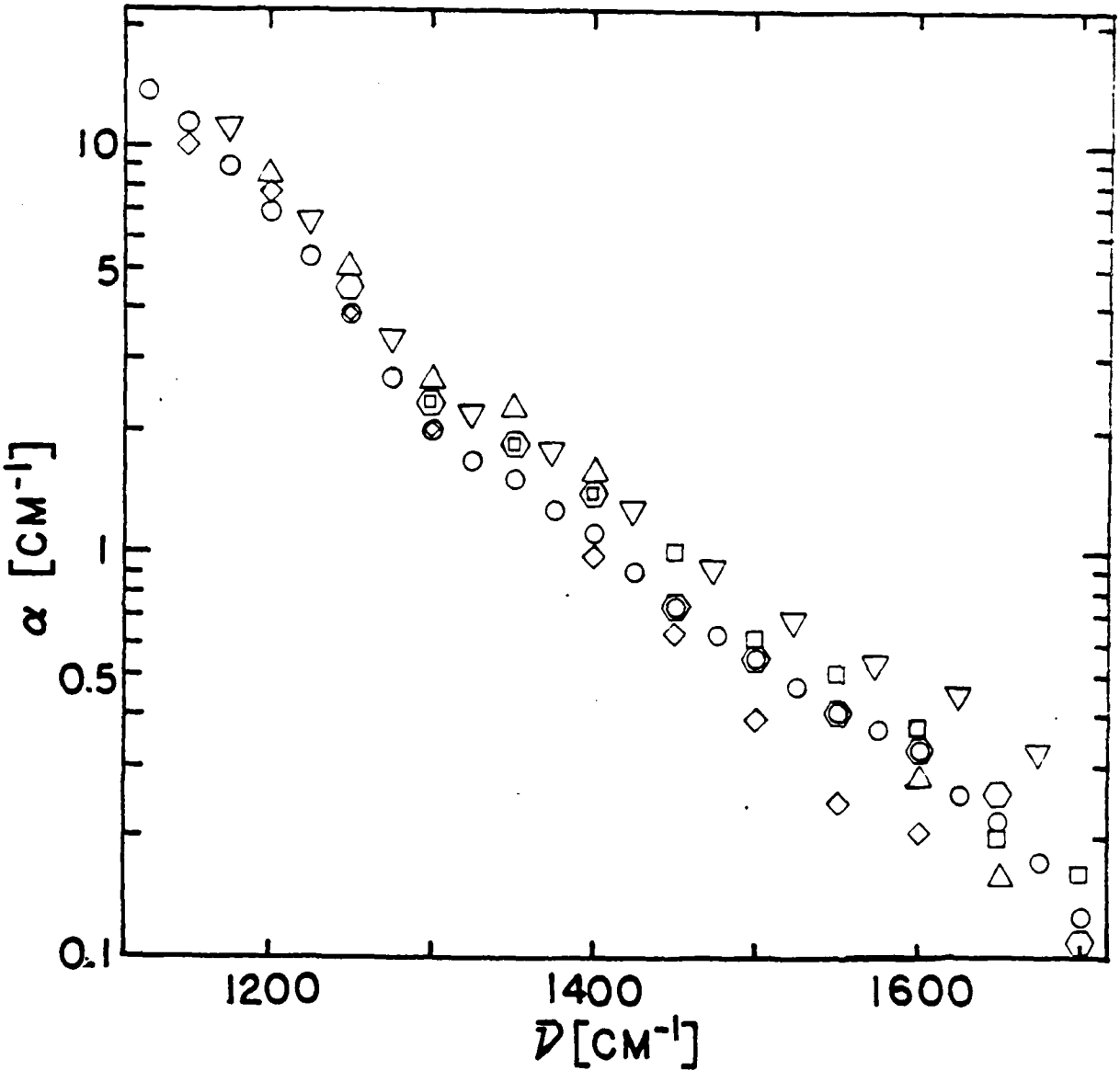

FIG. 38

Table XXVII. Compositions And Origins Of The Glass Of Fig. 38:

RADC = Rome Air Development Center;

HRL = Hughes Research Laboratories (Ref. 32);

LVF = Le Verre Fluore (Ref. 32);

CUA = Catholic University of America.

SYMBOL →	○	□	⬡	△	▽	◇
mol %						
ZrF_4	53	60	60	60	60	62
BaF_2	22	33	30	33	23	33
ThF_4	8	7	10	7		
LaF_3	4.2				7	5
KF	4.2					
RbF	4.2					
CsF	4.2				10	
Thickness (cm)	0.21 0.41	0.75	0.36	0.25	0.25	0.27
Melting Atmos.	Ar	CCl_4	INERT	HF	N_2	N_2
Source	RADC	HRL	LVF	HRL	CUA	CUA
Conc. Zr [$\frac{mol/cm^3}{X\,10^4}$]	14.7	16.0	15.7	16.0	—	16.8

glasses.

If rule (B) applies, AlF_3 should be more absorbing than ZrF_4 or HfF_4 ($\alpha_{MgF_2} < \alpha_{AlF_3}$ and $\alpha_{MgF_2} \sim \alpha_{HBL}$ or α_{ZBL}). Therefore addition of small amounts of AlF_3 to ZrF_4- or HfF_4-containing glasses will increase the multiphonon absorption. This is in accord with the data in Fig. 36, i.e., the α vs. $\bar{\nu}$ curves for ZBLA and HBLA glasses lie above those for ZBL and HBL.

The α vs. $\bar{\nu}$ curves for HBL and ZBL in Figs. 30 and 36 are almost parallel over the experimental frequency range measured, the HBL curve being shifted to lower frequency by about 30-40 cm^{-1} relative to the ZBL curve. (At a given frequency the ratio of absorption coefficients, $\alpha_{ZBL}/\alpha_{HBL}$, is roughly 1.4 - 1.7.) Drexhage et al. [8] speculated that the differences in IR edge absorption between the ZrF_4- and HfF_4-based glasses were due primarily to the difference in the fundamental vibration frequencies arising from the mass differences between Hf and Zr. On the basis of such differences, one would predict a shift to lower frequencies of about 20-25 cm^{-1} ($=\sqrt{\mu_{Hf-F}/\mu_{Zr-F}}$) in the fundamental IR frequencies associated with Hf-F vibrations relative to those for Zr-F. Recent measurements of IR restrahlen spectra [76], however, indicate that the shift is smaller than expected, about 10 - 15 cm^{-1}. Also the intensity of the fundamental peak at about 500 cm^{-1} in the HBL glass is somewhat lower than that observed in ZBL. These two facts possibly indicate a larger Hf-F force constant in the HfF_4-based glasses relative to the Zr-F force constant in the corresponding ZrF_4-based glasses. The observed 10 - 15 cm^{-1} displacement between the ZBL and HBL absorption curves in the fundamental

frequency region implies that the shift should be 20 - 30 cm^{-1} in the 2-phonon region around 1000 cm^{-1} and 30 - 45 cm^{-1} in the 3-phonon region around 1500 cm^{-1}. This is consistent overall with the observed shift in frequency of the HBL relative to the ZBL α vs. $\bar{\nu}$ curves (Fig. 30 and 36).

IX.3.2. BaF_2/ThF_4-Based Glasses

The IR edge of the BZnYbT glass in Fig. 36 is shifted to much lower frequencies relative to those of the ZrF_4- and HfF_4-containing glasses. This is due to the absence of ZrF_4 and HfF_4, which were by far the most strongly absorbing components in the latter glasses.

Again by using semiempirical rules and Table XXVI we can decide which components are probably contributing most strongly to IR edge absorption in the BZnYbT glass. It can be seen that $\alpha_{BaF_2} << \alpha_{BZnYbT}$, while α_{YbF_3} (probably similar to α_{LaF_3}) and α_{ThF_4} are of the same order of magnitude but somewhat smaller than α_{BZnYbT}. There are no available data on pure ZnF_2; however, the radius of Zn^{2+} (0.074 nm) is smaller than that of Ca^{2+} (0.099 nm), so that it is likely that $\alpha_{ZnF_2} > \alpha_{CaF_2}$ even though the difference in masses between Ca and Zn would have the opposite effect in the α values. Since α_{CaF_2} is just slightly lower than α_{BZnYbT}, it thus seems likely that the main contributor to the IR edge absorption in BZnYbT glasses is ZnF_2, along with substantial but lower contributions from YbF_3 and ThF_4.

Fig. 39 shows plots of α vs. $\bar{\nu}$ in the region of the IR edge for a number of BaF_2/ThF_4-based glasses. (These α vs. $\bar{\nu}$ data are also tabulated in Appendix I.) Replacement of YbF_3 in the BZnYbT glass by

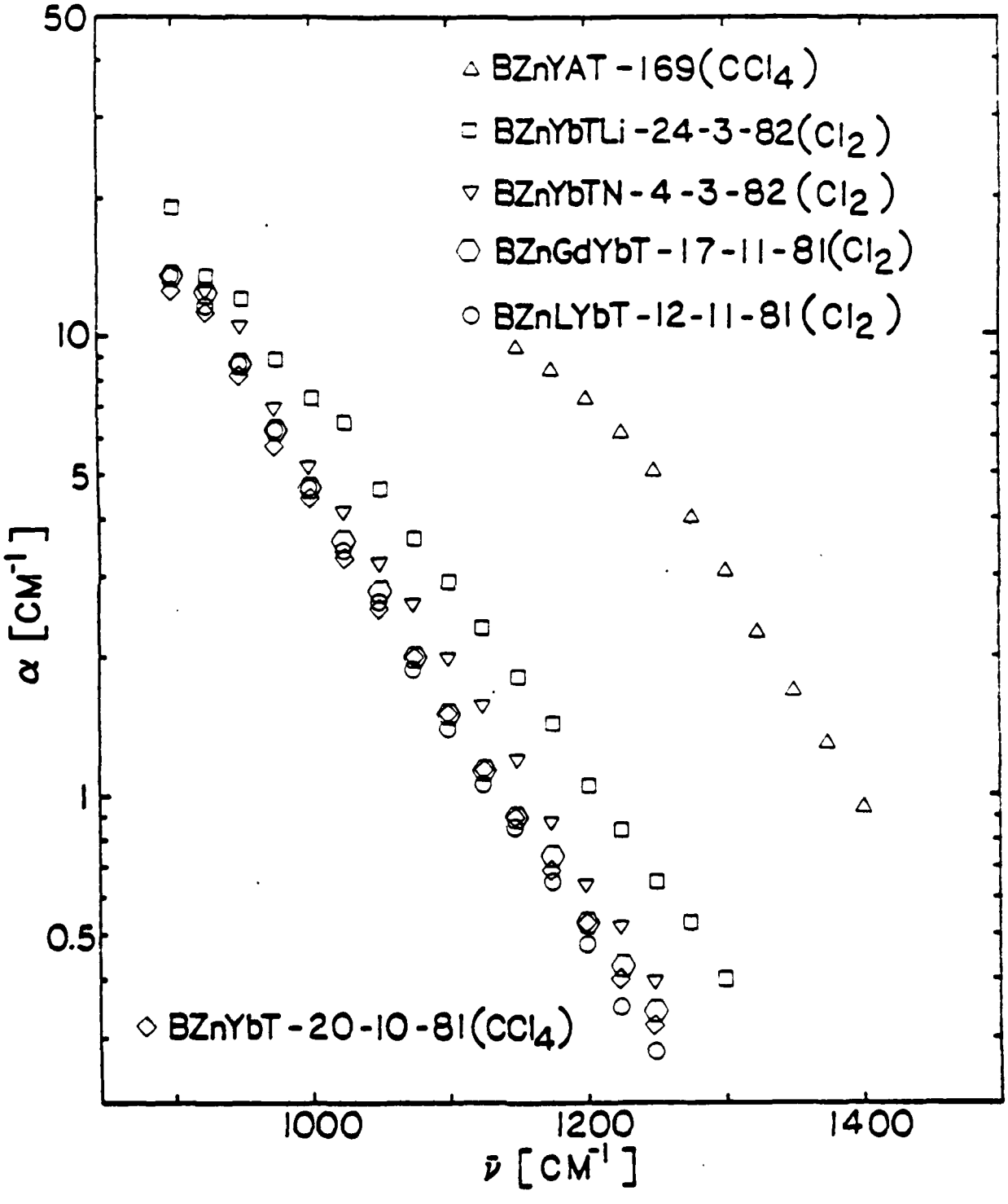
50
10
5
1
0.5
α [CM⁻¹]
1000
1200
1400
ν̄ [CM⁻¹]
△ BZnYAT-169(CCl4)
□ BZnYbTLi-24-3-82(Cl2)
▽ BZnYbTN-4-3-82(Cl2)
⬡ BZnGdYbT-17-11-81(Cl2)
○ BZnLYbT-12-11-81(Cl2)
◇ BZnYbT-20-10-81(CCl4)

FIG. 39

the lighter YF_3 and AlF_3 greatly enhances at a given frequency. Addition of LiF to BZnYbT glass has a similar, but smaller effect. On the other hand, replacement of YbF_3 by LaF_3 or GdF_3 or the addition of NaF has no effect relative to BZnYbT glass on the observed IR edge absorption. All these trends are in accord with the semiempirical rules of section IX.2 and the data in Table XXVI.

CHAPTER X

CONCLUSION

In this thesis, heavy metal fluoride glasses based on ZrF_4, HfF_4 and BaF_2/ThF_4 have been studied. The ZrF_4- and HfF_4- based glasses exhibit considerable promise as high transparency materials from the UV to the IR (0.2 - 7 μm) and the BaF_2/ThF_4-based glasses exhibit transparency over even a larger region (0.2 - 9 μm).

At present there are several problems associated with the usage of these glasses in high technology systems, and these have been the main motive for the present study. One major problem is that the materials are relatively poor glass formers and have a strong tendency to crystallize on cooling. Another is that absorption bands at 2.9 μm and 7 or 9 μm, due respectively to -OH and metal oxyfluoride impurities, can cause significant transmission losses in the mid-IR radiation, if they can not be eliminated or at least substantially reduced. These transmission characteristics are most important with regard to the potential telecommunication system applications of these glasses.

Concerning these problems, it was apparent that they were essentially related to the quality of glasses which could be produced (with respect to their homogeneity and impurity levels). Consequently, the main aim throughout this thesis has been to study the effects of processing conditions on the physical properties of the glasses, using a combination of techniques, including IR spectroscopy and differential scanning calorimetry.

The optimum glass forming compositions for the ternary fluorozirconate and fluorohafnate systems have been determined to be $62ZrF_4$- or $62HfF_4$-$33BaF_2$-$5LaF_3$ and close to $19BaF_2$-$27ZnF_2$-$27YbF_3$-$27ThF_4$ for the BaF_2/ThF_4-based glasses. Improvements in the glass forming abilities of the fluorozirconate and fluorohafnate glasses (as reflected by an increase in the difference between the glass transition and crystallization temperatures) were achieved by adding CsF, PbF_2 or AlF_3 as additional components, while the BaF_2/ThF_4-based glasses could be improved by adding NaF, LiF or AlF_3 or by the substitution of LuF_3 for YbF_3.

The heat capacities, $\bar{C}p$, of the fluorozirconate, fluorohafnate and BaF_2/ThF_4-based glasses were all found to be very similar on a per gram-atom basis. At ambient temperature the heat capacities were all close to 5.2 cal/g-atom.K, while near Tg the Dulong-Petit limit of 3R (5.97 cal/g-atom.K) was approached. The values of ΔCp at the glass transition were all $\sim$3.4 cal/g-atom.K, which is much larger than those reported for oxide glasses (1.1 $\sim$ 1.8 cal/g-atom.K).

The IR spectra of the fluoride glasses showed excess absorption at $\sim$2.9 μm and $\sim$7 or 9 μm due respectively to -OH and metal oxyfluoride impurities. However, the IR absorption data obtained for consecutively thinned samples has indicated that the peaks at 2.9 μm for glasses melted under CCl_4 or Cl_2 reactive atmospheres are due almost entirely to surface -OH. It has been found that melting in a closed reactor with a CCl_4 atmosphere is the most effective of the methods used for removing -OH. A CCl_4 atmosphere was also found best for removing oxide impurity. It has also been found that the -OH and oxide absorptions for the

BaF_2/ThF_4 glasses are not as intense as in the ZrF_4- or HfF_4-based glasses prepared under the same conditions, although it should be pointed out that higher melting temperatures were used for the former group of glasses.

For the fluorozirconate and fluorohafnate glasses the main contributors to multiphonon absorption on the IR edge at ~7 μm were found to be, respectively, the ZrF_4 and HfF_4 components; components such as BaF_2, LaF_3, ThF_4 and NaF have little effect on the IR edge absorption. The BaF_2/ThF_4- based glasses, as might be expected, have IR edges at longer wavelengths (~9 μm) due to the absence of these ZrF_4 or HfF_4 components. Additions of AlF_3 were found to shift the IR edges to shorter wavelengths for all the glasses.

APPENDIX I

IR TRANSMISSION AND ABSORPTION COEFFICIENT DATA ON THE IR EDGE OF HEAVY METAL FLUORIDE GLASSES

TO = transmission in region of spectrum where only reflectivity losses occur

R = reflectivity

THICKNESS = thickness of glass specimen

FREQ = measurement frequency in wave numbers

TRANS = transmission

ALPHA = attenuation coefficient α,

Uncertainties in α values were computed as described in Chapter III.

62ZRF4-33BAF3-5LAF3

SAMPLE NO. Z3L-27-1-82

T0=0.874 R=0.067

THICKNESS=0.223 CM

FREQ(1/CM)	TRANS	ALPHA(1/CM)
1100	0.030	15.10+-0.97
1125	0.035	14.41+-0.85
1150	0.060	11.99+-0.56
1175	0.111	9.23+-0.36
1200	0.186	6.92+-0.25
1225	0.296	4.84+-0.18
1250	0.407	3.41+-0.14
1275	0.513	2.38+-0.12
1300	0.588	1.77+-0.11
1325	0.643	1.37+-0.10
1350	0.678	1.13+-0.10
1375	0.693	1.03+-0.10
1400	0.719	0.87+-0.09
1425	0.744	0.72+-0.09
1450	0.764	0.60+-0.09
1475	0.779	0.51+-0.09
1500	0.789	0.46+-0.08
1525	0.799	0.40+-0.08
1550	0.804	0.37+-0.08
1575	0.814	0.32+-0.08
1600	0.824	0.26+-0.08

SOLAR-GARD-LOT-5L4F3

SAMPLE NO. ZBL-083

T0=0.776 R=0.126

THICKNESS=0.102 CM

FREQ(1/CM)	TRANS	ALPHA(1/CM)
1050	0.045	27.54+-1.87
1075	0.066	24.01+-1.46
1100	0.107	19.27+-1.06
1125	0.163	15.15+-0.80
1150	0.224	12.04+-0.64
1175	0.301	9.15+-0.52
1200	0.383	6.80+-0.42
1225	0.469	4.84+-0.35
1250	0.556	3.19+-0.29
1275	0.622	2.11+-0.26
1300	0.663	1.50+-0.24
1325	0.684	1.20+-0.23
1350	0.694	1.06+-0.22
1375	0.704	0.93+-0.22
1400	0.714	0.79+-0.22
1425	0.724	0.66+-0.21
1450	0.730	0.58+-0.21

S2ZRF4-338MP2-5LAF2

SAMPLE NO. ZBL-083

T0=0.916 R=0.101

THICKNESS=0.378 CM

FREQ(1/CM)	TRANS	ALPHA(1/CM)
1200	0.046	7.58+-0.37
1225	0.097	5.61+-0.21
1250	0.184	3.77+-0.13
1275	0.296	2.66+-0.09
1300	0.388	1.95+-0.08
1325	0.439	1.62+-0.07
1350	0.474	1.42+-0.07
1375	0.505	1.25+-0.07
1400	0.546	1.05+-0.06
1425	0.577	0.90+-0.06
1450	0.607	0.77+-0.06
1475	0.633	0.66+-0.06
1500	0.653	0.58+-0.06
1525	0.673	0.50+-0.06
1550	0.689	0.44+-0.05
1575	0.699	0.40+-0.05
1600	0.714	0.35+-0.05
1625	0.730	0.29+-0.05
1650	0.745	0.24+-0.05
1675	0.755	0.20+-0.05
1700	0.765	0.17+-0.05
1725	0.776	0.13+-0.05

62CRF4-33PF3-SL2F1

SAMPLE NO. ZRL-25-9-80

T0=0.918 R=0.043

THICKNESS=0.074 CM

FREQ(1/CM)	TRANS	ALPHA(1/CM)
950	0.025	48.14+-4.37
975	0.025	43.74+-3.50
1000	0.056	37.77+-2.63
1025	0.082	32.62+-2.07
1050	0.107	29.02+-1.76
1075	0.138	25.58+-1.50
1100	0.189	21.33+-1.23
1125	0.250	17.55+-1.01
1150	0.321	14.18+-0.84
1175	0.403	11.11+-0.69
1200	0.490	8.47+-0.57
1225	0.571	6.40+-0.48
1250	0.658	4.49+-0.40
1275	0.724	3.20+-0.35
1300	0.765	2.46+-0.32
1325	0.781	2.18+-0.31
1350	0.796	1.92+-0.30
1375	0.801	1.84+-0.29
1400	0.821	1.50+-0.28
1425	0.832	1.32+-0.27
1450	0.847	1.08+-0.26
1475	0.852	1.00+-0.26
1500	0.862	0.85+-0.25
1525	0.867	0.77+-0.25
1550	0.867	0.77+-0.25
1575	0.872	0.69+-0.25

S2ZRF4-33BAF2-5L4F3

SAMPLE NO. ZBL-25-9-80

T0=0.870 R=0.065

THICKNESS=0.190 CM

FREQ(1/CM)	TRANS	ALPHA(1/CM)
1125	0.036	16.79+-1.01
1150	0.056	14.46+-0.72
1175	0.097	11.57+-0.48
1200	0.168	8.68+-0.33
1225	0.255	6.49+-0.25
1250	0.367	4.57+-0.19
1275	0.469	3.28+-0.16
1300	0.551	2.44+-0.14
1325	0.582	2.15+-0.13
1350	0.607	1.93+-0.13
1375	0.633	1.71+-0.12
1400	0.663	1.47+-0.12
1425	0.694	1.23+-0.11
1450	0.719	1.04+-0.11
1475	0.745	0.86+-0.11
1500	0.765	0.72+-0.10
1525	0.776	0.65+-0.10
1550	0.786	0.58+-0.10
1575	0.796	0.51+-0.10
1600	0.801	0.48+-0.10
1625	0.811	0.41+-0.10
1650	0.821	0.35+-0.10
1675	0.832	0.28+-0.10
1700	0.837	0.25+-0.09

62ZRF4-33BAF2-5LAF3

SAMPLE NO. ZBL-25-9-80

T0=0.872 R=0.060

THICKNESS=0.254 CM

FREQ(1/CM)	TRANS	ALPHA(1/CM)
1150	0.036	12.53+-0.72
1175	0.051	11.16+-0.54
1200	0.097	8.63+-0.33
1225	0.173	6.35+-0.22
1250	0.281	4.44+-0.16
1275	0.388	3.17+-0.13
1300	0.469	2.43+-0.11
1325	0.515	2.06+-0.10
1350	0.546	1.83+-0.10
1375	0.571	1.66+-0.10
1400	0.612	1.38+-0.09
1425	0.648	1.16+-0.09
1450	0.679	0.98+-0.08
1475	0.704	0.84+-0.08
1500	0.730	0.69+-0.08
1525	0.750	0.59+-0.08
1550	0.760	0.54+-0.08
1575	0.770	0.49+-0.08
1600	0.781	0.43+-0.07
1625	0.796	0.36+-0.07
1650	0.806	0.31+-0.07
1675	0.816	0.26+-0.07
1700	0.832	0.18+-0.07

62ZSF4-33BAF2-5LAF3

SAMPLE NO. ZBL-8-10-81

T0=0.870 R=0.070

THICKNESS=0.329 CM

FREQ(1/CM)	TRANS	ALPHA(1/CM)
1175	0.040	9.35+-0.45
1200	0.070	7.64+-0.31
1225	0.150	5.38+-0.18
1250	0.210	4.31+-0.14
1275	0.380	2.51+-0.09
1300	0.480	1.80+-0.08
1325	0.555	1.36+-0.07
1350	0.595	1.15+-0.07
1375	0.620	1.02+-0.07
1400	0.655	0.86+-0.06
1425	0.675	0.77+-0.06
1450	0.695	0.68+-0.06
1475	0.710	0.61+-0.06
1500	0.735	0.51+-0.06
1525	0.750	0.45+-0.06
1550	0.765	0.39+-0.06
1575	0.770	0.37+-0.06
1600	0.785	0.31+-0.06
1625	0.795	0.27+-0.06
1650	0.805	0.23+-0.06
1675	0.820	0.18+-0.05
1700	0.830	0.14+-0.05

[illegible]

SAMPLE NO. HBL-07-

TO=0.000 T=0.851

THICKNESS=0.040 IN

FREQ(1/CM)	TRANS	ALPHA (1/CM)
1100	0.052	11.80+-0.56
1125	0.085	9.70+-0.38
1150	0.160	7.10+-0.25
1175	0.250	5.26+-0.18
1200	0.340	4.00+-0.15
1225	0.450	2.84+-0.12
1250	0.550	2.02+-0.10
1275	0.620	1.46+-0.08
1300	0.680	1.15+-0.06
1325	0.710	0.97+-0.06
1350	0.730	0.86+-0.06
1375	0.755	0.72+-0.06
1400	0.770	0.64+-0.06
1425	0.790	0.53+-0.06
1450	0.910	0.43+-0.06
1475	0.920	0.39+-0.07
1500	0.945	0.26+-0.07
1525	0.945	0.26+-0.07
1550	0.955	0.21+-0.07
1575	0.960	0.19+-0.07
1600	0.965	0.16+-0.07

62HFF4-339AF3-5L3F3

SAMPLE NO. 43L-999

T0=0.929 P=0.037

THICKNESS=0.058 CM

FREQ(1/CM)	TRANS	ALPHA(1/CM)
850	0.036	56.02+-5.99
875	0.051	50.02+-4.93
900	0.066	45.57+-3.46
925	0.092	39.84+-2.84
950	0.128	34.15+-2.33
975	0.163	29.98+-2.01
1000	0.219	24.89+-1.65
1025	0.255	22.27+-1.48
1050	0.301	19.41+-1.31
1075	0.342	17.21+-1.18
1100	0.408	14.17+-1.01
1125	0.490	11.01+-0.94
1150	0.571	8.38+-0.70
1175	0.653	6.07+-0.58
1200	0.719	4.41+-0.50
1225	0.770	3.23+-0.44
1250	0.811	2.34+-0.39
1275	0.837	1.79+-0.37
1300	0.857	1.39+-0.35
1325	0.862	1.29+-0.34
1350	0.867	1.19+-0.34
1375	0.867	1.19+-0.34
1400	0.872	1.09+-0.33
1425	0.878	0.97+-0.33
1450	0.883	0.87+-0.32

SEMI-INSULATING GaAs

SAMPLE NO. HBL-080

T0=0.923 R=0.040

THICKNESS=0.210 CM

FREQ(1/CM)	TRANS	ALPHA(1/CM)
1125	0.031	10.94+-0.64
1150	0.061	8.76+-0.37
1175	0.138	6.13+-0.20
1200	0.230	4.48+-0.14
1225	0.327	3.34+-0.11
1250	0.429	2.47+-0.09
1275	0.526	1.81+-0.08
1300	0.587	1.46+-0.07
1325	0.617	1.30+-0.07
1350	0.638	1.19+-0.07
1375	0.653	1.11+-0.07
1400	0.679	0.99+-0.07
1425	0.704	0.87+-0.06
1450	0.735	0.73+-0.06
1475	0.760	0.63+-0.06
1500	0.786	0.52+-0.06
1525	0.806	0.44+-0.06
1550	0.816	0.40+-0.06
1575	0.827	0.35+-0.06
1600	0.837	0.31+-0.06
1625	0.852	0.26+-0.06
1650	0.862	0.22+-0.06
1675	0.872	0.18+-0.05

62HFF4-33BAF2-5LAF3

SAMPLE NO. HBL-11-9-90

T0=0.969 R=0.016

THICKNESS=0.071 CM

FREQ(1/CM)	TRANS	ALPHA(1/CM)
900	0.036	46.37+-3.73
925	0.051	41.47+-2.99
950	0.061	38.94+-2.67
975	0.102	31.70+-1.95
1000	0.143	26.95+-1.59
1025	0.184	23.40+-1.35
1050	0.224	20.63+-1.19
1075	0.270	17.99+-1.04
1100	0.337	14.87+-0.88
1125	0.418	11.84+-0.73
1150	0.505	9.18+-0.61
1175	0.582	7.18+-0.52
1200	0.663	5.34+-0.44
1225	0.730	3.99+-0.38
1250	0.781	3.04+-0.34
1275	0.821	2.33+-0.31
1300	0.847	1.89+-0.30
1325	0.857	1.73+-0.29
1350	0.857	1.73+-0.29
1375	0.862	1.65+-0.29
1400	0.872	1.48+-0.28
1425	0.878	1.39+-0.27
1450	0.888	1.23+-0.27
1475	0.898	1.07+-0.26
1500	0.908	0.92+-0.26
1525	0.913	0.84+-0.25
1550	0.913	0.84+-0.25
1575	0.913	0.84+-0.25
1600	0.918	0.76+-0.25
1625	0.923	0.68+-0.25
1650	0.929	0.59+-0.24
1675	0.929	0.59+-0.24

62HFF4-30BAF2-5LAF3

SAMPLE NO. HBL-11-9-90

T0=0.990 R=0.005

THICKNESS=0.103 CM

FRE0(1/CM)	TRANS	ALPHA(1/CM)
950	0.036	32.14+-2.23
975	0.046	29.77+-1.88
1000	0.061	27.04+-1.55
1025	0.092	23.06+-1.19
1050	0.133	19.48+-0.94
1075	0.163	17.51+-0.82
1100	0.230	14.17+-0.65
1125	0.306	11.40+-0.53
1150	0.393	8.97+-0.44
1175	0.490	6.83+-0.36
1200	0.582	5.16+-0.31
1225	0.663	3.89+-0.27
1250	0.735	2.89+-0.23
1275	0.791	2.18+-0.21
1300	0.821	1.82+-0.20
1325	0.837	1.63+-0.20
1350	0.842	1.57+-0.19
1375	0.852	1.46+-0.19
1400	0.862	1.34+-0.19
1425	0.872	1.23+-0.18
1450	0.888	1.06+-0.18
1475	0.903	0.89+-0.17
1500	0.913	0.79+-0.17
1525	0.923	0.68+-0.17
1550	0.929	0.62+-0.17
1575	0.934	0.57+-0.16
1600	0.934	0.57+-0.16
1625	0.939	0.51+-0.16
1650	0.949	0.41+-0.16
1675	0.959	0.31+-0.16

S2HFFJ-33BAF2-5L9F3

SAMPLE NO. HBL-11-9-80

T0=0.944 R=0.029

THICKNESS=0.152 CM

FREQ(1/CM)	TRANS	ALPHA(1/CM)
1025	0.031	22.47+-1.50
1050	0.041	20.63+-1.21
1075	0.056	18.58+-0.96
1100	0.097	14.96+-0.66
1125	0.158	11.75+-0.47
1150	0.230	9.28+-0.37
1175	0.327	6.97+-0.29
1200	0.429	5.18+-0.23
1225	0.520	3.92+-0.20
1250	0.607	2.90+-0.17
1275	0.679	2.17+-0.15
1300	0.724	1.74+-0.14
1325	0.750	1.51+-0.14
1350	0.755	1.47+-0.14
1375	0.765	1.38+-0.14
1400	0.781	1.25+-0.13
1425	0.801	1.08+-0.13
1450	0.816	0.96+-0.13
1475	0.837	0.79+-0.12
1500	0.852	0.67+-0.12
1525	0.862	0.60+-0.12
1550	0.867	0.56+-0.12
1575	0.872	0.52+-0.12
1600	0.878	0.48+-0.12
1625	0.888	0.40+-0.11
1650	0.893	0.36+-0.11
1675	0.903	0.29+-0.11

58ZRF4-33BAF2-5L4F3-4RLF3

SAMPLE NO. ZDLA-10-2-32

T0=0.855 R=0.078

THICKNESS=0.237 CM

FREQ(1/CM)	TRANS	ALPHA(1/CM)
1150	0.040	12.89+-0.71
1175	0.070	10.53+-0.46
1200	0.125	8.09+-0.30
1225	0.200	6.11+-0.22
1250	0.295	4.47+-0.17
1275	0.360	3.40+-0.14
1300	0.435	2.83+-0.13
1325	0.490	2.33+-0.12
1350	0.535	1.96+-0.11
1375	0.580	1.62+-0.10
1400	0.630	1.28+-0.10
1425	0.675	0.99+-0.09
1450	0.710	0.78+-0.09
1475	0.735	0.63+-0.08
1500	0.765	0.46+-0.08
1525	0.780	0.38+-0.08
1550	0.790	0.33+-0.08
1575	0.800	0.28+-0.08
1600	0.805	0.25+-0.08
1625	0.810	0.23+-0.08
1650	0.820	0.17+-0.08

50ZRF4-30BAF2-5LAF3-4ALF3

SAMPLE NO. ZBLA-5-2-92

T0=0.894 R=0.056

THICKNESS=0.204 CM

FREQ(1/CM)	TRANS	ALPHA(1/CM)
1150	0.045	14.64+-0.70
1175	0.080	11.82+-0.51
1200	0.131	9.40+-0.36
1225	0.206	7.18+-0.26
1250	0.286	5.57+-0.21
1275	0.377	4.22+-0.17
1300	0.442	3.44+-0.15
1325	0.503	2.81+-0.14
1350	0.543	2.43+-0.13
1375	0.578	2.13+-0.12
1400	0.628	1.72+-0.12
1425	0.673	1.39+-0.11
1450	0.704	1.17+-0.10
1475	0.759	0.80+-0.10
1500	0.779	0.67+-0.09
1525	0.799	0.55+-0.09
1550	0.804	0.52+-0.09
1575	0.819	0.43+-0.09
1600	0.829	0.37+-0.09

58ZRF4-32BAF2-5LAF3-4ALF3

SAMPLE NO. ZBLA-14-7-81

T0=0.929 R=0.042

THICKNESS=0.256 CM

FREQ(1/CM)	TRANS	ALPHA(1/CM)
1175	0.040	12.24+-0.65
1200	0.065	10.34+-0.44
1225	0.130	7.64+-0.27
1250	0.205	5.86+-0.20
1275	0.300	4.37+-0.15
1300	0.375	3.50+-0.13
1325	0.435	2.92+-0.12
1350	0.480	2.54+-0.11
1375	0.535	2.11+-0.10
1400	0.580	1.80+-0.09
1425	0.640	1.41+-0.09
1450	0.680	1.18+-0.08
1475	0.730	0.90+-0.08
1500	0.765	0.72+-0.08
1525	0.790	0.59+-0.07
1550	0.810	0.50+-0.07
1575	0.820	0.45+-0.07
1600	0.835	0.38+-0.07
1625	0.850	0.31+-0.07
1650	0.875	0.20+-0.07

58ZRF4-33BAF2-5L3F3-4ALF3

SAMPLE NO. ZBLA-22-7-91

T0=0.880 R=0.064

THICKNESS=0.289 CM

FREQ(1/CM)	TRANS	ALPHA(1/CM)
1175	0.035	11.14+-0.63
1200	0.055	9.58+-0.44
1225	0.110	7.18+-0.26
1250	0.180	5.48+-0.18
1275	0.270	4.08+-0.14
1300	0.345	3.23+-0.12
1325	0.405	2.67+-0.11
1350	0.455	2.27+-0.10
1375	0.510	1.88+-0.09
1400	0.555	1.59+-0.08
1425	0.610	1.26+-0.08
1450	0.660	0.99+-0.07
1475	0.700	0.79+-0.07
1500	0.735	0.62+-0.07
1525	0.760	0.50+-0.07
1550	0.770	0.46+-0.07
1575	0.780	0.41+-0.07
1600	0.790	0.37+-0.06
1625	0.800	0.33+-0.06
1650	0.820	0.24+-0.06
1675	0.825	0.22+-0.06

50HFF4-33BAF2-5LAF2-4ALF3

SAMPLE NO. HSLA-1-12-81

T0=0.890 R=0.058

THICKNESS=0.272 CM

FREQ(1/CM)	TRANS	ALPHA(1/CM)
1150	0.055	10.22+-0.47
1175	0.095	8.21+-0.31
1200	0.145	6.66+-0.23
1225	0.200	5.48+-0.18
1250	0.265	4.44+-0.15
1275	0.340	3.53+-0.13
1300	0.410	2.84+-0.11
1325	0.460	2.42+-0.10
1350	0.495	2.15+-0.10
1375	0.535	1.86+-0.09
1400	0.570	1.63+-0.09
1425	0.620	1.32+-0.08
1450	0.675	1.01+-0.08
1475	0.715	0.80+-0.07
1500	0.765	0.55+-0.07
1525	0.785	0.46+-0.07
1550	0.800	0.39+-0.07
1575	0.810	0.34+-0.07
1600	0.830	0.25+-0.07

20BAF2-24ZNF2-24YBF3-30TMF4

SAMPLE NO. BZNYBT-20-10-91

T0=0.900 R=0.053

THICKNESS=0.246 CM

FREQ(1/CM)	TRANS	ALPHA(1/CM)
900	0.040	12.65+-0.68
925	0.055	11.35+-0.53
950	0.115	8.35+-0.31
975	0.215	5.81+-0.20
1000	0.300	4.46+-0.16
1025	0.400	3.29+-0.13
1050	0.480	2.55+-0.11
1075	0.550	1.99+-0.10
1100	0.620	1.51+-0.09
1125	0.680	1.13+-0.09
1150	0.720	0.90+-0.08
1175	0.760	0.68+-0.08
1200	0.790	0.53+-0.08
1225	0.810	0.43+-0.07
1250	0.830	0.33+-0.07
1275	0.840	0.28+-0.07
1300	0.860	0.18+-0.07
1325	0.870	0.14+-0.07
1350	0.875	0.11+-0.07
1375	0.875	0.11+-0.07
1400	0.880	0.09+-0.07
1425	0.885	0.07+-0.07

10BAF2-2TCNF2-2TYBF3-2TTHF4

SAMPLE NO. BZNYBT-30-10-81

T0=2.905 R=0.050

THICKNESS=0.216 CM

FREQ(1/CM)	TRANS	ALPHA(1/CM)
900	0.035	15.05+-0.89
925	0.060	12.55+-0.58
950	0.110	9.75+-0.37
975	0.190	7.22+-0.26
1000	0.240	6.13+-0.22
1025	0.270	5.59+-0.20
1050	0.315	4.88+-0.18
1075	0.370	4.13+-0.16
1100	0.440	3.33+-0.14
1125	0.530	2.47+-0.12
1150	0.640	1.60+-0.11
1175	0.730	0.99+-0.09
1200	0.780	0.69+-0.09
1225	0.810	0.51+-0.09
1250	0.830	0.40+-0.08
1275	0.850	0.29+-0.08
1300	0.860	0.24+-0.08

19BAF2-27CHF2-2FV3F3-2FTHF1

SAMPLE NO. DCNYBT-10-11-01

T0=0.890 R=0.058

THICKNESS=0.247 CM

FREQ(1/CM)	TRANS	ALPHA(1/CM)
925	0.040	12.55+-0.68
950	0.070	10.28+-0.44
975	0.120	8.10+-0.30
1000	0.140	7.47+-0.27
1025	0.150	7.20+-0.25
1050	0.160	6.93+-0.24
1075	0.190	6.24+-0.22
1100	0.225	5.55+-0.19
1125	0.290	4.53+-0.16
1150	0.375	3.49+-0.13
1175	0.490	2.41+-0.11
1200	0.590	1.66+-0.10
1225	0.690	1.03+-0.09
1250	0.765	0.61+-0.08
1275	0.805	0.42+-0.07
1300	0.830	0.28+-0.07
1325	0.850	0.18+-0.07
1350	0.860	0.14+-0.07

AD-A122 359 METALLIC HALIDE OPTICAL GLASSES: SYNTHESIS AND CHARACTERIZATION OF IR TRA..(U) CATHOLIC UNIV OF AMERICA WASHINGTON DC C T MOYNIHAN ET AL. OCT 82

3/3

UNCLASSIFIED RADC-TR-82-264 F19628-81-K-0010 F/G 11/2 NL

END

DATE FILMED

DTIC

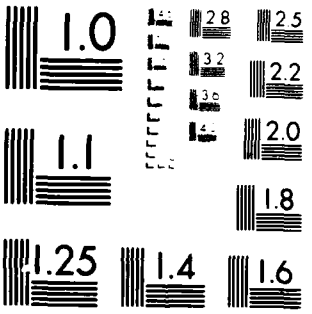

[illegible]

SAMPLE NO. [illegible]

T0=1.000 R=0.081

THICKNESS=0.160 CM

FREQ(1/CM)	TRANS	ALPHA(1/CM)
900	0.045	18.25+-1.00
925	0.085	14.35+-0.65
950	0.140	11.29+-0.46
975	0.190	9.42+-0.38
1000	0.195	9.26+-0.37
1025	0.215	8.66+-0.35
1050	0.190	9.42+-0.38
1075	0.090	14.00+-0.63
1100	0.060	16.49+-0.83
1125	0.055	17.02+-0.89
1150	0.045	18.25+-1.00
1175	0.050	14.00+-0.60
1200	0.150	10.87+-0.44
1225	0.330	6.33+-0.26
1250	0.580	2.79+-0.17
1275	0.740	1.09+-0.13
1300	0.815	0.50+-0.11
1325	0.845	0.28+-0.11

19BAF2-27ZNF2-13.5YF3-13.5YBF3-27THF4

SAMPLE NO. BZNYYBT-9-11-91

T0=0.895 R=0.061

THICKNESS=0.209 CM

FREQ(1/CM)	TRANS	ALPHA(1/CM)
900	0.035	15.44+-0.92
925	0.060	12.86+-0.61
950	0.120	9.54+-0.37
975	0.200	7.10+-0.26
1000	0.235	6.33+-0.23
1025	0.255	5.94+-0.22
1050	0.285	5.41+-0.20
1075	0.350	4.42+-0.18
1100	0.405	3.73+-0.16
1125	0.530	2.44+-0.13
1150	0.625	1.66+-0.11
1175	0.715	1.01+-0.10
1200	0.770	0.66+-0.09
1225	0.800	0.48+-0.09
1250	0.820	0.36+-0.09
1275	0.835	0.28+-0.09
1300	0.850	0.19+-0.08

19[illegible]F2-27CNF2-5GIF3-2CV3F3-17THF4

SAMPLE NO. [illegible]

T0=2.905 R=0.050

THICKNESS=0.238 CM

FREQ(1/CM)	TRANS	ALPHA(1/CM)
900	0.040	13.09+-0.71
925	0.050	12.16+-0.59
950	0.115	8.66+-0.32
975	0.205	6.23+-0.21
1000	0.300	4.63+-0.17
1025	0.380	3.53+-0.14
1050	0.475	2.70+-0.12
1075	0.560	2.01+-0.11
1100	0.630	1.52+-0.10
1125	0.685	1.17+-0.09
1150	0.725	0.93+-0.09
1175	0.765	0.70+-0.08
1200	0.795	0.54+-0.08
1225	0.815	0.44+-0.08
1250	0.835	0.34+-0.08
1275	0.850	0.26+-0.07
1300	0.865	0.19+-0.07
1325	0.870	0.16+-0.07
1350	0.875	0.14+-0.07
1375	0.885	0.09+-0.07
1400	0.890	0.07+-0.07

19BAF2-2TCNF2-3L9F3-24V5F3-27THF4

SAMPLE NO. BZHLY9T-12-11-81

T0=0.865 R=0.072

THICKNESS=0.258 CM

FREQ(1/CM)	TRANS	ALPHA(1/CM)
900	0.025	13.72+-0.95
925	0.045	11.44+-0.59
950	0.090	8.75+-0.35
975	0.175	6.17+-0.22
1000	0.265	4.57+-0.16
1025	0.360	3.38+-0.13
1050	0.440	2.60+-0.11
1075	0.530	1.89+-0.10
1100	0.595	1.44+-0.09
1125	0.660	1.04+-0.08
1150	0.695	0.84+-0.08
1175	0.735	0.63+-0.08
1200	0.765	0.47+-0.07
1225	0.790	0.35+-0.07
1250	0.805	0.28+-0.07
1275	0.815	0.23+-0.07
1300	0.835	0.14+-0.07
1325	0.845	0.09+-0.07
1350	0.850	0.07+-0.07
1375	0.855	0.04+-0.07

14BAF2-27ZNF2-27YBF3-27THF4-5NAF

SAMPLE NO. BZNYBTN-4-3-82

T0=0.899 R=0.053

THICKNESS=0.315 CM

FREQ(1/CM)	TRANS	ALPHA(1/CM)
925	0.020	12.07+-0.92
950	0.035	10.30+-0.57
975	0.101	6.93+-0.25
1000	0.172	5.24+-0.17
1025	0.242	4.16+-0.13
1050	0.318	3.29+-0.11
1075	0.394	2.61+-0.10
1100	0.470	2.05+-0.09
1125	0.545	1.58+-0.08
1150	0.621	1.17+-0.07
1175	0.682	0.87+-0.07
1200	0.732	0.65+-0.06
1225	0.763	0.52+-0.06
1250	0.793	0.40+-0.06
1275	0.813	0.32+-0.06
1300	0.833	0.24+-0.06
1325	0.854	0.16+-0.06
1350	0.859	0.14+-0.05
1375	0.869	0.11+-0.05
1400	0.886	0.05+-0.05
1425	0.886	0.05+-0.05

14BAF2-2T2NF2-2TV2F2-2TTHTV-5L1F

SAMPLE NO. B2NY2TLI-24-3-32

T0=0.905 R=0.050

THICKNESS=0.260 CM

FREQ(1/CM)	TRANS	ALPHA(1/CM)
900	0.015	15.76+-1.48
925	0.035	12.50+-0.71
950	0.045	11.53+-0.58
975	0.090	8.87+-0.34
1000	0.141	7.14+-0.25
1025	0.211	5.59+-0.19
1050	0.271	4.63+-0.16
1075	0.357	3.57+-0.13
1100	0.422	2.93+-0.12
1125	0.497	2.30+-0.10
1150	0.568	1.79+-0.09
1175	0.633	1.37+-0.09
1200	0.688	1.05+-0.08
1225	0.724	0.85+-0.08
1250	0.764	0.65+-0.07
1275	0.789	0.53+-0.07
1300	0.814	0.41+-0.07
1325	0.834	0.31+-0.07
1350	0.849	0.24+-0.07
1375	0.859	0.20+-0.07
1400	0.869	0.16+-0.07
1425	0.874	0.13+-0.07
1450	0.879	0.11+-0.07
1475	0.889	0.07+-0.06

205AF2-28.75CHF2-14.375VF2-11.375ALF3-22 5TH54

SAMPLE NO. R2YAT-169

T0=0.900 P=0.952

THICKNESS=0.329 CM

FREQ(1/CM)	TRANS	ALPHA(1/CM)
1150	0.040	9.18+-0.47
1175	0.050	8.52+-0.39
1200	0.075	7.32+-0.28
1225	0.110	6.19+-0.21
1250	0.160	5.09+-0.16
1275	0.230	4.02+-0.13
1300	0.315	3.09+-0.10
1325	0.410	2.31+-0.09
1350	0.500	1.72+-0.08
1375	0.580	1.29+-0.07
1400	0.650	0.96+-0.06
1425	0.700	0.74+-0.06
1450	0.735	0.59+-0.06
1475	0.760	0.50+-0.06
1500	0.785	0.40+-0.05
1525	0.800	0.35+-0.05
1550	0.810	0.31+-0.05
1575	0.820	0.27+-0.05
1600	0.830	0.24+-0.05
1625	0.840	0.20+-0.05
1650	0.845	0.19+-0.05
1675	0.855	0.15+-0.05
1700	0.860	0.13+-0.05

REFERENCES

1. H. Rawson, Inorganic Glass Forming Systems, Academic Press, New York, 1967.

2. K. H. Sun, Glass Tech., 20, 36 (1979).

3. J. D. Mackenzie, Final Tech. Report No. 8331705, Lawrence Livermore Laboratory, Livermore, CA (May 1978).

4. S. Shibata, T. Kanamori, S. Mitach and T. Manabe, Mat. Res. Bull., 15, 129 (1980).

5. M. Poulain, M. Poulain and J. Lucas, Mat. Res. Bull., 10, 243 (1975).

6. Michel Poulain, Private Communication to C. T. Moynihan at Univ. of Rennes (June 1981).

7. M. Poulain and J. Lucas, Verres Refract., 32, 505 (1978).

8. M. G. Drexhage, C. T. Moynihan and M. Saleh, Mat. Res. Bull., 15, 213 (1980).

9. A. Lecoq, M. Poulain and J. Lucas, J. Non-Cryst. Solids, 34, 101 (1979).

10. M. G. Drexhage, C. T. Moynihan, M. Saleh Boulos and K. P. Quinlan, pp. 57-73 in Physics of Fiber Optics, B. Bendow and S. S. Mitra, Eds. (Am. Ceram. Soc., Columbus, OH, 1981).

11. M. Matecki, M. Poulain, M. Poulain and J. Lucas, Mat. Res. Bull., 13, 1039 (1978).

12. R. M. Almeida, Ph.D. Thesis, UCLA (1980).

13. B. Bendow and M. G. Drexhage, Proc. SPIE, 266, 16 (1981).

14. J. Lucas, H. Slim and G. Fonteneau, J. Non-Cryst. Solids, 44, 31 (1981).

15. G. Fonteneau, F. Lahaie and J. Lucas, Mat. Res. Bull., 15, 1143 (1980).

16. G. Fonteneau, H. Slim, F. Lahaie and J. Lucas, Mat. Res. Bull., 15, 1245 (1980).

17. H. Slim, Ph.D. Thesis, Univ. of Rennes (1981).

18. M. Poulain, M. Poulain and M. Matecki, Mat. Res. Bull., 16, 555 (1981).

19. W. H. Zachariasen, J. Am. Chem. Soc., 54, 3841 (1932).

20. D. L. Kepert, The Early Transition Metals, Academic, London, 1972.

21. M. Poulain, M. Chanthanasinh and J. Lucas, Mat. Res. Bull., 12, 151 (1977).

22. R. M. Almeida and J. D. Mackenzie, J. Chem. Phys., 74, 5954 (1981).

23. M. Poulain, Nature, 293, 279 (1981).

24. K. H. Sun, J. Am. Ceram. Soc., 30, 277 (1947).

25. C. M. Baldwin and J. D. Mackenzie, J. Am. Ceram. Soc., 62, 573 (1979).

26. T. J. Loretz, J. L. Mansfield, M. G. Drexhage and C. T. Moynihan, Am. Ceram. Soc. Bull., 60, 413 (1981).

27. H. Hu and J. D. Mackenzie, "Viscosity of Molten Fluorozirconates", Presented at First International Symposium on Halide and Other Non-Oxide Glasses, Cambridge, UK (March 1982).

28. L. Kaufmann, J. Argen, J. Nell and F. Hayes, "CALPHAD Calculation of Ternary Fluoride Glass Compositions", Presented at First International Symposium on Halide and Other Non-oxide Glasses, Cambridge, UK (March 1982).

29. M. Poulain, M. Poulain and J. Lucas, Rev. Chim. Miner., 16, 267 (1979).

30. C. M. Baldwin, R. M. Almeida and J. D. Mackenzie, J. Non-Cryst. Solids, 43, 309 (1981).

31. M. Robinson, R. C. Pastor, R. R. Turk, D. P. Devor, M. Braunstein and R. Braunstein, Proc. SPIE, 266, 78 (1981).

32. M. Robinson, R. C. Pastor, R. R. Turk, M. Braunstein and R. Braunstein Mat. Res. Bull., 15, 735 (1980).

33. R. C. Pastor, J. A. Harrington, L. E. Gore and R. K. Chew, Mat. Res. Bull., 14, 543 (1979).

34. C. T. Moynihan, A. J. Easteal, D. C. Tran, J. A. Wilder and E. P. Donovan, J. Am. Ceram. Soc., 59, 137 (1976).

35. G. V. Chandrashekhar and M. W. Shafer, Mat. Res. Bull., 15, 221 (1980).

36. A. Lecoq and M. Poulain, Verres Refract., 34, 333 (1980).

37. S. Takahashi, S. Shibata, T. Kanamori, S. Mitachi and T. Manabe, pp. 74-83 in Physics of Fiber Optics, B. Bendow and S. S. Mitra, Eds. (Am. Ceram. Soc., Columbus, OH, 1981).

38. S. Mitachi, S. Shibata and T. Manabe, Jap. J. Appl. Phys., 20, L337 (1981).

39. S. Mitachi, S. Shibata and T. Manabe, Elec. Lett., 17, 128 (1981).

40. D. Ravaine and D. Leroy, J. Non-Cryst. Solids, 38 & 39, 575 (1980).

41. M. G. Drexhage, B. Bendow, C. T. Moynihan and J. Lucas, Bull. Am. Ceram. Soc., 60, 860 (1981).

42. M. G. Drexhage, B. Bendow, T. J. Loretz, J. Mansfield and C. T. Moynihan, Paper presented at the Third International Conference on Integrated Optics and Optical Fiber Communication, San Francisco, CA, April (1980).

43. J. J. Mecholsky, M. G. Drexhage and C. T. Moynihan, Paper presented at Fall Meeting of American Ceramic Society, Bedford Springs, PA, October (1981).

44. A. Lecoq and M. Poulain, J. Non-Cryst. Solids, 41, 209 (1980).

45. M. W. Shafer and P. Perry, Mat. Res. Bull., 14, 899 (1979).

46. J. Gannon, J. Non-Cryst. Solids, 42, 239 (1980).

47. T. Kanamori, K. Oikawa, S. Shibata and T. Manabe, Jap. J. Appl. Phys., 20, L326 (1981).

48. M. Poulain, M. Poulain and M. Matecki, "Rare Earths in Fluoride Glasses: The LnF_3-AlF_3-ThF_4-BaF_2 Systems and Related Glasses", preprint of paper.

49. Y. LePage, D. E. A. de Chimie, Univ. of Rennes (1980-1981).

50. M. Matecki, M. Poulain and M. Poulain, Mat. Res. Bull., 16, 749 (1981).

51. T. Kanamori, S. Shibata, S. Mitachi and T. Manabe, Jap. J. Appl. Phys., 19, L90 (1980).

52. J-P. Miranday, C. Jacoboni and R. DePape, J. Non-Cryst. Solids, 43, 393 (1981).

53. J-P. Miranday, C. Jacoboni and R. DePape, Rev. Chim. Min., 16, 277 (1979).

54. J. Gannon, Proc. SPIE, 266, 62 (1981).

55. M. P. Brassington, T. Hailing, A. J. Miller and G. A. Saunders, Mat. Res. Bull., 16, 613 (1981).

56. C. M. Baldwin and J. D. Mackenzie, J. Non-Cryst. Solids, 31, 441 (1979).

57. C. M. Baldwin and J. D. Mackenzie, J. Non-Cryst. Solids, 40, 135 (1980).

58. K. Matusita and S. Sakka, Phys. Chem. Glasses, 20, 81 (1979).

59. K. Jinguji, M. Honguchi, S. Mitachi, T. Kanamori and T. Manabe, Jap. J. Appl. Phys., 20, L329 (1981).

60. C. M. Baldwin and J. D. Mackenzie, J. Non-Cryst. Solids, 42, 455 (1980).

61. D. Leroy and D. Ravaine, C. R. Acad. Sc. Paris, 286, Ser. C 413 (1979).

62. D. Leroy, J. Lucas, M. Poulain and D. Ravaine, Mat. Res. Bull., 13, 1125 (1978).

63. O. H. Wyatt and D. Dew-Hughes, Metals, Ceramics and Polymers, Cambridge Univ. Press (1974).

64. M. G. Drexhage, B. Bendow, O. El-Bayoumi, T. Loretz, C. T. Moynihan, J. J. Shaffer, P. A. Temple and H. E. Bennett, "Progress in the Development of Multispectral Glasses Based on the Fluorides of Heavy Metals", Presented at the 13th Boulder Damage Symposium, Boulder, Colorado (Nov. 1981).

65. T. Miya, Y. Terunuma, T. Hosaka and T. Miyashita, Elec. Lett., 15 106 (1979).

66. S. Mitachi and T. Manabe, Jap. J. Appl. Phys., 19, L313 (1980).

67. S. Mitachi, T. Kanamori and T. Miyashita, Jap. J. Appl. Phys., 21, L55 (1982).

68. D. A. Pinnow, T. C. Rich, F. W. Ostermayer and M. DiDomenico, Jr., Appl. Phys. Lett., 22, 527 (1973).

69. S. H. Wemple and M. DiDomenico, Jr., Phys. Rev. B, 1, 193 (1970).

70. S. H. Wemple, J. Chem. Phys., 67, 2151 (1977).

71. M. G. Sparks and L. G. DeSchazer, Proc. SPIE, 266, 3 (1981).

72. J. Schroeder, R. Mohr, C. J. Montrose and P. B. Macedo, J. Non-Cryst. Solids, 13, 313 (1973/74).

73. R. N. Brown, B. Bendow, M. G. Drexhage and C. T. Moynihan, Appl. Opt., 21, 361 (1982).

74. M. G. Drexhage, B. Bendow and C. T. Moynihan, Laser Focus, 15, 62 (1980).

75. M. G. Drexhage, O. H. El-Bayoumi and C. T. Moynihan, "Progress in Heavy Metal Fluoride Glasses for Infrared Fibers", Proc. SPIE, 320, (1982, in press).

76. B. Bendow, P. K. Banerjee, M. G. Drexhage, J. Goltman, S. S. Mitra, and C. T. Moynihan, J. Am. Ceram. Soc., 65, C-8 (1982).

77. B. Bendow, M. G. Drexhage, H. G. Lipson, P. K. Banerjee, J. Goltman, S. S. Mitra and C. T. Moynihan, Appl. Opt., 20, 2875 (1981).

78. B. Bendow, M. G. Drexhage, P. K. Banerjee, J. Goltman, S. S. Mitra, and C. T. Moynihan, Solid State Commun., 37, 485 (1981).

79. P. K. Banerjee, B. Bendow, M. G. Drexhage, J. T. Goltman, S. S. Mitra and C. T. Moynihan, J. de Physique, 42, Suppl. C6, 75 (1981).

80. G. Rupprecht, Phys. Rev. Lett., 12, 580 (1964).

81. B. Bendow, H. G. Lipson and S. P. Yukon, Phys. Rev. B, 16, 2684, (1977).

82. B. Bendow, in Solid State Physics, H. Ehrenreich, F. Seitz and D. Turnbull, Eds., Academic, New York (1976).

83. J. R. Hardy and B. S. Agrawal, Appl. Phys. Lett., 22, 236 (1973).

84. B. Bendow, M. G. Drexhage and H. G. Lipson, J. Appl. Phys., 52, 1460 (1981).

85. A. G. Pincus, J. Am. Opt. Soc., 35, 92 (1945).

86. J. Lucas, M. Chanthanasinh, M. Poulain, M. Poulain, P. Brun and M. J. Weber, J. Non-Cryst. Solids, 27, 273 (1978).

87. B. Bendow, R. N. Brown, M. G. Drexhage, T. J. Loretz and R. L. Kirk, Appl. Opt., 20, 3688 (1981).

88. L. Jeunhomme, H. Poignant and M. Monerie, "Material Dispersion Evaluation in a Fluoride Glass", preprint of paper.

89. K. Nassau, Elec. Lett., 16, 924 (1980).

90. T. Izumitani, in Treaties on Materials Science and Technology, vol. 17, Glass II, edited by M. Tomozawa and R. H. Doremus (1979).

91. U. E. Schnaus, C. T. Moynihan, R. W. Gammon and P. B. Macedo, Phys. Chem. Glasses, 11, 213 (1970).

92. C. A. Angel, J. Am. Ceram. Soc., 51, 117 (1968).

93. J. S. Haggerty, A. R. Cooper and J. H. Heasley, Phys. Chem. Glasses, 9, 47 (1968 and 9, 132 (1968).

94. U. E. Schnaus and C. T. Moynihan, Mater. Sci. Eng., 7, 268 (1971).

95. M. G. Drexhage, B. Bendow, R. N. Brown, P. K. Banerjee, H. G. Lipson, G. Fontenau, J. Lucas and C. T. Moynihan, Appl. Opt., 21, 971 (1982).

96. E. Gbogi, K.-H. Chung, C. T. Moynihan and M. G. Drexhage, J. Am. Ceram. Soc., 64, C-51 (1981).

97. M. G. Drexhage, C. T. Moynihan, B. Bendow, E. Gbogi, K.-H. Chung and M. Boulos, Mat. Res. Bull., 16, 943 (1981).

98. B. Bendow, Sol. State Phys., 33, 249 (1978).

99. C. T. Moynihan, M. G. Drexhage, B. Bendow, M. Saleh Boulos, K. P. Quinlan, K.-H. Chung and E. Gbogi, Mat. Res. Bull., 16, 25 (1981).

100. R. E. Howard, P. S. Danielson, M. S. Maklad, R. K. Mohr, P. B. Macedo and C. T. Moynihan, p. 271 in Optical Properties of Highly Transparent Solids, edited by S. S. Mitra and B. Bendow.

101. D. S. Ma, Ph.D. Thesis, The Catholic University of America (1977).

102. B. Bendow, H. G. Lipson and S. S. Mitra, Phys. Rev. B, 20, 1747 (1979).

103. A. Hordvik and L. Skolnik, Appl. Opt., 16, 2919 (1977).

MISSION
of
Rome Air Development Center

RADC plans and executes research, development, test and selected acquisition programs in support of Command, Control Communications and Intelligence (C^3I) activities. Technical and engineering support within areas of technical competence is provided to ESD Program Offices (POs) and other ESD elements. The principal technical mission areas are communications, electromagnetic guidance and control, surveillance of ground and aerospace objects, intelligence data collection and handling, information system technology, ionospheric propagation, solid state sciences, microwave physics and electronic reliability, maintainability and compatibility.

Printed by
United States Air Force
Hanscom AFB, Mass. 01731

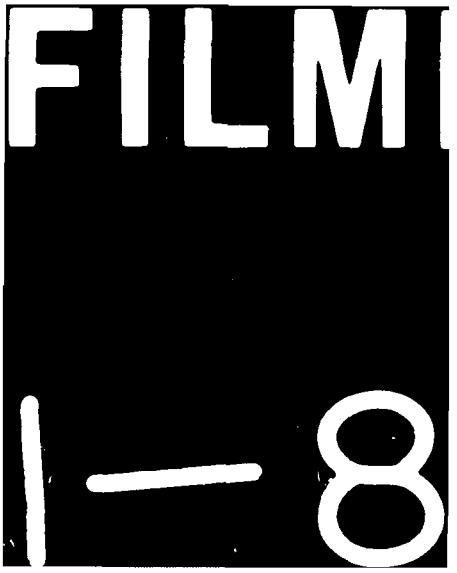
FILM
1-8